FZR-424

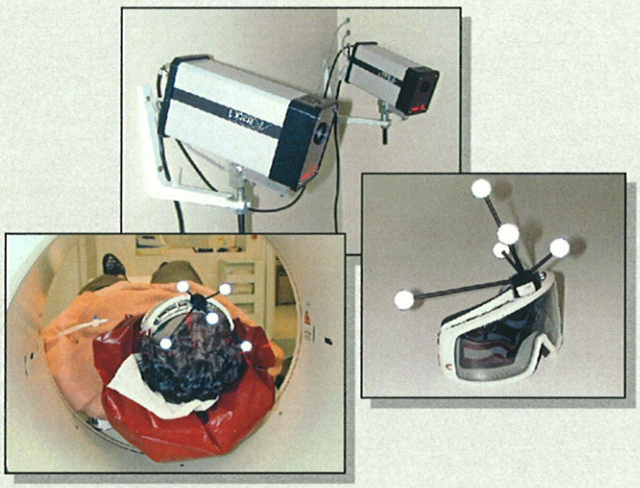

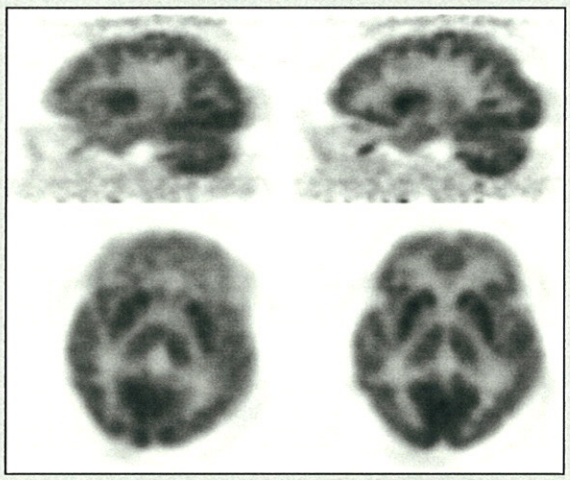

Wissenschaftlich-Technische Berichte
FZR-424 2005 · ISSN 1437-322X

Annual Report 2004

Institute of Bioinorganic and Radiopharmaceutical Chemistry

Forschungszentrum
Rossendorf

FORSCHUNGSZENTRUM ROSSENDORF

Mitglied der Wissenschaftsgemeinschaft Gottfried Wilhelm Leibniz

WISSENSCHAFTLICH-TECHNISCHE BERICHTE
FZR-424
Februar 2005
ISSN 1437-322X

Institute of Bioinorganic and Radiopharmaceutical Chemistry

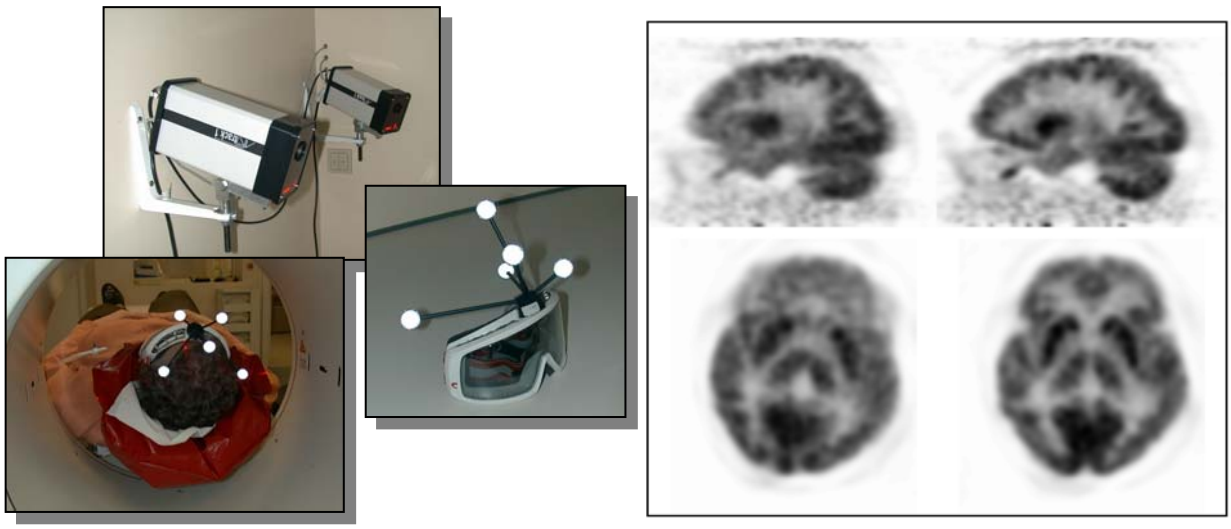

Annual Report 2004

Cover Picture:

Stereoscopic motion tracking in combination with list mode acquisition enables accurate correction of movement artifacts in PET: shown are snapshots of the motion tracker used at the PET center and tomographic images without (left column) and with (right column) correction of the list mode data prior to image reconstruction.

Forschungszentrum Rossendorf e.V.

Postfach 51 01 19 ; D-01314 Dresden
Bundesrepublik Deutschland
Telefon (0351) 260 2621
Telefax (0351) 260 3232
E-Mail j.van_den_hoff@fz-rossendorf.de

Wissenschaftlich-Technische Berichte
FZR-424
2005

Annual Report 2004

Institute of Bioinorganic and Radiopharmaceutical Chemistry

Editor: Prof. J. van den Hoff

Editorial staff: Dr. S. Seifert

Cover Picture:

Stereoscopic motion tracking in combination with list mode acquisition enables accurate correction of movement artifacts in PET: shown are snapshots of the motion tracker used at the PET center and tomographic images without (left column) and with (right column) correction of the list mode data prior to image reconstruction.

FOREWORD

In 2004 the Institute of Bioinorganic and Radiopharmaceutical Chemistry, one of six institutes in the Research Centre Rossendorf, continued to focus its basic and application-oriented research on the use of radiotracers as molecular *in vivo* probes, especially in the human body, on three main fields:

- radiotracers in tumour and metabolism research
- radiometal therapeutics
- PET in drug and food research

In the field of radiopharmaceutical chemistry, the Institute is predominantly engaged in research on PET nuclides as well as on radiometals.

In the latter field, our engagement in the coordination chemistry and radiopharmacology of technetium, rhenium and other metals has been further pursued. Here, chemical and radiopharmaceutical studies increasingly confront the radiotherapeutic aspect. This involves both the search for stable chelators for radiometals as well as attempts to optimize the *in vivo* behaviour of the molecule into which the chelate unit is integrated.

In the PET field, the improvement of labelling methods for carbon-11 and fluorine-18 continue to remain an area of considerable endeavour. The same is true for the task of increasing the range of PET-radiopharmaceuticals produced according to GMP regulations.

The Institute's chemically and radiopharmacologically oriented activities were complemented by more clinically oriented activities in the Positron Emission Tomography (PET) Centre Rossendorf, which closely links the Institute with the Department of Nuclear Medicine of the Medical Faculty of the University Dresden.

For these investigations, the lack of dedicated data processing tools has been identified as a potential bottleneck. Within the PET Centre, the Institute therefore is engaged in algorithm development for and implementation of such tools, notably in the area of accurate individual movement correction in PET investigations.

Generally, the activities in the PET Centre were further extended. In this context, the decision to install a dedicated 7 T micro-MRI apparatus to augment the imaging capabilities for small animal investigations should especially be mentioned. The machine was delivered in December 2004 and will be operational early in 2005.

The studies on bioactive substances in food, which may cause health risks or exert other, not yet identified effects on the body have been continued.

During the period under review, cooperations with external partners, particularly from the pharmaceutical industry, could be further extended.

After retirement of Dr. Spies, Prof. van den Hoff took over as Acting Director on April 1, 2004 until assumption of office by the successor of Prof. Johannsen, expected to take place in 2005.

The Institute would like to thank all partners from universities, industry and research institutes who supported its progress, as well as all members and guests of the Institute for their active contributions in 2004. The Institute wishes to acknowledge in particular the support and assistance received from the Executive Board of the Research Centre Rossendorf, from the competent authorities and funding agencies.

Prof. Dr. Jörg van den Hoff

Contents

I. RESEARCH REPORTS 1

RADIOTRACERS IN TUMOUR AND METABOLISM RESEARCH 3

Impact of Clinical Characteristics on the Pattern of the Regional Cerebral Glucose Metabolism in Patients with Major Depression 5
B. Beuthien-Baumann, G. Zündorf, S. Lüdecke, A. Triemer, K. Schierz, K. Herholz, V. A. Holthoff

Trigeminal Activation Measured with [^{15}O]H_2O-PET 6
B. Beuthien-Baumann, T. Hummel, L. Oehme, M. Heinke, J. Kotzerke, J. van den Hoff

4 h FDOPA Protocol for the Investigation of Parkinson's Disease with PET 7
P. Bühler, A. Strumpf, B. Beuthien-Baumann, R. Bergmann, J. Kotzerke, J. van den Hoff

FDG, OMFD and DOPA in the Diagnostic Work-up of Patients with Medullary Thyroid Carcinoma and Increasing Calcitonin Levels 9
B. Beuthien-Baumann, A. Strumpf, J. Zessin, J. Bredow, J. Kotzerke

User Guided Segmentation and Quantification of Three-Dimensional Structures in Oncological Whole Body PET - Continued 10
C. Pötzsch, J. van den Hoff

Development of an Algorithm for Respiratory Motion Correction in Gated PET Investigations of the Thorax 11
D. Möckel, U. Just, J. van den Hoff

Correction of Body Motion Artifacts in PET - Optimized 12
J. Langner, P. Bühler, E. Will, J. van den Hoff

Tomographic Image Reconstruction Software for the MicroPET P4 Scanner 13
H. Moelle, U. Just, P. Bühler, J. van den Hoff

Protein Oxidation in Human Disease: a Minireview 14
J. Pietzsch

Analysis of 6-Hydroxy-2-Aminocaproic Acid (HACA) as a Specific Marker of Protein Oxidation: the Use of *N(O,S)*-Ethoxycarbonyl Trifluoroethyl Ester Derivatives and Gas Chromatography/Mass Spectrometry 15
J. Pietzsch, R. Bergmann

Analysis of Non-Protein Amino Acids as Specific Markers of Low Density Lipo-protein Apolipoprotein B-100 Oxidation in Human Atherosclerotic Lesions 16
J. Pietzsch, R. Bergmann

Analysis of Specific Markers of Protein Oxidation in Rheumatoid Arthritis Plasma and Synovial Fluid LDL 17
J. Pietzsch, R. Bergmann, S. Kopprasch

Radiohalogenation of Lipoproteins: Limitations and Implications 18
J. Pietzsch, S. Hoppmann, J. van den Hoff

Fluorine-18 Radiolabelling of Low Density Lipoproteins (LDL): a Potential Approach for Characterization and Differentiation of Metabolism of Native and Oxidized LDL *in vivo* 20
J. Pietzsch, R. Bergmann, K. Rode, C. Hultsch, B. Pawelke, F. Wüst, J. van den Hoff

N-Arylation of Indoles with 4-[^{18}F]Fluoroiodobenzene: a Novel Radiolabelling Technique in ^{18}F Chemistry 21
F. Wüst, T. Kniess

N-Arylation of Indoles with 4-[^{18}F]Fluoroiodobenzene: Synthesis of ^{18}F-Labelled σ_2 Receptor Ligands 22
F. Wüst, H. Kasper

Determination of Radiochemical Purity of [^{18}F]3-OMFD and [^{18}F]FDOPA by HPLC 23
J. Zessin, B. Lipps

Synthesis of N-[6-(4-[^{18}F]Fluorobenzylidene)aminooxyhexyl]maleimide (MHAA). A New SH-Reactive ^{18}F-Labelling Agent 25
M. Berndt, F. Wüst

Modul-Assisted Synthesis of the Labelling Agent [^{18}F]SFB 26
P. Mäding, F. Füchtner, F. Wüst

Preparation of the Radiopharmaceutical [^{18}F]NaF for Medical Use 28
P. Mäding, F. Füchtner, J. Zessin, F. Wüst

Factors Affecting the Specific Activity of [^{18}F]Fluoride from a Water Target 30
F. Füchtner, S. Preusche, P. Mäding, J. Steinbach

Synthesis of a ^{11}C-Labelled Nonsteroidal Glucocorticoid Receptor Ligand for Imaging Brain Glucocorticoid Receptors (GR) 32
F. Wüst, T. Kniess, R. Bergmann

Synthesis of [^{11}C]CH_3I by Iodination of [^{11}C]CH_4 in a Synthesis Module 33
T. Kniess, F. Wüst

Synthesis of ^{11}C-Methylated Mercaptoimidazole Piperazinyl Derivatives as Potential Radioligands for Imaging 5-HT_{1A} Receptors by PET 34
T. Kniess, R. Garcia, A. Paulo, I. Santos, R. Bergmann, F. Wüst

A Novel Approach for ^{11}C-C Bond Formation: Hydrozirconation/^{11}C-Methylation of Prop-1-ynyl-benzene with [^{11}C]MeI 35
F. Wüst, P. Mäding

Metabolism of [^{11}C]SMe-ADAM in the Rat 36
B. Pawelke, R. Bergmann, J. Zessin

Animal PET Studies with [^{11}C]SMe-ADAM 37
R. Bergmann, J. Zessin

Evaluation of ^{18}F-Labelled Annexin V: Apoptosis Imaging in Mice 38
R. Bergmann, C. Hultsch, B. Pawelke, J. Pietzsch, S. Bergmann, S. Zijlstra, J. Gunawan, W. Burchert, J. van den Hoff

Molecular and Biochemical Characterisation of Neurotensin Receptor-1 (NTR-1) in Different Tumour Cell Lines 39
C. Haase, R. Bergmann

Prediction of Alternative Spliceforms of the Neurotensin Receptor-1 40
S. Heymann, R. Bergmann

Preparation of [^{86}Y]YCl_3 Solution for Labelling of Functionalised Biomolecules 41
S. Seifert, St. Preusche, J. Schlesinger, U. Schwarz, F. Wüst

Yttrium-86 Labelling of Neurotensin(8-13) Derivatives 42
J. Schlesinger, R. Bergmann, F. Wüst

Technetium and Rhenium Complexes with Modified Fatty Acid Ligands
7. Synthesis and Biological Evaluation of a New Type of Technetium-Labelled Fatty Acids for Myocardial Metabolism Imaging 43
M. Walther, C. M. Jung, R. Bergmann, J. Pietzsch, K. Rode, W. Kraus, H.-J. Pietzsch, H. Spies

Technetium and Rhenium Complexes with Modified Fatty Acid Ligands
8. Myocardial Extraction of a New Type of Technetium-Labelled Fatty Acids 44
M. Walther, C. M. Jung, S. Stehr, A. Heintz, G. Wunderlich, H.-J. Pietzsch, J. Kropp, A. Deussen, H. Spies

^{99m}Tc-Labelled RGD-Peptide Using the “4+1” Mixed-Ligand Chelate System 45
J.-U. Kuenstler, S. Seifert, R. Bergmann, H.-J. Pietzsch

Metabolic Stability and Biodistribution of Model Compounds Based on the ^{99m}Tc “4+1” Mixed-Ligand Chelate System 46
B. Pawelke, S. Seifert, R. Bergmann

Inhibition of Thymidine Phosphorylase as one Approach in Tumour Chemotherapy 47
M. Grote, St. Noll, B. Noll

Synthesis and ^{18}F-Labelling of Novel Acyclic Purine Nucleosides 48
B. Noll, St. Noll

Biodistribution of ^{18}F-Labelled Acyclic Guanosine and Thymine Derivatives 49
B. Noll, St. Noll, M. Grote, R. Bergmann

Biodistribution of ^{18}F-Labelled Acyclic *G*uanine and Uracile Derivatives 50
B. Noll, St. Noll, M. Grote, R. Bergmann

RADIOMETAL THERAPEUTICS 51

Hydrophilic Rhenium-188 Complexes for Attaching the Metal to Biomolecules 4. Synthesis and Characterisation of Hydroxymethyl Phosphine Containing '4+1' Complexes 53
E. Schiller, W. Kraus, H.-J. Pietzsch, H. Spies

Hydrophilic Rhenium-188 Complexes for Attaching the Metal to Biomolecules 5. Determination of *in Vitro* Stabilities 54
E. Schiller, S. Seifert, F. Tisato, F. Refosco, H.-J. Pietzsch

^{188}Re-EDTA – a Suitable Precursor for Preparing ^{188}Re(V) Complexes 55
S. Seifert

In Vitro Stability of ^{188}Re Complexes 56
S. Seifert, C. Jentschel

Novel and Efficient Preparation of Precursor $[^{188}Re(OH_2)_3(CO)_3]^+$ for the Labelling of Biomolecules 57
S. H. Park, S. Seifert, H.-J. Pietzsch

Biological Evaluation of ^{64}Cu-Labelled Tetrapropionitrile Derivatized Macrocyclic Ligands 58
P. McQuade, M. Wüst, M. Welch, F. Wüst

Formation of Stable Cu(II)-Complexes with Dendritic Oxybathophenanthroline Ligands 59
H. Stephan, G. Geipel, G. Bernhard, U. Hahn, F. Vögtle

Remarkable Enhancement of Cell Uptake for $[Ti_2W_{10}PO_{40}]^{7-}$ in the Presence of Chitosan 60
H. Stephan, R. Bergmann, K. Rode, A. Röllich, W. Kraus, K. Inoue, L. Jelínek, Z. Matějka

Colloid-Chemical Characterisation of Nanoparticles Formed by $[Ti_2W_{10}PO_{40}]^{7-}$ and Chitosan 61
W. Richter, H. Zänker, P. Krotká, Z. Matějka, A. Röllich, H. Stephan

Estimation of Partition Coefficient (log P) with Molecular Modelling of Rhenium and Technetium Complexes 62
K. Yoshizuka, H. -J. Pietzsch, H. Stephan

PET IN DRUG AND FOOD RESEARCH 63

Biodistribution and Catabolism of ^{18}F-Labelled Amadori Product Fructoselysine 65
C. Hultsch, M. Hellwig, R. Bergmann, B. Pawelke, T. Henle

Radiolabelled Flavonoids and Polyphenols
III. Synthesis of an ^{18}F-Labelled Resveratrol Derivative 67
S. Gester, J. Pietzsch, F. Wüst

CYCLOTRON OPERATION 69

Operation of the Rossendorf PET Cyclotron "CYCLONE 18/9" in 2004 71
St. Preusche, F. Wüst

Improved Version of the Rossendorf Solid Target System 73
St. Preusche, N. Dohn, H. Roß

Production of ^{86}Y and ^{56}Co at the Rossendorf PET Cyclotron "CYCLONE 18/9" 74
St. Preusche, F. Wüst, K.D. Schilling, N. Dohn, H. Roß

II. PUBLICATIONS, LECTURES, PATENTS AND AWARDS OF THE INSTITUTE AND THE PET-CENTRE ROSSENDORF 75

III. COLLABORATIONS, FUNDED PROJECTS AND FINANCIAL SUPPORT 89

IV. SEMINARS 99

V. PERSONNEL 103

I. RESEARCH REPORTS

RADIOTRACERS IN TUMOUR AND METABOLISM RESEARCH

Impact of Clinical Characteristics on the Pattern of the Regional Cerebral Glucose Metabolism in Patients with Major Depression

B. Beuthien-Baumann, G. Zündorf, S. Lüdecke, A. Triemer, K. Schierz, K. Herholz, V. A. Holthoff

Introduction

In the acute phase of Major Depression impairment of regional cerebral glucose metabolism is localized mainly in the frontal cortex [1]. The aim of this investigation was to assess the additional impact of clinical characteristics like age, gender, number of prior depressive episodes, severity and duration of the current depressive episode on the cerebral glucose pattern.

Patients and Methods

Patient group: 84 patients with Major Depression in acute phase, 64 female, 20 male; mean age 49.6±15.9 years; Hamilton Depression scale 21-items: 27.6±4.66 points.
Normal controls: 54 volunteers, 22 female, 32 males, mean age 51.7±13.7 years. The control group was derived from the European Database of the EU-project *"Network of Efficiency and Standardization of Dementia Diagnosis"* (NEST-DD).
FDG-PET: ECAT Exact HR+ (Siemens/CTI), 300 MBq [^{18}F]FDG, measured attenuation correction, acquisition 40-60 min post injection.
Data analysis: SPM99 (Statistical Parametric Mapping) [2], ANOVA, covariate: age at the time point of PET measurement. We retained as significant those clusters with a corrected $p<0.05$.

Results and Discussion

Comparing the group of patients in acute phase of Major Depression with the control group shows the impairment of regional cerebral glucose metabolism in the dorsolateral prefrontal cortex -more pronounced on the left side-(Brodmann area (BA) 9, BA 44-47; $p<0.0001$), impairment bilaterally in the orbitofrontal cortex (BA 10; $p< 0.0001$) and bilaterally in the superior temporal cortex (BA 41; $p<0.0001$) (Fig. 1).
Focussing on the clinical characteristic "age" one can observe a correlation between the increasing age at onset of the depressive episode and the degree of reduction of the dorsolateral prefrontal cortex ($p<0.001$) (Fig. 2), a pattern that does not correspond to the reductions due to age seen in a normal population [3].
No influence on the cerebral glucose pattern was seen from the other clinical characteristics: gender, number of prior depressive episodes, severity and duration of the current depressive episode.

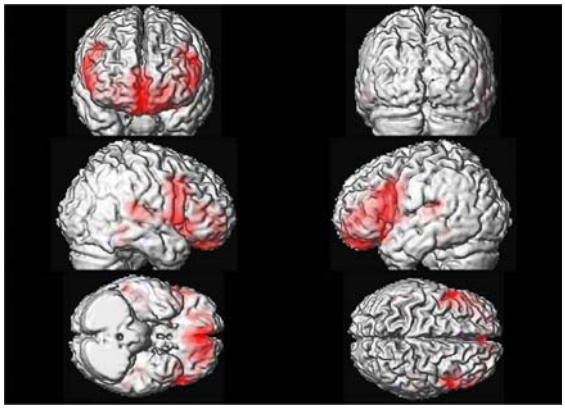

Fig.1. Brain areas marked in red indicate a reduction of brain glucose metabolism in patients with depression compared to the control group.

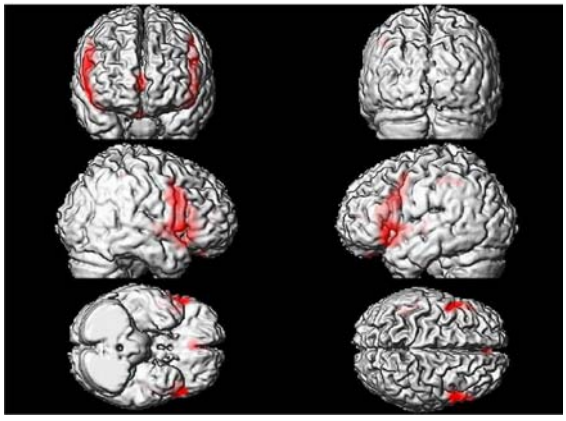

Fig. 2. Influence of age (marked in red) on the cerebral glucose pattern in patients with depression.

One substantial factor influencing the cerebral glucose pattern of patients with Major Depression in the acute phase seems to be the age of the patients, indicated by the regional reduction of metabolism in the dorsolateral prefrontal cortex, which is part of the pattern distinguishing patients and controls. It can be therefore hypothesized that the age is a risk factor for the development of Major Depression.

References

[1] Beuthien-Baumann, B. *et al.*, Acta Psychiatr. Scand. 110 (2004) 184-194.
[2] Friston, K., Hum. Brain Mapping 1 (1994) 214-220.
[3] Herholz, K. *et al.*, Neuroimage 17 (2002) 302-318.

Trigeminal Activation Measured with [^{15}O]H_2O-PET

B. Beuthien-Baumann, T. Hummel, L. Oehme, M. Heinke, J. Kotzerke, J. van den Hoff

Introduction

During their life time more than 5 % of the population will loose their sense of smell, mediated through the olfactory nerve, due to trauma or disease. In these patients the trigeminal nerve represents the only intranasal chemosensory modality. Up to date, most investigations studying olfactory processing apply mixed olfactory-trigeminal stimuli. The aim of this study was to investigate the cerebral processing of discrete trigeminal nerve activation in normal controls without olfactory impairment with [^{15}O]H_2O-PET.

Methods

Normal control group: 15 males (age 30-58 years, mean age 36 years) without neurological and internal diseases and without impairment of the olfactory senses.
Trigeminal activation: Application of short CO_2 pulses via intransal tube into the left nasal cavity (pulse length 1 s, interval between pulses 3 s) starting 20 s before injection of 1.7 GBq [^{15}O}H_2O.
PET: ECAT Exact HR+ (Siemens/CTI), dynamic acquisition over 5 min. Total of 4 PET scans per person, alternating activation and non-activation studies. Iterative reconstruction of the acquired data with measured attenuation correction. Parametric flow maps were calculated, applying a standard input function. These parametric flow maps were taken for the comparison of activation and non-activation studies. The analysis was performed with the software package SPM99 [1]. The study protocol was approved by the local ethics committee and the Federal Agency of Radiation Protection.

Results and Discussion

In 12 persons investigated, a total of 2 activation studies and 2 non-activation studies were successfully acquired. In the other 3 persons, due to technical problems, at least one pair of activation and non-activation was acquired. The first result of the ongoing data analysis of all studies performed shows a bilateral activation of the projection area of the trigeminal nerve, located in the lower part of the postcentral gyrus. This activation is more pronounced in the right hemisphere than in the left hemisphere (Fig. 1).

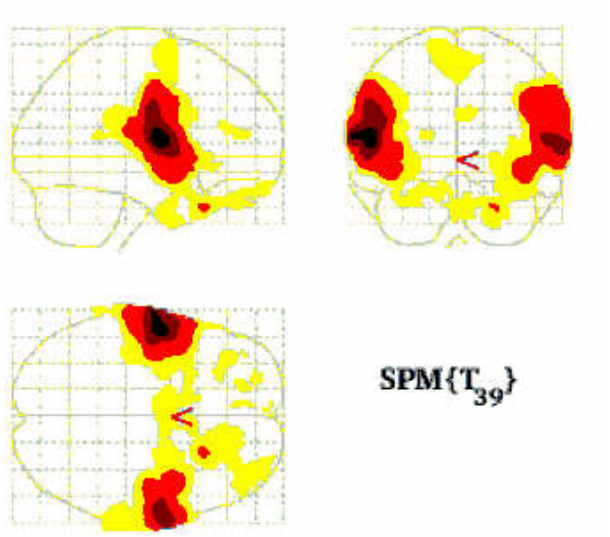

Fig. 1. SPM analysis, comparing activation versus non-activation of all subjects investigated. There is a clear bilateral activation in the projection field of the trigeminal nerve of both hemispheres with accentuation on the right side, contralateral to the activation side.

The evaluation of the stability of the intraindividual activation is one subject of the ongoing data analysis.

References

[1] Friston, K., Hum. Brain Mapping 1 (1994) 214-220.

4 h FDOPA Protocol for the Investigation of Parkinson's Disease with PET

P. Bühler, A. Strumpf, B. Beuthien-Baumann, R. Bergmann, J. Kotzerke, J. van den Hoff

Introduction

Positron Emission Tomography with the radiotracer [^{18}F]-fluorodopa (FDOPA) can be used to investigate deficiencies of the dopaminergic system in the brain. It is therefore a powerful tool in diagnosing Parkinson's disease (PD) and to differentiate it from other movement disorders. FDOPA is intravenously administered. After transport through the blood-brain-barrier it is metabolized into [^{18}F]-fluorodopamine (FDA), which is then trapped in the presynaptic vesicles in the striatum. Parts of the FDOPA and also FDA are metabolized to other products which are capable of leaving the brain. The uptake of FDA into the striatum, which can be quantified with PET, is used as a discriminator for PD. A reduced uptake is indicative for PD. At the PET centre of the FZR, the uptake is normally quantified by $k_{occ} = k_2k_3/(k_2+k_3)$ (see Fig. 1) which is determined using the data of the first 60 minutes post-injection of a dynamic PET scan and a reference tissue model. During this period FDOPA behaves practically like a irreversibly bound tracer ($k_{loss} = 0$).

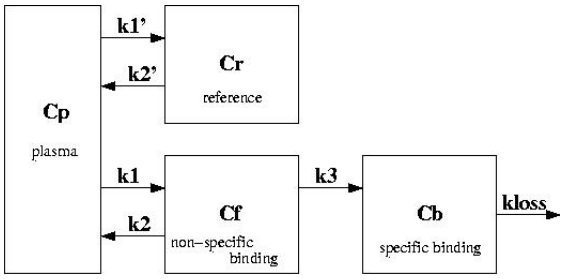

Fig. 1. Compartment model used to analyse FDOPA-PET data. In PD k_3 is supposed to be reduced and k_{loss}, to be enhanced. C: activity concentration, k: coupling constant.

This is no longer the case at later times, at which the effects of $k_{loss} \neq 0$ become important. As was demonstrated by Sossi *et al.* [1], data taken at later times can be used to measure the dopamine turnover k_{occ}/k_{loss} which they argue is the better discriminator for PD than k_{occ}. To determine the dopamine turnover they introduced a dynamic PET protocol with a total duration of 4 hours. With some assumptions the system of equations describing the compartment model can be reduced to the linear relation

$$\frac{\int_0^t Cb(t')\cdot dt'}{Cb(t)} = \text{const.} + \frac{k_{occ}}{k_{loss}} \cdot \frac{\int_0^t Cr(t')\cdot dt'}{Cb(t)}$$

and k_{occ}/k_{loss} is determined with a linear fit. Here we report on the recent implementation of a similar protocol at the PET centre of the FZR and first results of a trial study with 10 patients.

Method

The protocol comprises 3 dynamic PET scans of 90 and 2×40 minutes which are acquired within 4 hours. The data are acquired in 3D list mode. Prior to each emission scan a transmission scan is acquired and blood samples are taken in regular intervals throughout the entire investigation. Between the scans the patient is allowed to stand up and walk around. In order to allow an accurate coregistration of the 3 scans, the position of the patient head is continuously monitored with an infrared tracking system. This information is not only used for coregistration but can also be used for movement correction [2]. After sorting and reconstruction of the acquired list mode data, circular regions of interest (ROIs) are selected in the striatum (represent C_f+C_b) and the occipital cortex (represents $C_{r)}$ which are used to compute the time course of the activity concentrations.

Results and Discussion

So far we have carried out the procedure with 10 patients. The values obtained for k_{occ}/k_{loss} are comparable with the values published by Sossi *et al.* [1] as shown in the upper panel of Fig. 2. Each of the open diamonds represents a patient. The values for the dopamine uptake and turnover are highly correlated as is shown in the lower panel of Fig. 2, which suggests that both quantities are similarly good in differentiating PD. However, in order to judge the methods a discriminating analysis must be carried out with sufficiently large groups of PD and non-PD patients. Such a study will be started next year.

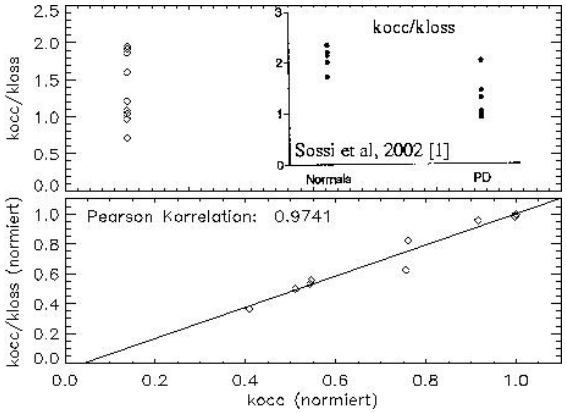

Fig. 2. Comparison of k_{occ}/k_{loss} values from study patients (open diamonds) with results published by Sossi *et al.*, 2002 [1] (inset) and correlation between k_{occ} and k_{occ}/k_{loss}.

References

[1] Sossi, V. *et al.*, J. Cereb. Blood Flow Metab. 22 (2002) 232.

[2] Bühler, P. *et al.*, IEEE Trans. Med. Imag. 23 (2004) 1176.

FDG, OMFD and DOPA in the Diagnostic Work-up of Patients with Medullary Thyroid Carcinoma and Increasing Calcitonin Levels

B. Beuthien-Baumann, A. Strumpf, J. Zessin, J. Bredow, J. Kotzerke

Introduction

In patients with medullary thyroid carcinoma (MTC) the only chance of cure is through surgery. Therefore the detection of local recurrence or metastases is mandatory for a curative intent, otherwise the diagnostic aim is the identification of malignant sites which can cause local problems like, i.e., bone metastases causing fractures or local recurrences invading vital structures of the neck. Comparing different nuclear medicine procedures in the diagnostic of MTC, FDG-PET shows a moderate detection rate [1]. Since MTC exhibits histologically neuroendocrine features it was described that [^{18}F]DOPA can identify metastases or local recurrence in patient with MTC [2]. [^{18}F]OMFD is a metabolite of DOPA which behaves in vivo like an amino acid and is used in the diagnostic of malignant brain tumours. In previous investigations it was found, that OMFD has only little accumulation in the muscles and is excreted via the urinary tract [3]. It was hypothesized, that MTC could be visualized by this amino acid tracer.

Patients and Methods

Patient group: 14 patients with MTC and increased calcitonin levels (range 48–4233 pg/ml) were investigated with FDG-PET (370 MBq FDG i.v., acquisition 60 min post injection). 10 out of these 14 patients were investigated with OMFD (300 MBq i.v., acquisition from 15 min p.i.). 12 out of these 14 patients were scanned with DOPA (premedication with 100 mg carbidopa 60 min pre-injection of 300 MBq DOPA, acquisition from 60 min p.i.).
PET: ECAT Exact HR+ (Siemens/CTI), iterative reconstruction with measured attenuation correction.

Results and Discussion

In 5 patients FDG revealed small focal increased areas (about 1 cm in diameter) in the neck, thorax or upper abdomen, highly suspicious for metastases and local recurrence respectively. 1 patient showed focal uptake at the left hip joint. 4 patients showed focal uptake with DOPA, in some areas corresponding to the FDG uptake in neck and thorax. In three of these patients uptake sites with DOPA were more numerous and some correlate findings were detected with ultrasound (neck) and CT (thorax). In 2 patients with DOPA uptake FDG-PET, CT or ultrasound was negative. With OMFD uptake was seen in 2 patients (1 x dorsal of the urinary bladder, 1 x in the liver) without correlate with FDG, DOPA or conventional diagnostic.
With FDG and DOPA focal increase uptake was noted in a total of 8/14 patients, highly suspicious for metastatic spread or local recurrence, although no histological verification was performed up to now. Therefore it can be concluded that there is a chance to detect MTC via increased glucose metabolism and increased neuroendocrine uptake of DOPA, but not via increased amino acid transport with OMFD.

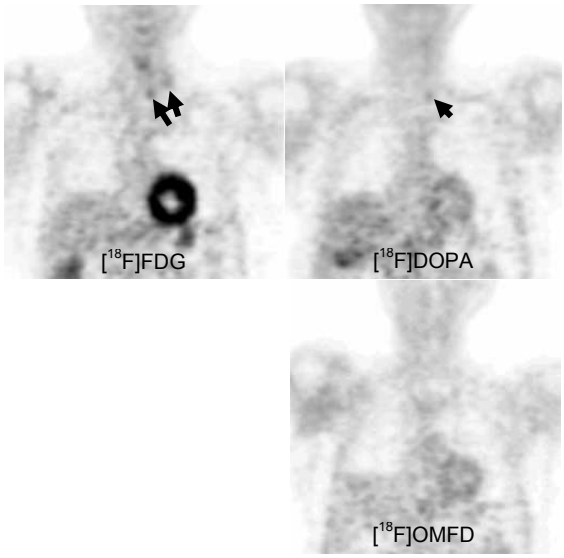

Fig. 1. 63-year old patient, initial stage pT4N1Mo, increased calcitonin level of 2151 pg/ml at time of PET. Focal increased uptake in the neck with FDG (2 spots) and DOPA (1 spot), no uptake with OMFD.

Correlate with ultrasound: Calcified structure in the left ventral cervical region.

References

[1] Diehl, M. *et al.,* Eur. J. Nucl. Med. 28 (2001) 1671-1676.
[2] Hoegerle, S. *et al.,* Eur. J. Nucl. Med. 28 (2001) 64-71.
[3] Beuthien-Baumann, B. *et al.,* Eur. J. Nucl. Med. Mol. Imaging 30 (2003) 11004-11008.

User Guided Segmentation and Quantification of Three-Dimensional Structures in Oncological Whole Body PET - Continued

C. Pötzsch, J. van den Hoff

Introduction

Oncological positron emission tomography (PET) studies typically contain several hundred tomographic images, which have to be analysed to derive informations such as the degree of metastatic spread of a tumour disease.
To fully exhaust the quantitative information provided by PET with respect to tracer accumulation and volume of target structures it is necessary to provide means for analysing these large data sets with manageable user interaction. Available programs, both, commercially as well as in the public domain do not offer the necessary functionality because quantitative evaluation is generally limited to processing of individual tomographic images. Therefore, it was the aim of this work to develop and implement volume oriented methods for quantification and provide a dedicated tool for the described situation. In the last report we described the basic functionality of the application. Here we will discuss the developments of this year and further aims.

Results and Discussion

One of the aims in the last report was the routine usability of the application for oncological studies performed in the PET center. To archive this, additional functionality was implemented and verified. In addition to the previously available orthogonal viewer mode two new views of the tomographic volumes are integrated. The first, is an overview of all slices in a specific angle (e.g. transaxial, coronal, sagittal), see Fig. 1. The user has the possibility to decide how many slices are displayed. The key functionality of defining masks and the threshold based search of VOI's is kept in this view.

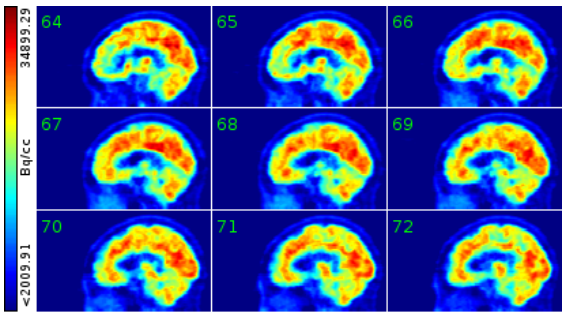

Fig. 1. Multiple planes view of a human brain

The second new view is a so-called maximum intensity view (MIPS) (see Fig. 2). Within this view two modes are possible. The first mode is the standard MIPS view where the whole volume is rotated over a user definable range of angles and the maximum projection computed for all angles and displayed afterwards. So the user has the impression of a rotating object where in all angle positions the hottest parts remain visible. In the second method a gaussian weight can be used to modify the projection, enhancing interior structures.

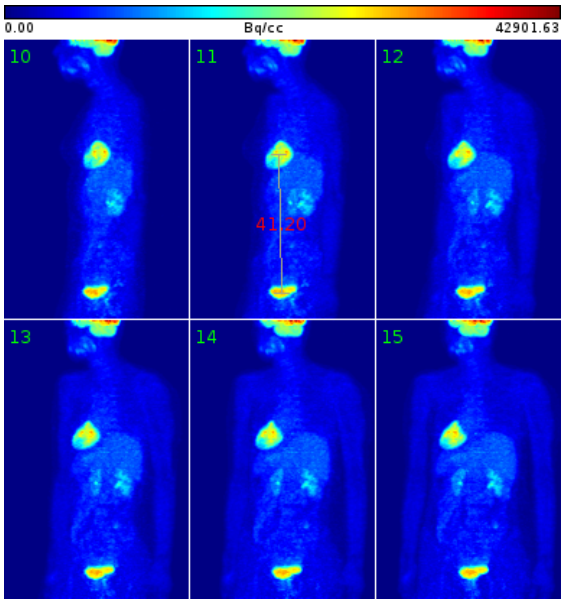

Fig. 2. Maximum Intensity Projection of an oncological study

A new image export with various setup parameters (e.g. a colorbar) is available for all three views. For distance and size determinations a ruler mode was implemented (see Fig. 2). To physically archive the results of the application a new print functionality is implemented where the user has the ability to define a header/footer to meet the in house design and layout standards.
Future developments will aim to improve the threshold based segmentation of the tomographic data. For follow up studies coregistration methods will be developed in cooperation with ABX (Advanced Biochemical Compounds, Radeberg). These coregistered volumes can be used to compare VOIs at different times to assess treatment success or failure.

Development of an Algorithm for Respiratory Motion Correction in Gated PET Investigations of the Thorax

D. Möckel, U. Just, J. van den Hoff

Introduction

Respiratory motion has a negative influence on the image quality of PET investigations of the human thorax. In the PET Centre Rossendorf a method was developed to register the respiratory motion and correlate the dataset with the PET data [1]. It is possible to create gated images of defined respiratory phases, thus reducing the effects of respiratory motion. However this method has a disadvantage. The statistics in respiratory motion gated images is decreased and the noise is increased, which results in a more difficult detection of structures with low activity concentration.
An algorithm was developed correcting the respiratory motion on the one hand and using the whole statistics on the other hand.

Methods

The developed algorithm transforms each of the single volume images of a respiratory motion gated study to a selected target image out of the gated sequence. The corrected image is finally created by averaging the image sequence. The transformation value for each voxel of the volume matrix is calculated by using a transformation function. The transformation function is modelled in consideration of the anatomy and physiology of the respiratory system. Only motions in craniocaudal direction are corrected because the main part of the respiratory motion proceeds in this direction. The transformation function depends on the craniocaudal position since motion amplitude changes dependent on it. Further, the transformation function can be dependent on lateral and ventrodorsal position to address additional anatomical dependencies.
The calculation of the transformation function requires input parameters such as the position of diaphragm and other moving structures. A graphical user interface was developed for the input of the transformation parameters.
The method was evaluated on eleven respiratory motion gated patient studies of the thorax. In these studies seven hearts and eight tumours were investigated.

Results

The measured tumour volumes in the corrected images are similar to those derived from the gated images for motion amplitudes greater than 0.5 cm (Fig. 1). For three tumour lesions with an amplitude of >0.9 cm the measured volume after correction was 6 %, 4 % and 12 % greater than the averaged volume of the gated images, in contrast to 19 %, 26 % and 21 % in images created without gating.
For low motion amplitudes (<0.5 cm) there was no difference between the measured tumour volumes in the corrected and uncorrected images. However in cases of small motion amplitudes the imaged tumour volume is little influenced and a respiratory motion correction is less needed.
With the developed correction method small tumours with high motion amplitude and low activity concentration may be detected that are not visible in non gated studies because of the respiratory motion and in the single gated images because of the high noise.
Images of the heart could be improved by the respiratory motion correction (Fig. 1). Especially for combined respiratory and heart gated investigations the use of the developed method is advantageous. Thus it is possible to study the heart cycle with the influence of respiration largely reduced and without the loss of statistics in single respiratory motion gated images.

References

[1] Just U. *et al.*, *Annual Report 2003*, FZR-394, p. 13.

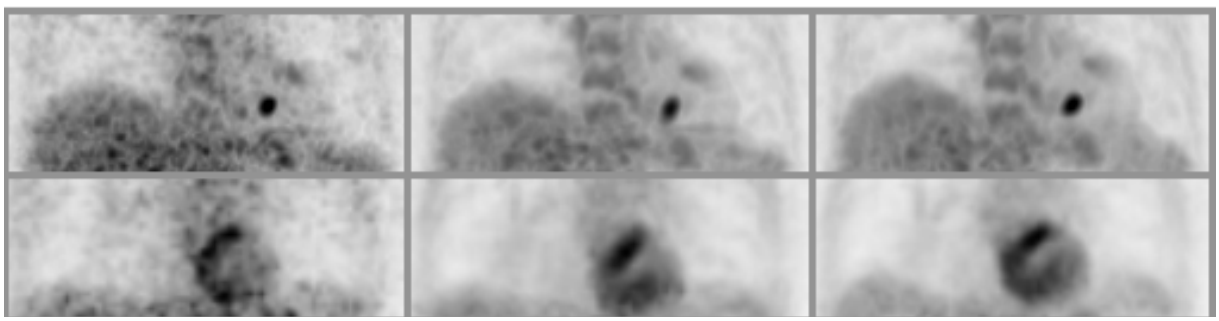

Fig. 1. Coronal slices of two FDG-PET studies of the thorax showing a tumour (top) and a heart (bottom). The displayed images of each row illustrate (from left to right)one single respiratory phase, the non gated study and the corrected image, respectively.

Correction of Body Motion Artifacts in PET - Optimized

J. Langner, P. Bühler, E. Will, J. van den Hoff

Introduction

Patient motion during PET investigations is unavoidable and can result in a noticeable loss of resolution and/or introduce artifacts in the final PET image. In a previous report [1] we presented that an event (list mode) based movement correction method, which is capable of minimizing such influences, results in an improved image quality. However, the application of the method showed that the processing times are large which hinders its introduction in routine operation. Therefore our recent work concentrated on developing methods to optimize the correction algorithm by making use of modern multiprocessor systems. Here we report on the progress and implementation and demonstrate how these methods allow to integrate list mode based movement corrections in routine operation by reducing the processing time considerable.

Method

The correction algorithm, which spatially reorientates each registered line of response (LOR) depending on movement information supplied by an external motion tracking system, underwent a parallelism analysis. In several steps the data dependencies of the algorithm were identified and independent areas encapsulated into separate threads. This also includes the time consuming "Out-of-FOV" corrections as well as the final sorting and binning into a sinogram file. These threads are then automatically distributed among the available processors during the correction. In addition, to support the idea of a routine use of motion correction procedures during neurological PET acquisitions, an implemen-tation of a graphical user interface was also part of the development. During the research on the user interface we decided to use the "Qt" development framework [2] that allows to keep applications portable over several platforms, aiming at a GUI usable by the technicians performing the PET acquisitions. Furthermore, this application also has the possibility to directly acquire the motion data from the *ARTtrack1* tracking system with which the head motion is measured.

Results and Discussion

The speed improvement and the accuracy of the optimized correction algorithm was validated with several test setups and measurements. Here we show results of a comparison between the sequential and the parallel implementation of the algorithm. For a selected study (21 frames) the sequential version required ~21 h for correcting list mode data based on an 1 h PET study while the parallel implementation only required ~1.5 h thanks to its multithreaded design.

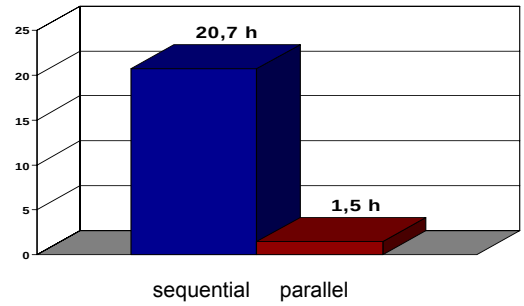

Fig. 1. Speed measurement where list mode data based on an one hour PET acquisition was first corrected by the sequential implementation and afterwards by the parallel version of the correction algorithm, showing a considerable speed up of the computations.

The capabilities of the method are demonstrated in Fig. 2. The data show a phantom study, in which the phantom was first kept at rest and during the second half of the acquisition was moved in axial direction. Comparison of images from the first and second half of the study prove, that the movement correction notably reduces the movement artifacts.

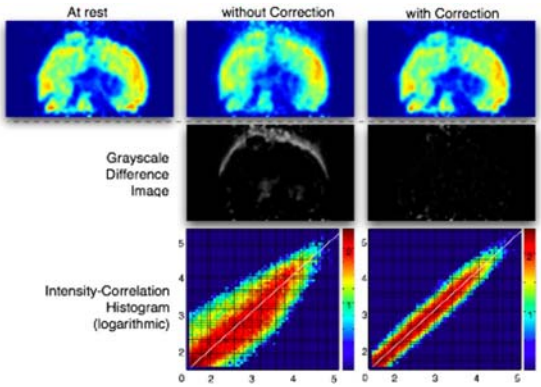

Fig. 2. Results of a test measurement with movement in axial direction (z). Sagittal views at the top row show reconstructed images in different positions (at rest, w/o, and w/ correction, respectively).

Our future work will focus on validation of these methods for the application in routine operation. In addition, further optimizations should eliminate still existing problems and also probably allow to correct motion artifacts in real time.

References

[1] Bühler, P. *et al.*, *Annual Report 2002*, FZR-363, p. 29.
[2] Trolltech, AS. Qt: A multiplatform, C++ application development framework, http://www.trolltech.com.

Tomographic Image Reconstruction Software for the MicroPET P4 Scanner

H. Moelle, U. Just, P. Bühler, J. van den Hoff

A program to reconstruct tomographic images from the data delivered by our microPET scanner (CTI Concorde Microsystems) has been developed. It allows an easy and fast image reconstruction in batch mode and supports the evaluation of the reconstruction parameters. The possibility to systematically assess reconstruction properties offers new opportunities to improve the image quality.

Introduction

The PET Center Rossendorf is equipped with a microPET P4 scanner (CTI Concorde Microsystems, LLC, Knoxville, TE., USA). The reconstruction software provided with the scanner has various limitations which hamper the efficient processing of the data. It is available only for MS-Windows and provides no opportunity for batch processing. So user interaction is needed for every single reconstruction. Furthermore, only one instance of the software is allowed on a system. This limits the usage to one person. The software works unstable if data is not located on a local drive, which makes copying of huge files over the network necessary. The reconstruction of a normal study with 35 frames takes about 12 hours with the OSEM / MAP method provided with the software. Iterative reconstruction procedures in PET require specification of various reconstruction parameters upon which the number of iterations is crucial for the quality of the reconstructed image. Optimization of the reconstruction parameters is a heavily time consuming procedure with the standard software. The goal of this work was to develop a simple to use tool for reconstruction of microPET data and to facilitate optimization of the reconstruction parameters.

Methods

Two reconstruction methods of the open source reconstruction software STIR [1] have been implemented (OSMAPOSL, FBP2D). The reconstruction process is controlled by a set of parameters which can be set either in the graphical user interface (GUI) written with Qt or on the command line. For evaluation of the optimum number of iterations an iteration sequence method has been implemented. It produces a volume file which consists of one frame for each iteration step applied to a selected frame of a study. The calibration factor to calculate the absolute activity can be added or can be selected from a list of stored values. All reconstructions are executed in a batch mode which makes human interaction unnecessary after having started the process. The frames of a study are distributed to the processors available on the system during the reconstruction. This speeds up the reconstruction. The progress of the reconstruction of a whole study and its frames is visible to the user in the GUI and on the command line. The reconstructed images are stored in ECAT7 volume format to allow use of existing postprocessing software.

Results

Identification of the best set of reconstruction parameters for a specific study is possible in a justifiable amount of time. Multiple instances of the software are possible and the data is not limited to a local drive. The software is available for SUN OS and Linux.

References

[1] Thielemans, K., STIR: **http://stir.irsl.org**, 2004.

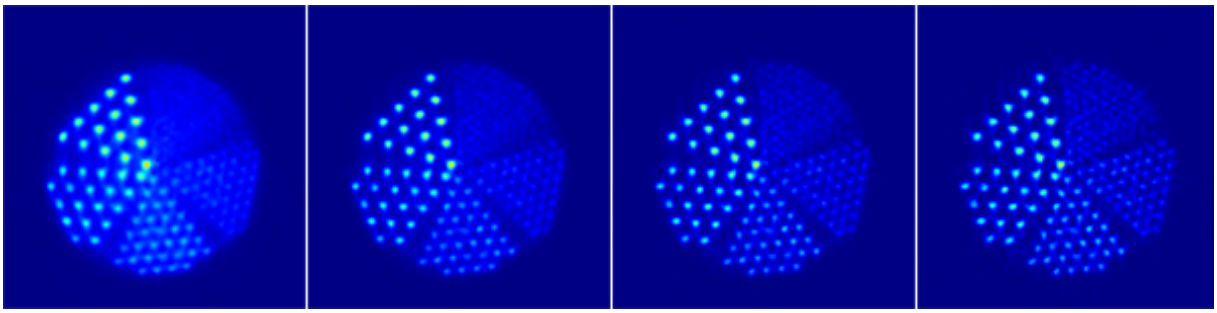

Fig. 1. [^{18}F]FDG microPET images of a line phantom: all images are produced with OSMAPOSL method (7 subsets, all segments, no filter) but different number of iterations, left most slice image is the result after two iterations. Next image is produced after four iterations, the next after eight iterations and the last after 16 iterations. The contrast increases with the number of iterations.

Protein Oxidation in Human Disease: a Minireview

J. Pietzsch

Oxidative modification of enzymes and structural proteins plays an essential role in the etiology, manifestation, and progression of an important number of human diseases. During the past two decades, considerable evidence has implicated oxidative stress, e.g., in rheumatoid arthritis, sepsis, atherosclerosis, diabetes mellitus, chronic renal failure, Alzheimer's disease, and amyotrophic lateral sclerosis, as well as in ageing. Recent advances in our understanding of oxidative stress have included: identification by mass spectrometry of the chemical nature of specific oxidative modifications in various proteins; identification of oxidized proteins in several disease-related tissue compartments; establishing the role of specific receptors that recognize oxidized proteins; and characterization of redox signaling pathways and of transcription factors that respond to oxidative stress. In this line, the minireview summarizes recent results of the Pathological Biochemistry Group providing further evidence that oxidative modification of human low density lipoproteins (LDL) plays a pivotal role in the pathogenesis of atherosclerosis. Better understanding of mechanisms generating oxidized LDL (oxLDL) and their metabolic consequences should help the development of new strategies for the prevention of cardiovascular diseases.

Atherosclerosis and chronic vascular diseases remain a major health problem in industrialized countries. Recent evidence suggests that oxidized LDL (oxLDL) play an important role in atherogenesis [1]. However, whether oxLDL is an initiator or accelerator of disease and what is the diagnostic significance of circulating oxLDL in human blood, is subject of debate and intensive study. The atherogenicity of LDL is increased by oxidative modification of both its protein and lipid moiety, occurring within the vascular wall and other inflammatory sites. Many pathways are known to oxidize LDL, at least *in vitro* [2, 3]. These include the myeloperoxidase pathway, the reactive nitrogen pathway, and the glycoxidation pathway, which generate various potent oxidants, e.g., the hydroxyl radical ($^{\bullet}OH$), the superoxide radical anion ($O_2^{\bullet-}$), hypochlorite (OCl^-), and peroxynitrite ($ONOO^-$) [1]. However, the specific pathways that are responsible in the atherogenic process have not been conclusively identified. Modification of apolipoprotein (apo) B-100, the major structural protein of LDL, can occur directly by these oxidants, or indirectly by covalent binding of lipid hydroperoxide breakdown products, such as 4-hydroxy-nonenal. Additionally, there is evidence supporting the hypothesis that among important mechanisms of apoB-100 oxidation are also metal-catalyzed processes. These processes involve binding of either free or, physiologically more relevant, complexed (porphyrin-bound) redox-active ferric iron to discrete binding sites of LDL and apoB-100, respectively, thus forming centers for redox cycling and repeated radical production [3]. For apoB-100 these modifications finally result in the formation of new epitopes. The latter are specifically recognized by scavenger receptors, followed by an excessive uptake and accumulation of oxLDL in macrophages, vascular smooth muscle cells, and endothelial cells in an unregulated fashion that can lead to foam cell formation [4]. The presence of foam cells in the vascular wall is considered to be the first morphological substrate of atherosclerosis. In contrast, native LDL (nLDL) will not promote the formation of foam cells under most circumstances, as uptake of nLDL by the LDL receptor pathway results in down-regulation of endogenous cholesterol synthesis and LDL receptor expression. Very recently, direct oxidation of apoB-100 has been measured in LDL recovered from human aortic vascular lesions [5]. Moreover, direct oxidation of apoB-100 has been measured in circulating LDL *in vivo* in conditions, which are accompanied by accelerated atherosclerosis including rheumatoid arthritis, impaired glucose tolerance, and overt diabetes mellitus [6, 7]. The role of these circulating oxLDL in disease is poorly understood. One reason for this is the lack of suitable sensitive and specific radiolabeling methods, which would allow direct assessment of metabolism of oxLDL *in vivo*. Thus, the development of novel methodologies for radiolabelling of both nLDL and oxLDL with ^{18}F and the use of small animal PET to investigate the metabolism of several species of oxLDL *in vivo* is currently in progress [9].

The author wishes to thank Mareike Barth, Uta Lenkeit, and Susan Hoppmann for their expert technical assistance.

References

[1] Itabe, H., Biol Pharm Bull 26 (2003) 1-9.
[2] Pietzsch, J. *et al.,* Rapid Commun. Mass Spectrom. 17 (2003) 767-770.
[3] Pietzsch, J. and Bergmann, R., Amino Acids 26 (2004) 45-51.
[4] Kopprasch, S. *et al.,* Int. J. Biochem. Cell Biol. 36 (2004) 460-471.
[5] Pietzsch, J. *et al.,* Spectroscopy 18 (2004) 177-183.
[6] Pietzsch, J. *et al.,* Atherosclerosis 5 (2004) 16. (Abstract)
[7] Julius, U. and Pietzsch, J., Antiox. Redox Signal (2005) *in press*.
[8] Pietzsch, J., Nucl. Med. Biol. 31 (2005) 1043-1050.

Analysis of 6-Hydroxy-2-Aminocaproic Acid (HACA) as a Specific Marker of Protein Oxidation: the Use of *N(O,S)*-Ethoxycarbonyl Trifluoroethyl Ester Derivatives and Gas Chromatography/Mass Spectrometry

J. Pietzsch, R. Bergmann

α-Aminoadipyl semialdehyde (αASA) is supposed to be a primary product of transition metal catalyzed oxidation of protein lysine side chain residues [1]. αASA may arise via initial hydrogen abstraction at carbon six and formation of a reactive lysyl radical. The latter is a target for hydroxylation and subsequent loss of the ε-amino group. By reduction with sodium borohydride, αASA forms the non-protein amino acid 6-hydroxy-2-aminocaproic acid (HACA). For other proteins than apolipoproteins (apo), the formation of HACA has been measured i*n vitro* and *in vivo* [1]. In this respect, the value of HACA as a specific marker of metal catalyzed oxidation of apoB-100 has not been established. The mature apoB-100 (M_r 516,000; without carbohydrate content) consists of a single polypeptide chain of 4536 amino acids, and there is only one copy of the protein on each LDL particle. ApoB-100 contains 357 lysine residues that are supposed to be partially susceptible to direct oxidative damage. The objective of this report is the investigation of the feasibility of the use of *N(O,S)*-ethoxycarbonyl trifluoroethyl ester (ECEE-F_3) derivatives and gas chromatography/mass spectrometry (GC/MS) to quantify low-abundance αASA residues in isolated LDL apoB-100. Isolation, delipidation of human LDL, and enzymatic hydrolysis of apoB-100 were performed as previously described [2]. The free amino acids were isolated from protein hydrolysates, derivatized to their ECEE-F_3 derivatives, and analyzed by electron-impact ionization stable isotope dilution GC-MS as described elsewhere [2].

Results and Discussion

Initial studies of the ECEE-F_3 derivatives of protein amino acids by GC/MS showed them to be well separated under the conditions employed, with retention times being very reproducible [2-4]. The derivative studied yielded diagnostically useful fragment ions for use in HACA determination (Fig. 1). The limit of determination of HACA was 1 nmol/L (1 fmol/injection). The physiological level of HACA found in native circulating LDL obtained from normolipidemic, young male volunteers was 7.1 ± 10^{-4} mol/mol apoB-100 (0.02/10,000 lysine residues).

Furthermore, the data show that lysine side chain residues of apoB-100 are highly sensitive to form αASA and HACA, respectively, if LDL is exposed to low concentrations of iron or copper as pro-oxidants by using established oxidation systems *in vitro*. As an example, Fig. 2 shows the formation of HACA in human LDL particles exposed to various oxidation systems *in vitro*.

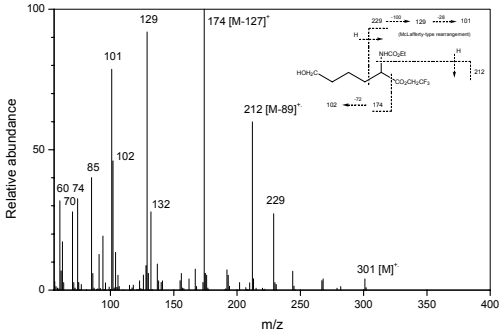

Fig. 1. EI ionization (70 eV) mass spectra of the ECEE-F_3 derivatives of HACA (Mr 301). Spectra show the prominent $[M-89]^{+\bullet}$ and $[M-127]^+$ ions, due to the losses of NH_2CO_2Et and $^{\bullet}CO_2CH_2CF_3$, respectively, from the ionized molecules. GC/MS conditions have been described elsewhere [2].

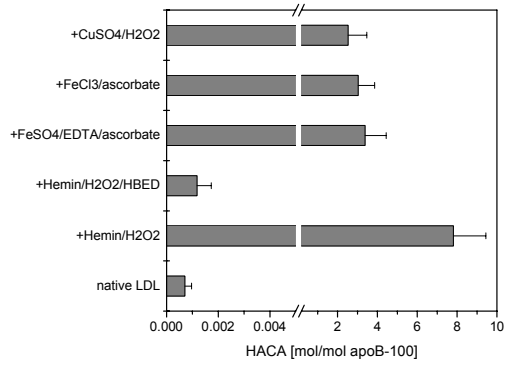

Fig. 2. Formation of HACA in human LDL particles exposed to various oxidation systems *in vitro* (n = 3) [2].

The approach is currently being applied to studies dealing with mechanisms of protein oxidation *in vitro* and *in vivo*.

References

[1] Requena, J. R. *et al.*, Proc. Natl. Acad. Sci. USA 98 (2001) 69-74.
[2] Pietzsch, J. e*t al.,* Amino Acids 26 (2004) 45-51.
[3] Pietzsch, J. *et al.,* Rapid Commun. Mass Spectrom. 11 (1997) 1835-1138.
[4] Pietzsch, J. *et al.,* Rapid Commun. Mass Spectrom. 17 (2003) 767-770.

Analysis of Non-Protein Amino Acids as Specific Markers of Low Density Lipoprotein Apolipoprotein B-100 Oxidation in Human Atherosclerotic Lesions

J. Pietzsch, R. Bergmann

There is effectual evidence supporting the hypothesis that among important mechanisms of apoB-100 oxidation are metal catalyzed processes. Two highly specific products of metal catalyzed protein oxidation are γ-glutamyl semialdehyde (γGSA) and α-aminoadipyl semialdehyde (αASA). γGSA is a product of oxidation of arginine and proline, and αASA, of oxidation of lysine. By reduction γGSA forms 5-hydroxy-2-aminovaleric acid (HAVA), and αASA, 6-hydroxy-2-aminocaproic acid (HACA). Sensitive gas chromatography-mass spectrometry methods allow their quantification in LDL recovered from human atherosclerotic lesions.

Direct oxidation of apolipoprotein (apo) B-100, the major protein of low density lipoprotein (LDL), is thought to finally result in the formation of new epitopes that are specifically recognized by scavenger receptors followed by an excessive uptake and accumulation of LDL particles in macrophages and vascular smooth muscle cells that can lead to foam cell formation [1]. The latter appears to be the earliest morphologic substrate of atherogenesis. With respect to the pathogenesis of atherosclerosis, it has been emphasized that the analysis of specific products protein oxidation in LDL isolated from atherosclerotic tissue could provide quantitative chemical and clinical evidence for metal catalyzed oxidative processes in the human artery wall [2]. We performed a systematic investigation on determination of levels of HAVA and HACA in LDL apoB-100 recovered from human aortic vascular lesions. Lesional LDL were isolated from the intima of normal and atherosclerotic specimen of human thoracic aortas as published elsewhere [3]. Isolation of apoB-100, enzymatic hydrolysis of apoB-100, and determination of HAVA and HACA, respectively, followed the protocols described previously by us [4, 5]. The content of both γGSA and αASA was significantly higher in LDL recovered from all types of lesion (including fatty streaks that represent the earliest lesion of atherosclerosis) when compared with normal aortic tissue (paired Student`s t test). Fig. 1 shows the content of HAVA and HACA in the intima from various stages of lesion evolution as determined by sensitive and specific GC-MS analysis. These results clearly support the hypothesis that metal catalyzed processes contribute to LDL oxidation both early and late in the atherosclerotic process [6]. The overall yield of HAVA and HACA, respectively, that has been found in lesion LDL (mean HAVA content: 10.45±0.66 mol/mol apoB-100, equally to 328/10,000 proline plus arginine residues; mean HACA content: 8.55±2.06 mol/mol apoB-100, equally to 243/10,000 lysine residues) is remarkably high and indicates that proline, arginine, and lysine residues are good targets for metal catalyzed oxidative attack. The content of HAVA and HACA in both atherosclerotic and normal aortic tissue exceeded the physiological level of HAVA (0.012±0.004 mol/mol apoB-100 (0.4/10,000 proline plus arginine residues)) and HACA (7.1×10^{-4} mol/mol apoB-100 (0.02/10,000 lysine residues)) found in native plasma LDL obtained from healthy normolipidemic, normoglycemic subjects [4, 5]. However, additional work is needed to understand both the nature of the original oxidative insult and the specific consequences of γGSA and αASA formation for the metabolic fate of apoB-100-containing lipoproteins in *vivo.*

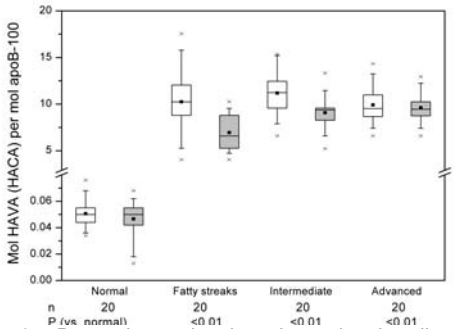

Fig. 1. Box plots showing low density lipoprotein apolipoprotein B-100 (apoB-100) 5-hydroxy-2-aminovaleric acid (HAVA; white boxes) and 6-hydroxy-2-aminocaproic acid (HACA; grey boxes) content in intima from various stages of lesion evolution in human thoracic aorta. Samples were obtained from 20 male accident victims (aged 26 to 45 years, no signs of severe acute diseases) within 10 hours of sudden death [6]. Normal and atherosclerotic tissue (fatty streaks, intermediate, and advanced plaques) was classified according to the criteria of the Pathobiological Determinants of Atherosclerosis in Youth Study.

References

[1] Itabe, H., Biol. Pharm. Bull. 26 (2003) 1-9.
[2] Requena, J. R. *et al*., Amino Acids 25 (2003) 221-226.
[3] Pietzsch, J. and Bergmann, R., J. Clin. Pathol. 56 (2003) 622-623
[4] Pietzsch, J. *et al*., Rapid Commun. Mass Spectrom. 17 (2003) 767-770.
[5] Pietzsch, J. and Bergmann, R., Amino Acids 26 (2004) 45-51.
[6] Pietzsch, J. *et al*., Spectroscopy 18 (2004) 177-183.

Analysis of Specific Markers of Protein Oxidation in Rheumatoid Arthritis Plasma and Synovial Fluid LDL

J. Pietzsch, R. Bergmann, S. Kopprasch[1]

[1]*Department of Internal Medicine III, Medical Faculty, University of Technology Dresden, Germany*

Rheumatoid arthritis (RA) is a chronic inflammatory disease in which reactive oxygen species have been implicated. The antioxidant capacity of synovial fluid is impaired. We hypothesized that LDL in the inflamed synovial joint of patients with active RA undergo pronounced oxidation. To better understand mechanisms of LDL oxidation in RA a novel GC-MS methodology using N(O,S)-ethoxycarbonyl trifluoroethyl amino acid esters (ECEE-F_3) has been applied for sensitive determination of 3-chlorotyrosine (3-Cl-Tyr), 5-hydroxy-2-aminovaleric acid (HAVA), and 6-hydroxy-2-aminocaproic acid (HACA) in apoB-100 of plasma and synovial fluid LDL subfractions. 3-Cl-Tyr is a specific marker of myeloperoxidase-catalyzed protein oxidation, whereas HAVA and HACA are specifically formed by metal-catalyzed protein oxidation.

In subjects with seropositive rheumatoid arthritis (RA) LDL particles accumulate in an accessible inflammatory site, the inflamed synovial joint, and are supposed to be susceptible targets of oxidative attack. Oxidized LDL are likely to serve as mediators for joint damage, further exacerbating the inflammatory process. Furthermore, there is clinical and experimental evidence that subjects with RA show higher cardiovascular mortality when compared with the general population [1].

Paired knee synovial fluid and plasma samples were collected from 30 patients with active RA (12 men/18 women; 21-63 years) and 30 control subjects (15 men/15 women; 20-51 years). The diagnosis of RA was based on criteria proposed by the American College of Rheumatology [2]. Patients were considered to have active RA because they had subjective symptoms, objective tender/swollen joints, and erythrocyte sedimentation rate (ESR) >20 mm/h or C-reactive protein (CRP) >0.6 mg/dL. All subjects were free of renal, hepatic, hematological, and thyroid abnormalities. Nobody was taking medications which influenced lipid metabolism. All subjects were normoglycemic. Nobody was a smoker. Determination of 3-Cl-Tyr, HAVA, and HACA content of LDL_1 and LDL_2 apoB-100 was performed as published elsewhere [3-5].

Results suggest that amino acid side chain residues of apoB-100 are highly reactive toward oxygen radicals in both plasma and synovial fluid in RA. Particularly small dense LDL_2 particles were prone to direct oxidation of apoB-100. Strong correlations between content of oxidation markers in plasma and synovial fluid LDL in RA may allow the use of 3-Cl-Tyr, HAVA, and HACA as clinical markers of antioxidant barrier impairment in RA. Results further suggest that oxidized synovial fluid LDL contribute to increased human monocyte chemotaxis and adhesion (not shown in detail). In summary, these data support the hypothesis of a pathophysiological link between RA and atherogenesis [6-7].

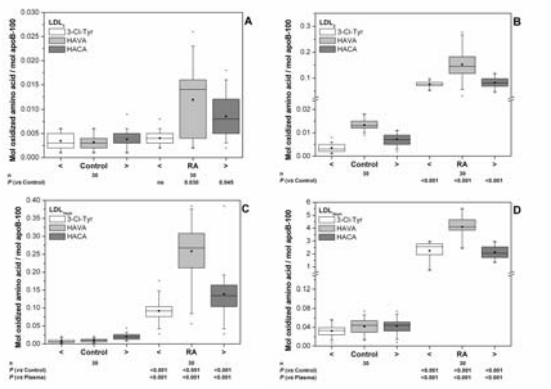

Fig. 1. Box plots showing LDL apoB-100 3-Cl-Tyr, HAVA, and HACA content in plasma LDL_1 (**A**), plasma LDL_2 (**B**), synovial fluid LDL1syn (**C**), and synovial fluid LDL_{2syn} (**D**) in patients with active RA and controls, respectively. Oxidation marker content is expressed as mol/mol apoB-100.

Table 1. Correlation analysis (Spearman's rank correlation coefficient) in both patients with RA and controls

	RA	**Control**
LDL_{1syn} vs. LDL_1		
3-Cl-Tyr	0.400 (.010)	-
HAVA	0.545 (.009)	0.325 (.037)
HACA	0.623 (.000)	-
LDL_{2syn} vs. LDL_2		
3-Cl-Tyr	0.578 (.004)	-
HAVA	0.739 (.000)	0.554 (.009)
HACA	0.714 (.000)	0.617

References

[1] Hitchon, C. A. and El-Gabalawy, H. S., Arthritis Res. Ther. 6 (2004) 265-278.

[2] Schumacher, H. R. *et al*., Clin. Exp. Rheumatol. 21 (2003) S15-S19. (Suppl. 1)

[3] Pietzsch, J. and Julius, U., FEBS Lett. 491 (2001) 123-126.

[4] Pietzsch, J. *et al*., Rapid Commun. Mass Spectrom. 17 (2003) 767-770.

[5] Pietzsch, J. and Bergmann, R., Amino Acids 26 (2004) 45-51.

[6] Pietzsch, J. *et al*., Atherosclerosis 5 (2004) 16a. (Abstract)

[7] Pietzsch, J. *et al*., Atherosclerosis 5 (2004) 16b. (Abstract).

Radiohalogenation of Lipoproteins: Limitations and Implications

J. Pietzsch, S. Hoppmann, J. van den Hoff

In the past, radiohalogenation of peptides, proteins, and lipoproteins has been established as an essential tool for assessment of their biological function *in vitro* and *in vivo* [1, 2]. Halogen radioisotopes are attractive since they exhibit nuclear properties suitable for various applications. At the same time, their chemistry shows great similarities, which enables the use of similar labeling procedures for different nuclides. Among radiohalogens, the use of iodine radionuclides, principally iodine-125 and iodine-131, for labeling of peptides, proteins, and lipoproteins is of widespread use [1, 2]. However, several authors showed that most commonly used oxidative radioiodination procedures such as the iodogen, chloramine-T, or iodine monochloride procedures lead to severe structural modifications of various proteins dramatically affecting their biological activity and functionality [3-6]. Recently, for lipoproteins, particularly low density lipoproteins (LDL) the significant oxidative modification of both the lipid and the apolipoprotein moiety by radioiodination has been demonstrated [7-9]. As strongly emphasized in these studies, it has to be considered that radioiodinated LDL no longer reflect the native LDL particle or, when obtained from *in vitro* oxidation experiments, the initially characterized modified LDL particle [7-9]. Therefore, the valid use of radioiodinated LDL to reflect kinetics and behaviour of native LDL as well as to differentiate kinetics and behaviour of native and oxidized LDL are essentially limited [9]. However, the relevance of these limitations varies greatly depending on the type of studies being done and the types of modified lipoproteins being studied [10-14]. In relation to this subject, several attempts have been made to overcome adverse modification of proteins and lipoproteins by iodination procedures such as the use of mild oxidizing reagents [15], the use of antioxidants [7], and the use of conjugative labeling employing Bolton-Hunter-type reagents [16-18]. For the majority of proteins, the use of iodinated Bolton-Hunter-type reagents such as *N*-succinimidyl-3-(4-hydroxy-5-[^{125}I]iodophenyl)propionate, *N*-succinimidyl-4-[^{125}I]iodobenzoate or *N*-succinimidyl-3-[^{131}I]iodo-4-phosphonomethyl-benzoate is supposed to be a promising approach, because these *n.c.a.* systems for protein radioiodination prevent direct exposure of the protein to excess oxidizing and reducing agents [16-18]. However, high incorporation of radioactivity into the LDL lipid moiety (>30%) limits the use of the majority of iodinated Bolton-Hunter-type reagents for radiolabeling of lipoproteins [1, 2, 16, 17]. To overcome these limitations, we hypothesized the use of *N*-succinimidyl-[4-^{18}F]fluorobenzoate ([^{18}F]SFB) to be a promising alternative [19]. Using this more hydrophilic fluorinated Bolton-Hunter-type reagent apoB-100, the major protein of human LDL, can be specifically labeled via [^{18}F]fluorobenzoylation in the *N*-terminus or the lysine side chain residues, respectively [20]. As a very recent result, the total radiochemical yields, effective specific radioactivities, and *in vitro* stability of [^{18}F]FB-nLDL and [^{18}F]FB-oxLDL, respectively, could demonstrated to be sufficiently high for both *in vitro* and *in vivo* investigations [20]. Importantly, only trace amounts of ^{18}F-radioactivity were incorporated into the lipid moiety of the radiolabeled LDL particles. More than 95% of the ^{18}F-radioactivity was covalently coupled to apoB-100, the structural protein of LDL [20, 21]. Furthermore, our data demonstrate that the use of [^{18}F]SFB for radiolabeling of LDL does not affect native and modified LDL specimen by initial or further oxidative modification or by alteration of their biological function *in vitro* [20]. This has been confirmed by cell binding and uptake studies. Furthermore, determination of non-specific and specific parameters of lipid and protein oxidation, respectively, prior to and after the radiolabelling procedure showed no differences between radiolabelled LDL and their corresponding non-radioactive counterparts [21]. We conclude that the use of [^{18}F]SFB for radiolabeling of LDL is an attractive alternative to LDL iodination methods. Moreover, it can be applied for measurement of kinetics and behavior of both native and oxidized LDL *in vivo* by means of small animal positron emission tomography (PET).

References

[1] Wilbur, D. S., Bioconjug. Chem. 3 (1992) 433-470.
[2] Shepherd, J. *et al.*, Clin. Chim. Acta 66 (1976) 97-109.
[3] Ganguly, S., FEBS Lett. 224 (1987) 198-200.
[4] Zhorov, O. V., *et al.*, Biokhimiia 56 (1991) 828-838.
[5] Bauer, R. J., *et al.*, Biopharm. Drug Dispos. 17 (1996) 761-774.
[6] Thibault, G., *et al.*, Mol. Pharmacol. 48 (1995) 1046-1053.
[7] Khouw, A. S., *et al.*, J. Lipid. Res. 34 (1993) 1483-1496.

[8] Romero, J. R., *et al.,* J. Physiol. Biochem. 57 (2001) 291-301.
[9] Sobal, G., *et al.*, Nucl. Med. Biol. 31 (2004) 381-388.
[10] Tashtoush, B. M. *et al.*, Anal. Biochem. 288 (2001) 16-21.
[11] Ramakrishnan, R. *et al.*, J. Lipid Res. 31 (1990) 1031-1042.
[12] Atsma, D. E. *et al*., J. Lipid Res. 32 (1991) 173-181.
[13] Ling, W. *et al.,* J. Clin. Invest. 100 (1997) 244-252.
[14] Van Berkel, T. J. *et al.,* J. Biol. Chem. 266 (1991) 2282-2289.
[15] Sinn, H. J. *et al.,* Anal. Biochem. 170 (1988) 186-192.
[16] Frantzen, F. *et al.*, Biotechnol. Appl. Biochem. 22 (1995) 161-167.
[17] Ross, J. *et al*., J. Biochem. Biophys. Methods 26 (1993) 343-350.
[18] Shankar, S. *et al.*, Nucl. Med. Biol. 31 (2004) 909-919.
[19] Pietzsch, J., et al. Amino Acids 25 (2003) 120. (Abstract)
[20] Pietzsch, J., Nucl. Med. Biol. 31 (2005) 1043-1050.
[21] Pietzsch, J. *et al.,* this report, p. 12.

Fluorine-18 Radiolabelling of Low Density Lipoproteins (LDL): a Potential Approach for Characterization and Differentiation of Metabolism of Native and Oxidized LDL *in vivo*

J. Pietzsch, R. Bergmann, K. Rode, C. Hultsch, B. Pawelke, F. Wüst, J. van den Hoff

Assessing the metabolic fate of oxidized LDL (oxLDL) in vivo with radiotracer techniques is hindered by the lack of suitable sensitive and specific radiolabelling methods. We evaluated an improved methodology based on the radiolabelling of native LDL (nLDL) and oxLDL with the positron emitter fluorine-18 (^{18}F) by conjugation with N-succinimidyl-4-[^{18}F]fluorobenzoate ([^{18}F]SFB). We investigated whether radiolabelling of LDL induces adverse structural modifications. Results suggest that radiolabelling of both nLDL and oxLDL using [^{18}F]SFB causes neither additional oxidative structural modifications of LDL lipids and proteins nor alteration of their biological activity and functionality, respectively. Thus, radiolabelling of LDL using [^{18}F]SFB could prove to be a promising approach for studying the kinetics of oxLDL in vivo.

Although different radionuclides have been used to radiolabel LDL, investigations to evaluate localization, clearance, and biological effects of modified LDL, e.g., acetylated LDL and oxidized LDL, respectively, have used extensively radionuclides of iodine such as iodine-125 and iodine-131. Recently, it has been clearly demonstrated that most commonly used radioiodination methods lead to oxidative modification of both the lipid and the protein moiety of LDL, affecting their cytotoxicity, interaction with LDL receptors or scavenger receptors, and *in vivo* clearance [1-3]. In consequence, the use of radioiodinated LDL labeled via direct iodination has serious limitations, particularly it does not allow to differentiate kinetics and behavior of native and oxidized LDL. As an attractive alternative we present a new methodology for *n.c.a.* labeling of LDL with the positron emitter fluorine-18 (^{18}F) using the Bolton-Hunter-type reagent *N*-succinimidyl-[4-^{18}F]fluorobenzoate ([^{18}F]SFB) [4].

Isolation of LDL, LDL oxidation, measurement of specific oxidation parameters, radiolabelling of native and oxidized LDL with [^{18}F]SFB, biochemical and biological characterization of radiolabelled LDL were performed as published elsewhere [4].

This work reports for the first time experiments on radiolabelling of both nLDL and oxLDL using the acylating reagent [^{18}F]SFB (Figure 1). The present data indicate that radiolabelling with [^{18}F]SFB did not alter biological activity and functionality of nLDL and oxLDL, respectively (not shown in detail).

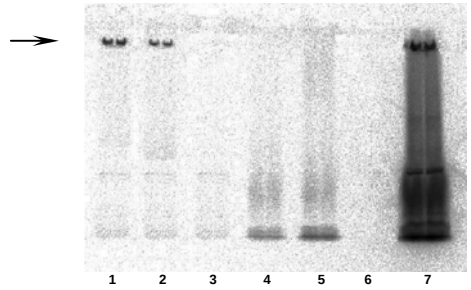

Fig. 1. Representative SDS polyacrylamide gel electrophoresis pattern of a complete separation of [^{18}F]FB-oxLDL. The figure shows radioactivity distribution as determined by radioluminography. Lane 7 is the reaction mixture, lanes 1 to 6 represent individual fractions obtained from DG 10 size exclusion chromatography column as determined in duplicate. Arrow indicates the apoB-100 band.

This radiolabelling does not lead either to adverse oxidation of nLDL particles or to additional adverse oxidative modification of oxLDL particles (Table 1). Thus, the present method is likely to provide a suitable radiotracer for assessment of metabolism of oxidized LDL in vivo by means of dynamic positron emission tomography (PET).

References

[1] Khouw, A. S. *et al*., J. Lipid. Res. 34 (1993) 1483-1496.

[2] Romero, J. R. *et al*., J. Physiol. Biochem. 57 (2001) 291-301.

[3] Sobal, G. *et al.*, Nucl. Med. Biol. 31 (2004) 381-388.

[4] Pietzsch, J., Nucl. Med. Biol. 31 (2005) 1043-1050.

Table 1. Parameters of protein oxidation prior to and after radiolabeling of nLDL and oxLDL with [^{18}F]SFB

Parameter	nLDL	[^{18}F]FB-nLDL	*P* *nLDL /[^{18}F]FB-nLDL*	oxLDL	[^{18}F]FB-oxLDL	*P* *oxLDL/ [^{18}F]FB-oxLDL*	*P* *nLDL/oxLDL*
REM	1	1.01±0.04	*ns*	3.94±0.23	3.91±0.36	*ns*	*0.000*
HAVA (*mol/mol apoB-100*)	0.009±0.003	0.011±0.003	*ns*	14.661±0.884	14.044±0.862	*ns*	*0.000*
HACA (*mol/mol apoB-100*)	0.0007±0.0003	0.0007±0.0003	*ns*	7.82±1.62	7.86±1.45	*ns*	*0.000*

Results are means ± SD (n=10); Mann-Whitney U tests were used for comparison of numerical variables between groups; REM, relative electrophoretic mobility; HAVA, 5-hydroxy-2-aminovaleric acid; HACA, 6-hydroxy-2-aminocaproic acid

N-Arylation of Indoles with 4-[^{18}F]Fluoroiodobenzene: a Novel Radiolabelling Technique in ^{18}F Chemistry

F. Wüst, T. Kniess

The palladium-mediated N-arylation of indoles with 4-[^{18}F]fluoroiodobenzene as novel radiolabelling method has been developed. Optimised reaction conditions ($Pd_2(dba)_3$/(2-(dicyclohexyl-phosphino)-2'-(N,N-dimethylamino)-biphenyl, NaOBu^t, toluene, 100 °C for 20 min) gave radiochemical yields of up to 71 % related to 4-[^{18}F]fluoroiodobenzene.

Introduction

N-Arylindoles are central structural motifs in many drugs and other pharmaceutically important compounds, and several Pd- and Cu-mediated reactions were shown to be very effective for the preparation of *N*-arylated compounds including indoles [1-4]. However, the transition-mediated *N*-arylation of indoles has not been adapted to ^{18}F chemistry yet.

Results and Discussion

Four different catalyst systems were tested for sufficient coupling of 4-[^{18}F]fluoroiodobenzene with indole **1** to give 1-(4-[^{18}F]fluorophenyl)-1*H*-indole **[^{18}F]-2** (Fig. 1), being **A**: CuI/*trans* 1,2-diaminocyclohexane; **B**: CuI/ethylenediamine; **C**: $Pd_2(dba)_3$/Xantphos and **D**: $Pd_2(dba)_3$/2-(dicyclohexyl-phosphino)-2'-(*N*,*N*-dimethyl-amino)-biphenyl).

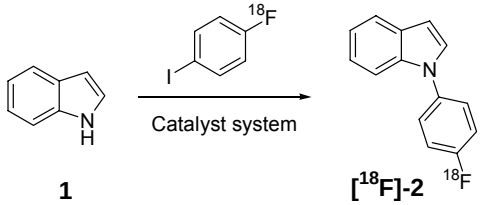

Fig. 1. Synthesis of the labelling precursor **7**.

Best results were obtained with catalyst system **D** containing electron-rich phosphine ligand 2-(dicyclohexyl-phosphino)-2'-(*N*,*N*-dimethyl-amino)-biphenyl), whereas Cu-mediated reactions (entries 1-4) or the use of Xantphos as phosphine ligand (entries 5-10) only gave low to moderate radiochemical yields (Table 1). The reaction is strongly influenced by the used base and solvent. In this connection a combination of NaOBu^t as base and toluene as the solvent seems to be the best choice. No product formation was observed when DMF as a polar solvent was used (entry 12). In contrast, high radiochemical yields were obtained when toluene was used as the solvent (entry 13). Thus, cross-coupled product **[^{18}F]-2** was formed in 25 % after 10 min, and the radiochemical yield could be increased significantly to 69 % after 20 min. Extension of the reaction time to 30 min and 60 min did not further improve the radiochemical yield, being 71 % and 70 %, respectively. Lowering the reaction temperature to 65 °C (entry 14) was accompanied with a drastic decrease of radiochemical yield and only 3 % of the desired product was formed. On the other hand, performance of the reaction at 140 °C did not further improve radiochemical yield of product **[^{18}F]-2** when compared with the reaction at 100 °C (entry 15 vs. entry 13).

Table 1. *N*-Arylation of indole with [^{18}F]fluoro-iodobenzene

No	Catalyst system	Base	Solvent[c]	RCY in %[a,b]
1	**A**	K_3PO_4	THF/toluene	0
2	**A**	K_3PO_4	toluene	0
3	**B**	K_3PO_4	THF/toluene	7
4	**B**	K_3PO_4	toluene	36
5	**C**	NaOBu^t	THF	5
6	**C**	KOBu^t	THF	6
7	**C**	NaOBu^t	THF/toluene	13
8	**C**	Cs_2CO_3	THF/toluene	0
9	**C**	K_3PO_4	THF/toluene	16
10	**C**	NaOBu^t	toluene	28
11	**D**	NaOBu^t	THF/toluene	22
12	**D**	NaOBu^t	DMF	0%
13	**D**	NaOBu^t	toluene	25 (10 min) 69 (20 min) 71 (30 min) 70 (60 min)
14	**D**	NaOBu^t	toluene	3 %[d]
15	**D**	NaOBu^t	toluene	70 %[e]

[a] Radiochemical yield (RCY) determined by radio-HPLC representing the percentage of radioactivity area of cross-coupled product **[^{18}F]-2** related to the total radioactivity area
[b] All reactions were conducted at 100 °C for 30 min.
[c] Solvents in a 1:1 mixture
[d] Reaction was carried out at 65 °C
[e] Reaction was carried out at 140 °C

References

[1] Old, D. W. *et al.*, Org. Lett. 2 (2000) 1403-1406.
[2] Grasa, G. A. *et al.*, J. Org. Chem. 66 (2001) 7729-7737.
[3] Antilla, J. C. *et al.*, J. Am. Chem. Soc. 124 (2002) 11684-11688.
[4] Klapars, A. *et al.*, J. Am. Chem. Soc. 123 (2001) 7727-7729.

N-Arylation of Indoles with 4-[^{18}F]Fluoroiodobenzene: Synthesis of ^{18}F-Labelled σ_2 Receptor Ligands

F. Wüst, H. Kasper

*Optimised reaction conditions ($Pd_2(dba)_3$/(2-(dicyclohexyl-phosphino)-2'-(N,N-dimethylamino)-bi-phenyl, $NaOBu^t$, toluene, 100 °C for 20 min) for the palladium-mediated N-arylation of indoles with 4-[^{18}F]fluoroiodobenzene were applied for the synthesis of ^{18}F-labelled σ_2 receptor ligands **[^{18}F]-11** and **[^{18}F]-13** in 91 % and 84 % radiochemical yield, respectively, related to 4-[^{18}F]fluoroiodobenzene.*

Introduction

In a previous report in this Annual Report we described the development of an efficient *N*-arylation approach of indoles with 4-[^{18}F]fluoroiodobenzene [1]. Now we report on the radiosynthesis of two ^{18}F-labelled σ_2 receptor ligands **[^{18}F]-11** and **[^{18}F]-13** exhibiting an 4-[^{18}F]fluorophenyl-substituted indole motif by application of optimised reaction conditions as elaborated for the palladium-mediated *N*-arylation of indole with 4-[^{18}F]fluoroiodobenzene.

Results and Discussion

Optimised reaction conditions ($Pd_2(dba)_3$/(2-(dicyclohexyl-phosphino)-2'-(*N*,*N*-dimethylamino)-biphenyl, $NaOBu^t$, toluene, 100 °C for 20 min) were applied for the synthesis of ^{18}F-labelled σ_2-receptor ligands **[^{18}F]-11** and **[^{18}F]-13** by the reaction of indoles **10** and **12** with 4-[^{18}F]fluoroiodobenzene. The synthesis of labelling precursors **10** and **12** and the synthesis of reference compounds **11** and **13** is shown in Fig. 1.

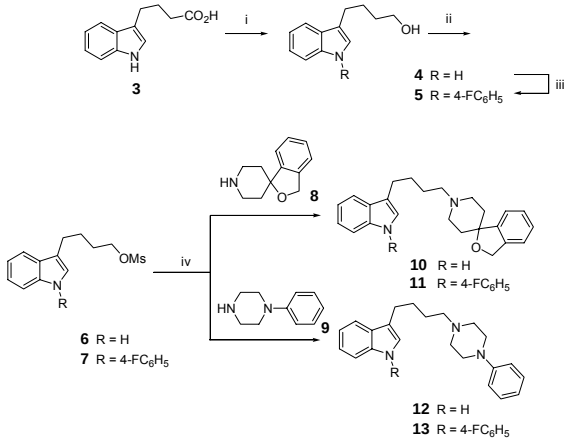

Fig. 1. Reagents and conditions: (i) $LiAlH_4$, THF, 0 °C-r.t.; (ii) MsCl, TEA, CH_2Cl_2, 0 °C; (iii) 4-fluoroiodobenzene, CuI, ZnO, K_2CO_3 NMP, 160 °C; (iv) amine **8** or **9**, Na_2CO_3, acetone, r.t..

The synthesis started with reduction of commercially available 4-(3-indolyl)-butyric acid **3** by means of $LiAlH_4$ to give the corresponding alcohol **4** in 57 % yield. 4-(1*H*-Indol-3-yl)-1-butanol **4** was converted into methanesulfonate ester **6** followed by *N*-alkylation reactions with amines **8** [2] and **9** to give labelling precursors **10** and **12** in 59 % and 67 % yield, respectively, for the two steps. For the synthesis of reference compounds **11** and **13** alcohol **4** was subjected to an Ullmann arylation reaction with 4-fluoroiodobenzene to give 1-(4-fluorophenyl)-substituted compound **5** [3] in 44 % yield prior to conversion into methanesulfonate ester **7**. *N*-Alkylation was carried out using the same procedure as was used for the synthesis of labelling precursors **10** and **12** using amines **8** [2] and **9**. Following this procedure reference compounds **11** and **13** could be obtained in 52 % and 62 % yield relative to methanesulfonate ester **7**.

The radiolabelling of σ_2-receptor ligands **[^{18}F]-11** and **[^{18}F]-13** via *N*-arylation with 4-[^{18}F]fluoroiodobenzene is depicted in Fig. 2.

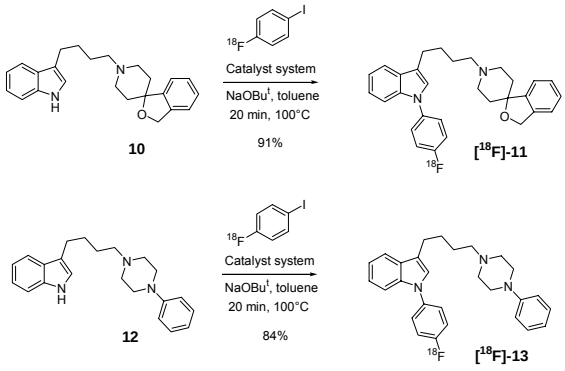

Catalyst system: $Pd_2(dba)_3$ /2-(dicyclohexyl-phosphino)-2'-(N,N-dimethylamino)-biphenyl

Fig. 2. Radiosynthesis of σ_2-receptor ligands **[^{18}F]-11** and **[^{18}F]-13**.

Starting from labelling precursors **10** and **12** the desired compounds **[^{18}F]-11** and **[^{18}F]-13** could be obtained in excellent radiochemical yields of 91 % and 84 %, respectively, related to 4-[^{18}F]fluoroiodobenzene.

References

[1] Wüst, F. *et al.*, *this report*, p. 17.
[2] Kubota, H. *et al.*, Chem. Pharm. Bull. 46 (1998) 351-354.
[3] Perregaard, J. *et al.*, J. Med. Chem. 38 (1995) 1998-2008.

Determination of Radiochemical Purity of [^{18}F]3-OMFD and [^{18}F]FDOPA by HPLC

J. Zessin, B. Lipps

A combination of a short polymer and a RP18 column was used for determination of the radiochemical purity of [^{18}F]OMFD to improve the quantification of impurities.

Introduction

The radiochemical purity is an important parameter for the release of PET radiopharmaceuticals. This parameter can be easily determined by reserved phase HPLC. Two types of stationary phases are available for RP-HPLC: silica and styrene/divinylbenzene copolymer.
The use of silica-based columns for the analysis of ^{18}F-labelled radiopharmaceuticals is restricted by the high affinity of [^{18}F]fluoride to the silica matrix. A correct quantification of this main side product is prevented due to this obstacles. Polymer-based stationary HPLC phases do not show an irreversible binding of [^{18}F]fluoride [1], but the decreased resolution ability implied difficulties in the quantification of compounds with comparable retention times.
[^{18}F]3-OMFD and [^{18}F]FDOPA contain [^{18}F]fluoride as well as other radioactive impurities with retention times comparable to that of the radiopharmaceuticals. A correct determination of the radiochemical purity is impossible using either a silica- or a polymer-based HPLC column.
In this report, we describe the improvement of this analysis by use of a column combination, which consists of a short polymer column and a silica-based column.

Methods

The analysis of radiochemical purity was performed with an HPLC system (Series 1100) from Agilent consisting of an autosampler, pump with a low pressure gradient system, vacuum degasser, and a photodiode array detector (DAD). The gamma radioactivity monitor “GABI” from Raytest was used as radioactivity detector. The HPLC eluent was a acetonitrile/water (containing trifluoroacetic acid and Na_2EDTA) gradient.
Columns and detectors were arranged in the following order: SecurityGuard RP-1 (4x3 mm, Phenomenex) - radioactivity detector - Purospher RP18 (125x3 mm, Merck) - radioactivity detector – DAD. After passing the columns, the compounds go through the radioactivity detector in separated loops.

Results and Discussion

Fig. 1 shows a typical radiochromatogram, which was obtained by the established HPLC method using a PolymerX RP1 column. This chromatogram demonstrates the restricted resolution of [^{18}F]3-OMFD and an impurity with a comparable polarity.

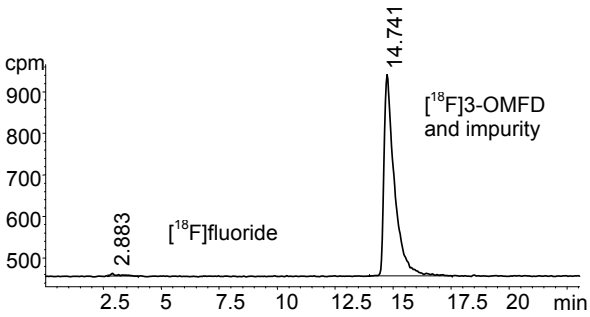

Fig. 1. Radiochromatogram of [^{18}F]3-OMFD from PolymerX column

Fig. 2 shows the radiochromatogram of the same [^{18}F]3-OMFD batch, which was obtained from the analysis of radiochemical purity using a combination of a short polymer column and a silica-based RP18 column. The first part of the radiochromatogram demonstrates, that a polymer column with a length of 3 mm was sufficient enough to separate [^{18}F]fluoride from the more unpolar compounds.

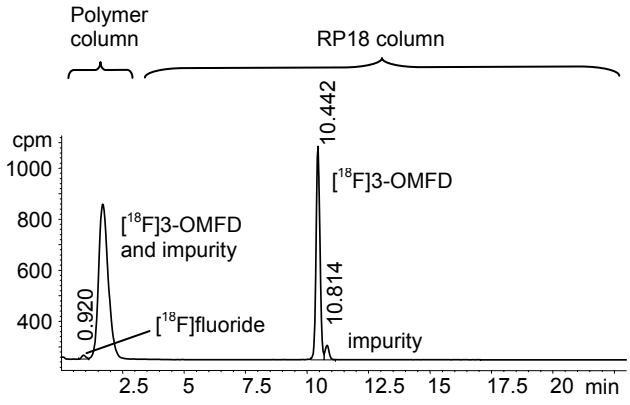

Fig. 2. Radiochromatogram of [^{18}F]3-OMFD (same batch as shown in Fig. 1) from SecurityGuard RP1/Purosphere RP18 column combination

After passing the radioactivity detector, the pre-separated HPLC sample passed a silica-based RP18 column. As expected, [^{18}F]fluoride was completely retained by this stationary phase, but the peaks of [^{18}F]3-OMFD and the radioactive impurity were separated.
The quantification was performed by analysis of the [^{18}F]fluoride peak in the first part and the [^{18}F]3-OMFD and impurity peaks in the second part of the radiochromatogram. These results were comparable to the results obtained with the PolymerX RP1 column. The differences of the [^{18}F]fluoride amount were in the range of accuracy of HPLC.
The described HPLC method is also applicable for the analysis of [^{18}F]FDOPA, but a 10 mm polymer column (RSPak DE-G 4.6x10 mm, Shodex) was necessary to separate the peaks of [^{18}F]fluoride and [^{18}F]FDOPA completely. The longer polymer column has no influence of the resolution of the silica-based RP-HPLC.
Furthermore, we tested the [^{18}F]fluoride recovery from a hybrid phase (Gemini, Phenomenex), which has a coating of the silica surface with organic residues. The [^{18}F]fluoride recovery of such a hybrid phase was in the same range as by use of conventional RP phase. Such a coating of silica do not show an advantage for the HPLC determination of [^{18}F]fluoride.

Conclusions

A combination of a short polymer column and a silica-based RP column was used for a determination of the radiochemical purity of the PET radiotracer [^{18}F]3-OMFD. This arrangement of columns improves the resolution of compounds with similar retention times by a similar sensitivity to [^{18}F]fluoride.

References

[1] Angelberger, P. *et al.*, J. Labelled Compd. Radiopharm. 44 (2001) 844-846.

Synthesis of N-[6-(4-[^{18}F]Fluorobenzylidene)aminooxyhexyl]maleimide (MHAA). A New SH-Reactive ^{18}F-Labelling Agent

M. Berndt, F. Wüst

We describe the synthesis of a new ^{18}F-labelling agent containing a thiol-reactive maleimide group. The labelling precursor was obtained in a three-step synthesis. Preparation of [^{18}F]fluorobenzaldehyde from [^{18}F]fluoride und subsequent conversion with the substituted maleimide led to the labelling reagent in 29-39 % radiochemical yield.

Introduction

For the ^{18}F-labelling of peptides and proteines *N*-succinimidyl-4-[^{18}F]fluorobenzoate (SFB) was found to be a suitable labelling reagent. Recently, a convenient remotely-controlled module radiosynthesis of SFB was developed in our group [1]. However, in some applications the use of this amine-reactive agent failed. Therefore further labelling strategies are needed. In this connection, particularly maleimide were shown to react efficiently and selectively with SH-groups under mild conditions.

Results and Discussion

Toyokuni *et al.* recently reported the synthesis of a bifunctional linker containing a thiol-reactive maleimide group and a carbonyl-reactive aminooxy group [2]. Admittedly the synthetic route was quite extensive. We found a very efficient synthetic pathway to a related labelling precursor **4** with only three steps (Fig. 1). 6-bromo-1-hexanole (**1**) was converted with *tert*-butyl-*N*-hydroxycarbamate and DBU in dichloromethane [3]. The maleimide group was introduced via Mitsunobu reaction [4]. Finally, the Boc-protecting group was removed using HCl/EtOAc and *N*-(6-aminooxyhexyl)maleimide (**4**) was obtained as the stable HCl salt.

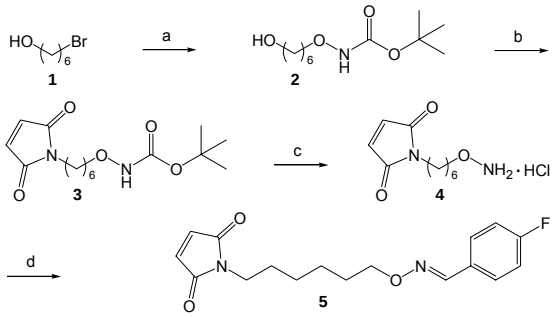

a) BocNHOH, DBU, CH_2Cl_2, 24 h, RT, 75 %; b) maleimide, PPh_3, DIAD, THF, 77 %; c) HCl, EtOAc, 84 % ; d) [^{19}F]fluorobenzaldehyde, DMF, 89 %.

Fig. 1. Synthesis of labelling precursor **4** and reference substance **[^{19}F]-5**.

Transformation of **4** with [^{19}F]fluorobenzaldehyde led to the reference substance **[^{19}F]-5**. Exclusively the *E*-isomer was formed, which was verified by the ^{1}H NMR signal of the oxime proton [2].

The radiosynthesis started with the preparation of [^{18}F]fluorobenzaldehyde. In a one-pot procedure *N*-(6-aminooxyhexyl)maleimide (**4**) was added to the generated aldehyde and afterwards *N*-[6-(4-[^{18}F]fluorobenzylidene)aminooxyhexyl]maleimide (**[^{18}F]-5**) was isolated by HPLC. In a typical experiment 3.88 GBq of [^{18}F]fluoride could be converted to 723 MBq (29 %, decay corrected) **[^{18}F]-5** within 69 min, including HPLC purification. The specific activity was determined to be 76 GBq/µmol.

The labelling properties of **[^{18}F]-5** were examined by using glutathione (GSH) as a SH-group-containing model peptide (Fig. 2). **[^{18}F]-5** in ethanol (50 µl, 5 MBq) was added to 900 µl of glutathione solutions (1.0 mg/ml to 10 ng/ml) in phosphate buffer (pH = 7.2) at 20 °C. The conversion was monitored by radio-TLC. After 5 min the **[^{18}F]-5** was transferred into **[^{18}F]-6** completely in the vials containing 1.0 mg/ml to 10 µg/ml. At lower concentrations of glutathione the conversion was incomplete (for 1 µg/ml 95 % radiochemical yield after 1 h, for 100 ng 20 % after 1 h, for 10 ng 5 % after 1 h).

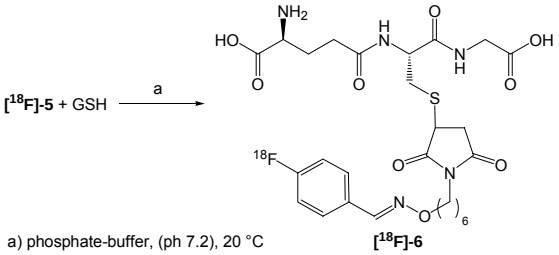

Fig. 2. Coupling of **[^{18}F]-5** and glutathione (GSH).

Currently we extend this labelling procedure to more complex biomolecules such as proteines and antibodies.

References

[1] Mäding, P. *et al., this report*, p. 22.
[2] Toyokuni, T. *et al.*, Bioconjugate Chem. 14 (2003**)** 1253-1259.
[3] Jones, D. S. *et al.*, Tetrahedron Lett. 41 (2000) 1531-1533.
[4] Walker, M. A., J. Org. Chem. 60 (1995) 5352-5355.

Modul-Assisted Synthesis of the Labelling Agent [^{18}F]SFB

P. Mäding, F. Füchtner, F. Wüst

The known three-step synthesis of N-succinimidyl-4-[^{18}F]fluorobenzoate ([^{18}F]SFB) was adapted and transferred to an automated module. After optimization of the reaction conditions [^{18}F]SFB was obtained in decay-corrected radiochemical yields of 34-37 % (related to [^{18}F]fluoride; n = 8) within a synthesis time of 68 min. The radiochemical purity was in the range of 93-96 %.

Introduction

[^{18}F]SFB **5** was shown to be a suitable acylation agent for labelling of peptides, proteins and antibodies [1-4 among others]. Such bioactive compounds containing the [^{18}F]fluorobenzoyl group can be useful radiotracers for in vivo studies by means of PET.
Permanent utilisation of [^{18}F]SFB call for a reliable and reproducible routine preparation of [^{18}F]SFB without increased radiation exposure to personnel.
Therefore we have adapted the three-step two-pot procedure according to Fig. 1 [4] to a modified double module "TRACERlab Fx$_{FDG}$" from GE Medical Systems.

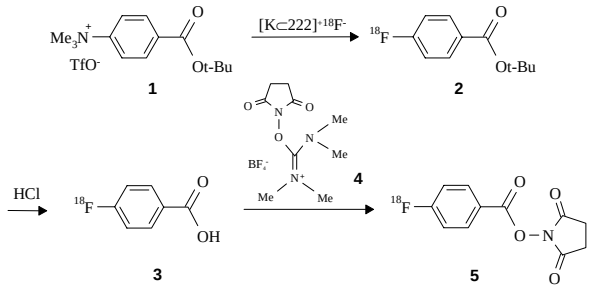

Fig. 1. Synthesis of [^{18}F]SFB (**5**)

Results and Discussion

In [4] the synthesis of 4-[^{18}F]fluorobenzoic acid **3** was carried out within a very short reaction time using microwave activations (2 min for the [^{18}F]fluorination step, 30 s for the saponification step). As the use of the microwave is not possible in the module, the reaction vessels are heated conventionally. Therefore, the synthesis of **3** was investigated and optimised in the automated synthesis module. The first reaction step (**1** into **2**) was tested using several solvents, such as DMSO, DMF and MeCN, at different temperatures and reaction times. MeCN was the solvent of choice along with heating at 90 °C for 10 min. Furthermore diluted HCl was tested for the saponification step (**2** into **3**) to avoid the use of trifluoroacetic acid. It was found that 1 M HCl was suitable to hydrolyse the *tert.*-butyl ester group of **2** by heating at 100 °C for 5 min. After dilution of the acidic reaction mixture with water, **3** was purified by solid phase extraction (Chromafix HR-P; Macherey-Nagel). **3** was eluted from the cartridge with MeCN in radiochemical yields of up to 67 % and a radiochemical purity of 97-98 %.
Then, **3** was converted with Me_4NOH into its tetramethylammonium salt, which was dried. Addition of the activating agent *O*-(*N*-succinimidyl)-*N,N,N',N'*-tetramethyluronium-tetrafluoroborate (TSTU; (**4**)) in MeCN and heating at 90 °C for 2 min yielded [^{18}F]SFB **5**. After the two purification steps using a polystyrene cartridge [2] (Chromafix HR-P; Macherey-Nagel), **5** was eluted with MeCN in radiochemical yields of 34-37 %. The total synthesis time was 68 min and the radiochemical purity ranged between 93-96 %. Thus, in a typical experiment 12 GBq of [^{18}F]fluoride could be converted into 2.8 GBq [^{18}F]SFB within 68 min. The process flow scheme is given in Fig. 2.

Conclusions

A remotely-controlled procedure for the synthesis of [^{18}F]SFB **5** was developed based on a modified double module "TRACERlab Fx$_{FDG}$" from GE Medical Systems. In this way, [^{18}F]SFB could be obtained in reproducible yields and purities. It was suitable for the labelling of peptides and proteins.

References

[1] Vaidyanathan, G. *et al.*, J. Nucl. Med. 33 (1992) 1535-1541.
[2] Wester, H.-J. *et al.*, Nucl. Med. Biol. 23 (1996) 365-372.
[3] Zijlstra, S. *et al.*, Appl. Radiat. Isot. 58 (2003) 201-207.
[4] Wüst, F. *et al.*, Appl. Radiat. Isot. 59 (2003) 43-48.

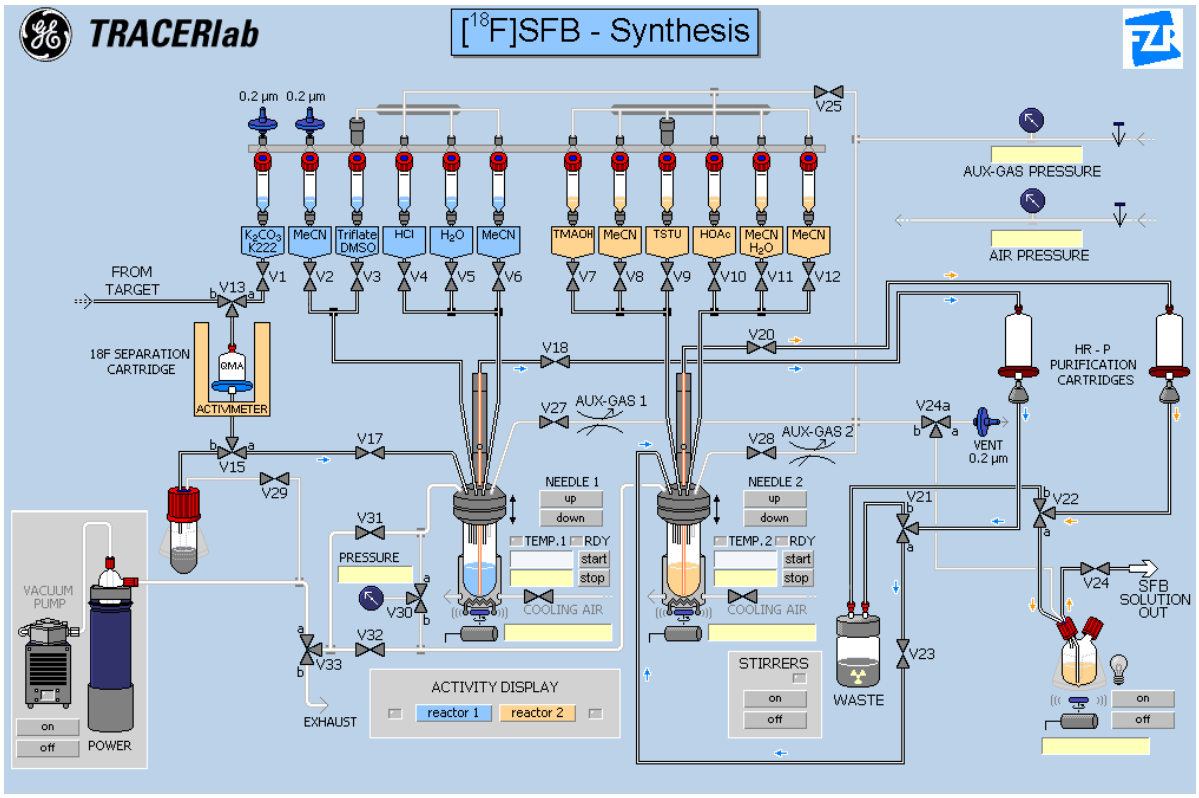

Fig. 2. Process flow scheme for the remotely-controlled synthesis of [^{18}F]SFB **5**.

Preparation of the Radiopharmaceutical [^{18}F]NaF for Medical Use

P. Mäding, F. Füchtner, J. Zessin, F. Wüst

The preparation of sodium [^{18}F]fluoride was developed in an automated module. The separated [^{18}F]fluoride was eluted from the anion exchange cartridge using 1 ml of isotonic saline. After dilution with isotonic saline the radioactive solution was sterilized by filtration through a 0.22 µm sterile filter. The yield of sodium [^{18}F]fluoride was in the range of about 90 % within a preparation time of 6 min.

Introduction

The importance of sodium [^{18}F]fluoride as a radiotracer for bone imaging originated from 1962 [1]. It became the standard agent for bone scanning until the development of ^{99m}Tc-labelled bisphosphonates in the 1970s [2]. In 1992 Hawkins had introduced a kinetic model for [^{18}F]fluoride in humans [3]. The use of [^{18}F]fluoride for whole body skeletal PET imaging in patients was published in 1993 for the first time [4]. Sodium [^{18}F]fluoride is indicated in PET imaging to define areas of bone metastases and altered osteogenic activity [2, 5, 6 among others].

Therefore we have developed a simple procedure for the preparation of sodium [^{18}F]fluoride for medical use based on a ^{18}F-remotely-controlled synthesis module from GE Medical Systems.

In [7] the preparation of sodium [^{18}F]fluoride was carried out by dilution of the irradiated [^{18}O]water with isotonic saline solution. In this way [^{18}O]water can not be re-used. Non-separated radionuclide impurities are an other disadvantage of this method. To avoid this disadvantages, Brenner *et al.* [2] performed a purification of [^{18}F]fluoride using an anion exchange cartridge. Sodium [^{18}F]fluoride was eluted with sodium bicarbonate solution and diluted with isotonic saline.

Results and Discussion

We have found that the adsorbed [^{18}F]fluoride can also be eluted off the anion-exchange cartridge with small amounts of isotonic saline (about 1 ml). The use of larger amounts of isotonic saline will cause co-elution of radionuclidic impurities. Thus, we have transferred this procedure on a modified ^{18}F synthesis module according to Fig. 1. The preparation of sodium [^{18}F]fluoride was carried out as follows:

(1) Adsorption of the [^{18}F]fluoride on an strong anion exchange cartridge (Accell^{TM} Plus QMA, Waters),

(2) Elution of [^{18}F]fluoride with 1 ml isotonic sodium chloride,

(3) Dilution with 14 ml isotonic saline and sterile filtration through a 0.22 µm sterile filter. The yield of sodium [^{18}F]fluoride was in the range of 90 % within a preparation time of 6 min. In this way a chemical and radiochemical pure product was obtained. The radiochemical and chemical purity was determined by ion chromatography using a CarboPac PA1 column (250x4 mm; DIONEX) and 0.1 M sodium hydroxide as eluent. The radiochemical purity exceeds 99.5 %. The radionuclear purity, which was checked by gamma spectroscopy and measurement of the half-life, exceeds 99.9 %.

The maximum amounts of the residual solvents acetonitrile (to activate the QMA cartridge) and ethanol (as cleaning solvent) are within the limits of the European Pharmacopoeia. The pH of the solution varies from 7.2 to 8.6. The product was isotonic, sterile and pyrogen-free.

Conclusions

A procedure for the routine production of sodium [^{18}F]fluoride was developed based on a ^{18}F synthesis module from GE Medical Systems. The described procedure is very simple and robust. The final product conforms to the specifications for this radiopharmaceutical according to the monograph “sodium fluoride (^{18}F) injection” of the European Pharmacopoeia.

References

[1] Blau, M. *et al.*, J. Nucl. Med. 3 (1962) 332-334.

[2] Brenner, W. *et al.*, J. Nucl. Med. 45 (2004) 1493-1500.

[3] Hawkins, R. A. *et al.*, J. Nucl. Med. 33 (1992) 633-642.

[4] Hoh, C. K. *et al.*, J. Comput. Assist. Tomogr. 17 (1993) 34-41.

[5] Schirrmeister, H. *et al.*, J. Clin. Oncol. 17 (1999) 2381-2389.

[6] Berding, G. *et al.*, Eur. J. Nucl. Med. 22 (1995) 1133-1140.

[7] Piert, M. *et al.*, J. Nucl. Med. 42 (2001) 1091-1100 and J. Nucl. Med. 44 (2003) 117-124.

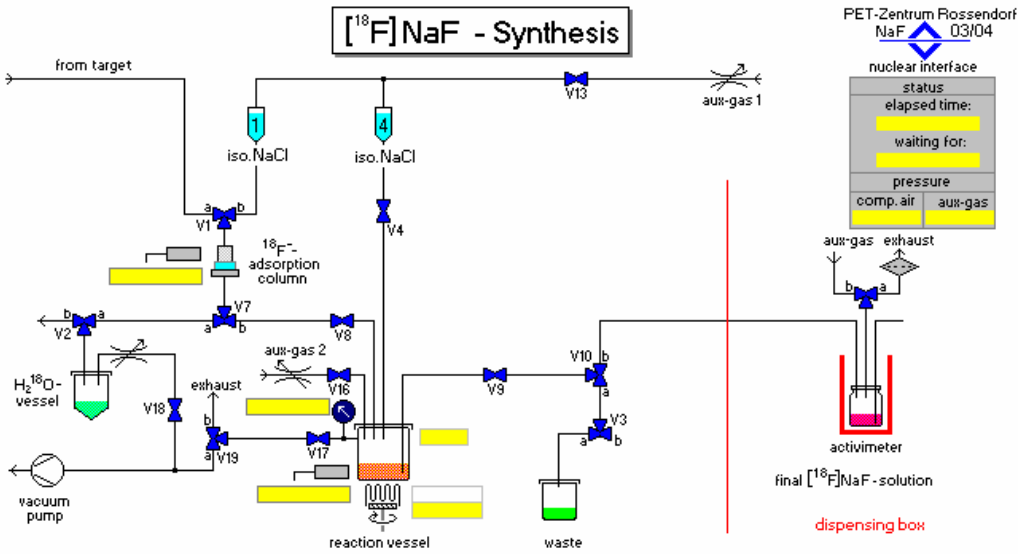

Fig. 1. Scheme of the module for the preparation of sodium [^{18}F]fluoride.

Factors Affecting the Specific Activity of [^{18}F]Fluoride from a Water Target

F. Füchtner, S. Preusche, P. Mäding, J. Steinbach[1]

[1] *Institut für Interdisziplinäre Isotopenforschung, Permoserstr.15, 04318 Leipzig, Germany*

By replacing PTFE tubes to PP tubes the contribution of the water target dispensing system to the contamination of [^{18}F]/[^{18}O]water with [^{19}F]fluoride can be reduced by the factor of about two.

Introduction

The nuclear reaction $^{18}O(p,n)^{18}F$ is the method of choice for routine production of n.c.a. [^{18}F]fluoride to synthesise labeled compounds on high activity level as well as with high specific activity (SA). For quite a few PET radiopharmaceuticals the SA has to be high in order to prevent physiological response at the studied system. We found that the SA shows considerable variation, as also reported in the literature [1-6]. The SA is an important quality parameter in accordance with the GMP guidelines and should be reproducible. The SA of the radiopharmaceuticals mainly depends on the SA of the [^{18}F]fluoride dispensed from the cyclotron target system after radiation. Initial investigations indicated that the main origin of ^{19}F is the [^{18}O]water dispensing and delivery system of the target and not the starting [^{18}O]water itself. Detailed ion chromatographic investigations were carried out to determine the contamination sources of the ^{19}F.

Results and Discussion

[^{18}O]water and [^{18}F]/[^{18}O]water samples from different places of the target dispensing and delivery system were analyzed for [^{19}F]fluoride using ion chromatography.

The SA of the labeled receptor ligand [^{18}F]ZK811460 [7] (n = 58) was determined by RP chromatography using a UV detector.

The starting [^{18}O]water is of good quality and contains no significant amounts of [^{19}F]fluoride (0.5 nMol/8 ppb). A considerable contribution of the target irradiation process to the [^{19}F]fluoride amount was not found.

The [^{19}F]fluoride amount ***of the dispensing system*** mainly depends on the tubing materials and the radiation dose, which is exposed to the tube near the target/cyclotron, as well as on the water/tube contact time. The PTFE tube of the dispensing system is the main origin of [^{19}F]fluoride (contamination up to 380 nMol/5550 ppb). Avoiding PTFE tubes and changing to PP (polypropylene) tubes the [^{19}F]fluoride amount can be decreased considerably (maximum value 10 nMol/170 ppb).

The average value and its standard deviation of the cold amount | SA of the [^{18}F]ZK811460 using PP tubes (n = 36) in the target dispensing system in contrast to PTFE tubes (n = 22) could improved from 66±32 nMol | 56±35 GBq/µMol (PTFE) to 38±15 nMol | 126±38 GBq/µMol (PP) (see Fig.).

On the other hand: In our experience PTFE tubes of the target water ***delivery system*** have the best transport properties related to the [^{18}F]/[^{18}O]water bolus. In general, its contribution to the [^{19}F]fluoride amount (contamination up to 20 nMol/300 ppb) is minor. If very high SA is required repeated rinsing of the whole delivery system with ultra pure water becomes necessary.

References

[1] Dence, C. *et al.*, Proceedings WTTC 6, Vancouver (1995) 199-205.

[2] Kilbourn, M. R. *et al.*, Int. J. Appl. Radiat. Isot. 35 (1984) 599-602.

[3] Nishijima, K. *et al.*, Appl. Radiat. Isot. 57 (2002) 443-449.

[4] Schlyer, D. J. *et al.*, Appl. Radiat. Isot. 44 (1993) 1459-1465.

[5] Shiue, C. Y. *et al.*, J. Nucl. Med. 26 (1985) 181-186.

[6] Solin, O. *et al.*, Appl. Radiat. Isot. 39 (1988) 1065-1071.

[7] Maeding, P. *et al.*, *Annual Report 2002*, FZR-363, p. 40 and *Annual Report 2003,* FZR-394, p. 31.

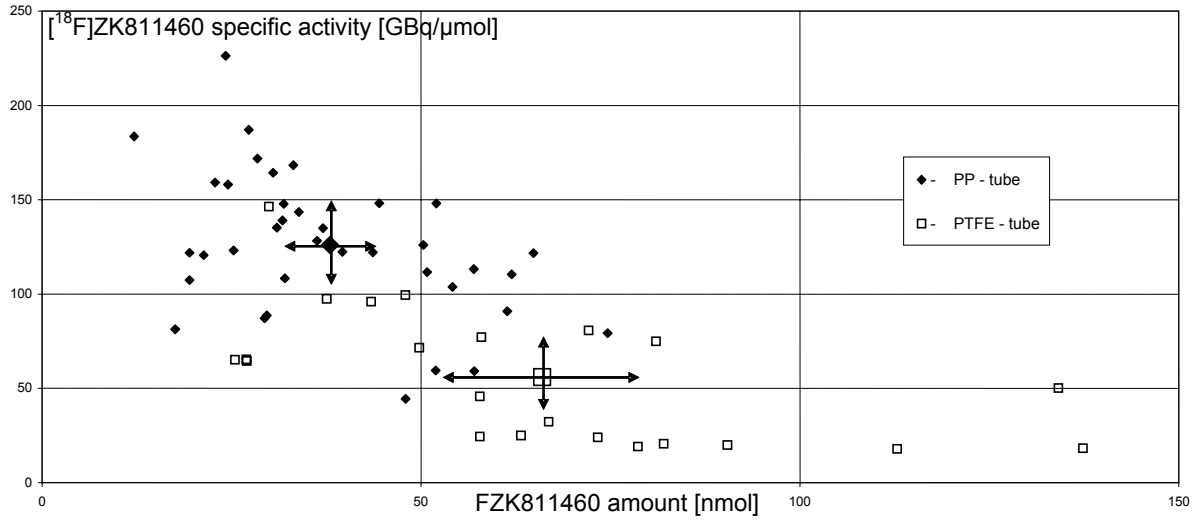
[18F]ZK811460 specific activity [GBq/µmol]
250
200
150
100
50
0
0
50
100
150
FZK811460 amount [nmol]
PP - tube
PTFE - tube

Synthesis of a ^{11}C-Labelled Nonsteroidal Glucocorticoid Receptor Ligand for Imaging Brain Glucocorticoid Receptors (GR)

F. Wüst, T. Kniess, R. Bergmann

*The radiosynthesis of a ^{11}C-labelled nonsteroidal GR ligand **11** is described as an alternative approach for imaging brain GR by means of PET. Compound **11** could be synthesised in 30-40 % radiochemical yield at an specific radioactivity of 20 GBq/µmol within 40-45 min. Preliminary biodistribution studies in Wistar rats showed promising brain uptake of 1.5 % ID/g after 5 min p.i., which decreased to 0.65 % ID/g after 60 min.*

Introduction

The development of GR ligands which are appropriately labelled with short-lived positron-emitting radioisotopes would allow the non-invasive in vivo imaging and mapping of brain GRs by means of PET. For this purpose, various steroidal glucocorticoids have been labelled with the positron emitter ^{18}F. However, none of the investigated compounds were suitable for in vivo visualization of brain GRs with PET [1-3].
An alternative approach is based on the discovery of structurally novel, nonsteroidal small molecules, which show high binding to the GR in the nanomolar range [4-5]. The benzopyrano quinoline-based structure of these GR-binding compounds bears a methoxy group, which is a potential site for radiolabelling with [^{11}C]methyl iodide starting from the corresponding desmethyl labelling precursor **10**.

Results and Discussion

The preparation of compound **10** commenced with commercially available 2,6-dimethoxyphenylboronic acid **1** and involves a multi-step synthesis sequence as shown in Fig. 1 [5].

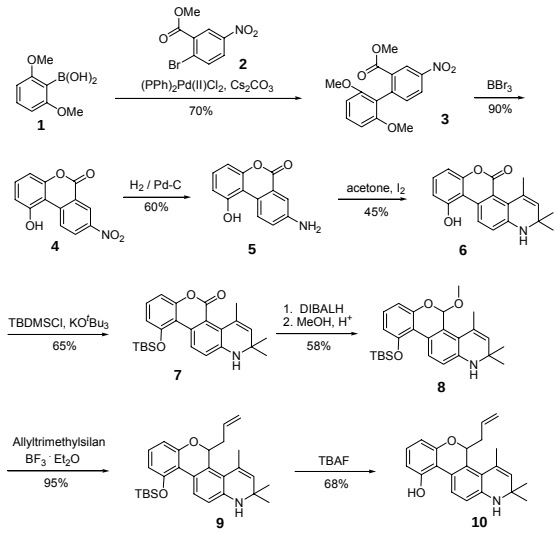

Fig. 1. Synthesis of labelling precursor **10**.

The reaction of phenol **10** with [^{11}C]methyl iodide was performed in an automated synthesis module (Nuclear Interface, Münster). [^{11}C]Methyl iodide was prepared via the "wet" chemistry route, involving $LiAlH_4$ reduction of [^{11}C]CO_2 and subsequent treatment with HI (57 %).
[^{11}C]Methyl iodide was trapped in a DMF solution containing labelling precursor **2** and NaOH as the base (Fig. 2).

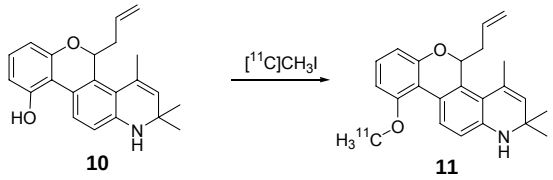

Fig. 2. Radiolabelling of **10** with [^{11}C]MeI.

The methylation reaction was accomplished within 5 min at 100 °C, and the product was purified by semi-preparative HPLC. The total synthesis time including [^{11}C]methyl iodide preparation, synthesis of ^{11}C-labelled compound **11** and HPLC-purification was 40-45 min. Compound **11** was obtained in a radiochemical yield of 30-40 % (decay-corrected, related to [^{11}C]CO_2). Starting from 20 GBq [^{11}C]CO_2, specific radioactivities ranging from 15 to 20 GBq/µmol were reached at the end of the synthesis. The radiochemical purity of **11** exceeded 98 %.
Preliminary biodistribution studies of compound **11** in Wistar rats demonstrated a brain uptake of 1.5 % ID/g after 5 min p.i., which decreased to 0.65 % ID/g after 60 min.

Financial support of this work by the IIS Central European Division is gratefully acknowledged.

References

[1] Wüst, F. *et al.*, J. Labelled Compd. Radiopharm. 46 (2003) S142.
[2] Pomper, M. G. *et al.*, Nucl. Med. Biol. 19 (1992) 461.
[3] Feliu, A. L. *et al.*, J. Nucl. Med. 28 (1986) 998.
[4] Elmore, S. W. *et al.*, J. Med. Chem. 44 (2001) 4481.
[5] Kym, P. R. *et al.*, J. Med. Chem. 46 (2003) 1016.

Synthesis of [^{11}C]CH_3I by Iodination of [^{11}C]CH_4 in a Synthesis Module

T. Kniess, F. Wüst

The synthesis procedure of [^{11}C]CH_3I via [^{11}C]CH_4 using the remotely controlled synthesis module TRACERlab FX_C is described.

Introduction

[^{11}C]CH_3I is an important labelling precursor in ^{11}C-chemistry. It is usually prepared by the "wet chemistry route" involving reduction of cyclotron produced [^{11}C]CO_2 with $LiAlH_4$ to [^{11}C]CH_3OH, followed by hydrolysis and iodination with hydrogen iodide. In general this procedure suffers from low specific activity of [^{11}C]CH_3I since $LiAlH_4$ readily adsorbs CO_2 from air. Thus, $LiAlH_4$ has to be handled with great care in suitable glove boxes prior use to avoid any potential CO_2 contamination from air. Moreover, the aqueous iodination with HI requires careful and laborious cleaning and drying procedures of the synthesis module, which limits the number of [^{11}C]CH_3I syntheses to not more than one per day.

To circumvent these obstacles an alternative gas phase iodination of [^{11}C]CH_4 has been developed [1, 2]. An automated synthesis module for [^{11}C]CH_3I preparation employing this principle has been commercially available recently by GE Medical Systems. The PET Center Rossendorf is operating such a TRACERlab FX_C module since 2004, and first experiences of operation are reported herein.

Results and Discussion

The scheme of [^{11}C]CH_3I production is shown in Fig. 1, which also serves as operation panel for the synthesis module. [^{11}C]CO_2 produced via ^{14}N[p,α]^{11}C nuclear reaction is converted into [^{11}C]CH_4 by reduction with hydrogen on a Ni-catalyst at 400 °C.

The produced [^{11}C]CH_4 is trapped on Carbosphere under liquid nitrogen cooling at -140 °C for purification and concentration. Unconverted [^{11}C]CO_2 and formed H_2O are trapped on Ascarite (NaOH). The purified [^{11}C]CH_4 is than allowed to react with iodine at 720 °C to form [^{11}C]CH_3I in a gas circulating process system, where formed HI is trapped in an additional Ascarite trap. [^{11}C]CH_3I is trapped on a Porapak Q trap at room temperature while unconverted [^{11}C]CH_4 re-enters the circulation process. At the end of the circulation process the collected [^{11}C]CH_3I is released from the Porapak Q trap in a stream of He at 190 °C and distilled into the reaction vessel to perform the labelling reaction.

In a typical experiment 8.0 GBq of [^{11}C]CO_2 could be converted into 5.3 GBq of [^{11}C]CH_4 and 3.0 GBq of [^{11}C]CH_3I after 15 minutes. The radiochemical yield of [^{11}C]CH_3I synthesis is 60 % (decay-corrected).

References

[1] Prenant, C. *et al.*, J. Labelled Compd. Radiopharm. 30 (1991) 125-131.

[2] Larsen, P. *et al.*, Appl. Radiat. Isot. 48 (1997) 153-157.

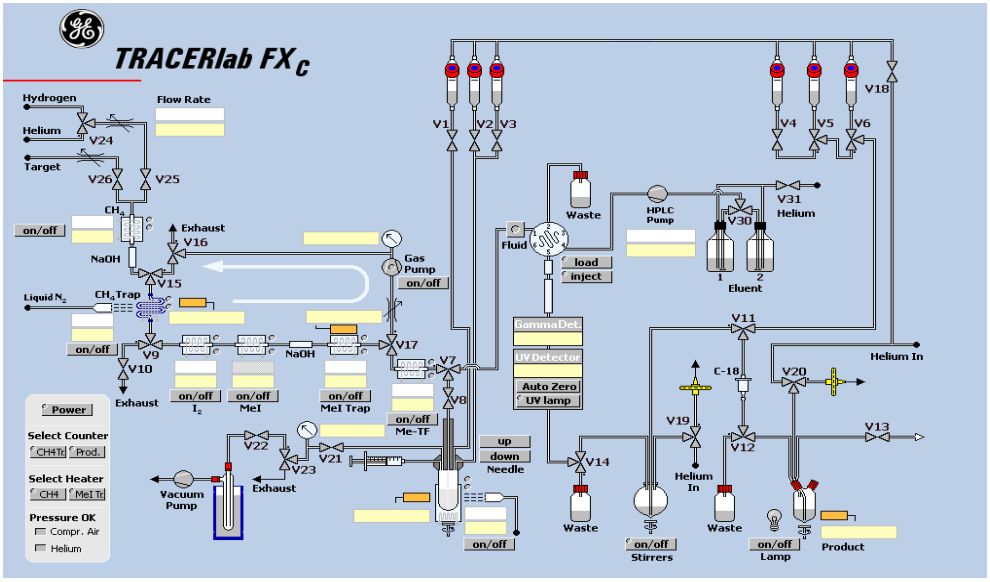

Fig. 1. [^{11}C]CH_3I production scheme.

Synthesis of ^{11}C-Methylated Mercaptoimidazole Piperazinyl Derivatives as Potential Radioligands for Imaging 5-HT$_{1A}$ Receptors by PET

T. Kniess, R. Garcia[1], A. Paulo[1], I. Santos[1], R. Bergmann, F. Wüst
[1]*Instituto Tecnologico e Nuclear (ITN), Sacavem, Portugal*

*Two novel 5-HT$_{1A}$ receptor binding 2-mercaptoimidazole derivatives **1** and **2** were labelled with ^{11}C through methylation of the thioketone functionality with [^{11}C]CH$_3$I in radiochemical yields of 20-30 % within 40 min including HPLC-purification in 99 % radiochemical purity. The brain uptake of the radioligands was determined by preliminary biodistribution studies.*

Introduction

Central 5-HT$_{1A}$ receptors are implicated in the pathophysiology of major neuropsychiatric diseases such as schizophrenia, anxiety and depression. The functional imaging of the 5-HT$_{1A}$ receptors by PET represents an innovative approach for a non-invasive assessment of those disorders. The identification of WAY-100635 as a potent and selective antagonist for the 5-HT$_{1A}$ receptor was accompanied by attempts to label the compound with ^{11}C [1, 2]. The replacement of the piperazinyl amide group by fragments of the mercaptoimidazole type would allow straightforward alkylation of thioketone functionality with [^{11}C]CH$_3$I. Herein we report on the radiosynthesis and biodistribution of two ^{11}C-methylated mercaptoimidazole piperazinyl derivatives **3** and **4**.

Results and Discussion

The synthesis of labelling precursors **1** and **2** was accomplished by multi-step procedures starting from 4-[(2-methoxyphenyl)-1-piperazinyl]-butylamine [3]. Corresponding reference compounds were synthesised by the reaction of thioketones **1** and **2** with methyl iodide in ethanolic solution in the presence of NaOH at room temperature.
S-Methylation of thioketones **1** and **2** with [^{11}C]CH$_3$I was performed by means of an automated synthesis module to give the desired radiolabelled compounds **3** and **4**, respectively (Fig. 1).

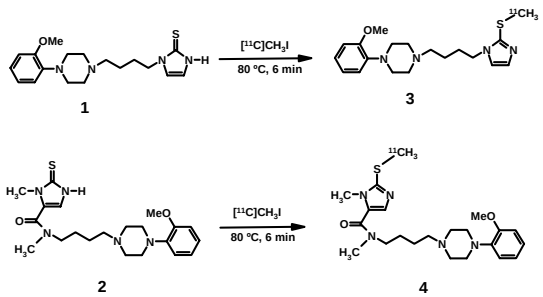

1 3

2 4

Fig. 1

[^{11}C]CH$_3$I was synthesised in a ^{11}C-methylation synthesis module (GE-Medical Systems) by reduction of cyclotron produced [^{11}C]CO$_2$ with LiAlH$_4$ followed by hydrolysis and iodination with HI.
After distillation of approximately 3700 MBq of [^{11}C]CH$_3$I into a second reaction vessel containing 1.0-1.5 mg of labelling precursor in ethanol the methylation was carried out at 80 °C for 6 min. Afterwards, radioligands **3** and **4** were purified by semi-preparative HPLC using isocratic elution with acetonitrile/aqueous NEt$_3$ (70/30). Under these conditions **3** and **4** could nicely be separated from excess of precursor and very low amount of non-reacted [^{11}C]CH$_3$I. Typically, 900 MBq of the radioligand were obtained in radiochemical yields of 20-30 % within 40 min.
Biodistribution studies of **3** and **4** were performed in male Wistar rats to evaluate brain uptake and brain radioactivity retention. Table 1 summarizes the biodistribution data.

Table 1

Organ	% ID/g			
	[^{11}C]**3**		[^{11}C]**4**	
	5 min	60 min	5 min	60 min
Blood	0.11 ± 0.02	0.10 ± 0.03	0.12 ± 0.03	0.04 ± 0.00
Cerebellum	0.82 ± 0.13	0.14 ± 0.03	0.29 ± 0.04	0.14 ± 0.01
Brain	1.14 ± 0.11	0.18 ± 0.04	0.37 ± 0.04	0.16 ± 0.01
Pancreas	4.16 ± 0.51	5.85 ± 0.84	3.34 ± 0.57	1.86 ± 0.13
Spleen	1.48 ± 0.26	0.92 ± 0.19	1.27 ± 0.17	0.51 ± 0.07
Adrenals	3.77 ± 1.03	1.11 ± 0.16	7.95 ± 3.09	7.32 ± 0.75
Kidneys	2.85 ± 0.43	0.81 ± 0.16	2.56 ± 0.32	1.09 ± 0.15
Heart	0.49 ± 0.08	0.19 ± 0.03	0.41 ± 0.08	0.10 ± 0.01
Lung	1.68 ± 0.19	0.48 ± 0.06	1.14 ± 0.17	0.33 ± 0.07
Liver	0.80 ± 0.18	1.37 ± 0.35	1.33 ± 0.28	2.75 ± 0.72

Both compounds **3** and **4** were able to cross the blood brain barrier showing an initial brain uptake after 5 min of 1.14 and 0.37 % ID/g, respectively. However, a drastically reduced level of radioactivity in the brain was observed after 60 min.

References

[1] Mathis, C. A., *et al.,* Life Sci. 55 (1994) 403-407.
[2] McCarron, J. A. *et al.,* J. Labelled Compd. Radiopharm. 38 (1996) 941-953.
[3] Garcia, R. *et al.,* J. Labelled Compd. Radiopharm. (submitted).

A Novel Approach for ^{11}C-C Bond Formation: Hydrozirconation/^{11}C-Methylation of Prop-1-ynyl-benzene with [^{11}C]MeI

F. Wüst, P. Mäding

*The hydrozirconation/^{11}C-methylation of prop-1-ynyl-benzene **1** with [^{11}C]MeI as novel approach for ^{11}C-C bond forming reactions is described.*

Introduction

Distinct ^{11}C-C bond forming reactions via various transition metal-mediated reactions have been in the focus of radiochemical research for more than one decade [1-3]. Many metal-mediated reactions known from synthetic organic chemistry have successfully been introduced into ^{11}C chemistry, and research on novel ^{11}C-C bond formations is still of great interest.

In this report we describe the palladium-mediated reaction of alkenyl-zirconium derivatives with [^{11}C]MeI as a novel synthetic route for ^{11}C-C bond formations.

Results and Discussion

The α,α`-dimethyl alkene group is a common structural motif in many biological active compounds, namely phenyl group-containing molecules. The isotopic substitution of one of the two methyl groups present in α,α`-dimethyl alkene groups with a [^{11}C]methyl group represents an interesting approach to form corresponding ^{11}C-labelled compounds.

A commonly employed strategy to form α,α`-disubstituted alkenes comprises the formation of alkenylzirconium(IV) complexes by the cis-insertion of a C-C triple bond into the Zr-H bond of Schwartz`s reagent [$Cp_2Zr(H)Cl$] followed by metal-mediated C-C bond formation with electrophiles under retention of the configuration of the C-C double bond [4-5].

The principle feasibility of the approach was elaborated by the synthesis of 2-[^{11}C]methyl-propenyl benzene **3** via hydrozirconation/^{11}C-methylation of prop-1-ynyl-benzene **1** with [^{11}C]MeI as a model reaction (Fig. 1).

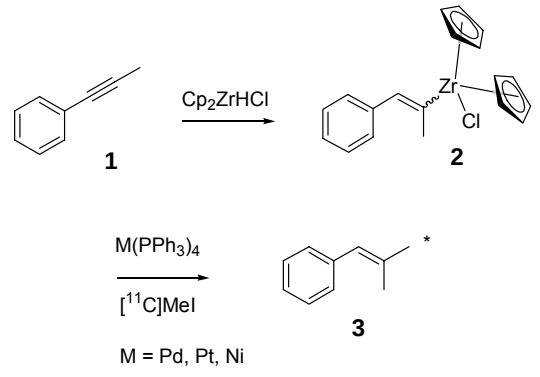

Fig. 1. ^{11}C-labelling via hydrozirconation/^{11}C-methylation

Prop-1-ynyl-benzene **1** was treated with 1.2 equiv. of Schwartz reagent in THF at room temperature. Formation of alkenylzirconium(IV) complex **2** could be monitored by formation of a clear orange-coloured solution. Alkenyl-zirconium(IV) complex **2** was treated with 5 mol % $M(PPh_3)_4$ (M = Ni, Pd, Pt) prior distillation of [^{11}C]MeI into the solution. The reaction mixture was heated at 60 °C for 5 min. The results are summarised in Table 1.

Table 1. Radiochemical yields of transition metal-mediated reaction of alkenyl-zirconium(IV) complex **2** with [^{11}C]MeI

Transition metal complex	Radiochemical yield [%]
$Ni(PPh_3)_4$	4
$Pd(PPh_3)_4$	70
$Pt(PPh_3)_4$	11

The radiochemical yields were determined by radio-HPLC representing the percentage of radioactivity area of ^{11}C-labelled product **3** related to the total radioactivity area.

The results clearly show that the use of transition metal complex $Pd(PPh_3)_4$ is superior to $Ni(PPh_3)_4$ and $Pt(PPh_3)_4$, respectively. Thus, sufficient radiochemical yields of 70 % could be obtained when $Pd(PPh_3)_4$ was used as the metal complex in the cross-coupling reaction.

Conclusion

The palladium-mediated cross-coupling reaction of in-situ-generated alkenyl-zirconium(IV) complexes with [^{11}C]MeI as novel method for ^{11}C-C bond formations was developed. The extension of this labelling approach toward phenyl group-containing compounds with biological relevance is currently in progress.

References

[1] Wüst, F. Trends Org. Chem. 10 (2003) 61-70.

[2] Langström, B. *et al.*, Acta Chem. Scand. 53 (1999) 651-669.

[3] Antoni, G. *et al.,* in: Welch, M. J., Redvanly, C. S. (eds.), Handbook of Radiopharmaceuticals (2003) pp. 441-465.

[4] Wipf, P. *et al.,* Tetrahedron 52 (1996) 12853-12910.

[5] Negishi, E. *et al.*, J. Am. Chem. Soc. 99 (1977) 3168-3170.

Metabolism of [^{11}C]SMe-ADAM in the Rat

B. Pawelke, R. Bergmann, J. Zessin

The blood kinetics and metabolisation of the radiotracer N,N-dimethyl-2-(2-amino-4-[^{11}C]methylthiophenylthio)-benzylamine ([^{11}C]SMe-ADAM) was evaluated in rats.

Introduction

Alterations of serotonin transporters (SERT) are implicated in a large number of psychiatric disorders. The first generation radiotracer for SERT imaging by PET techniques was (+)-[^{11}C]McN 5652 [1]. New compounds should exhibit lower nonspecific binding in the brain, higher plasma free fraction, and faster plasma clearance and brain uptake kinetics, enabling measurement of SERT parameters in a shorter scanning time. The purpose of this study was to evaluate the blood kinetics and metabolism in rats of the new PET radioligand for the SERT, N,N-Dimethyl-2-(2-amino-4-[^{11}C]methyl-thiophenylthio)benzylamine ([^{11}C]SMe-ADAM). The tracer was synthesized from its thiophenol precursor by reaction with [^{11}C]methyl iodide [2].

Results and Discussion

Blood kinetics

The ^{11}C-activity clearance from rat blood was evaluated by arterial blood samples and by measurements of the time activity distribution in a region of interest (ROI) over the heart.
After an initial, rapid distribution phase, plasma activity stabilized at relatively constant levels for the tracer.

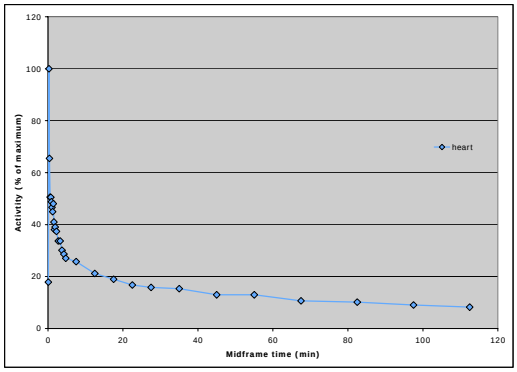

Fig. 1. Time-activity curve extracted from a heart ROI of dynamic microPET images after single intravenous injection of [^{11}C]-SMe-ADAM in a rat.

Metabolic investigations

Metabolisation of the radioligand [^{11}C]-SMe-ADAM was investigated in blood and brain of rats after *i.v.* application. A quite fast peripheral metabolism of the radiotracer was stated. 10 min after administration the main portion of radioactivity in plasma samples was assigned to hydrophilic metabolites whereas less than 18 % of the activity represented the un-changed radiotracer. 60 min after injection the portion of the non-metabolized tracer had dropped to only 2 %.
In contrast to these observations, only the signal of the original compound [^{11}C]-SMe-ADAM was detected in brain sections 60 min after tracer application (striatum + thalamus, cerebellum) revealing that no passage of me-tabolites through the blood-brain-barrier occurs (for examples, see Fig. 2).

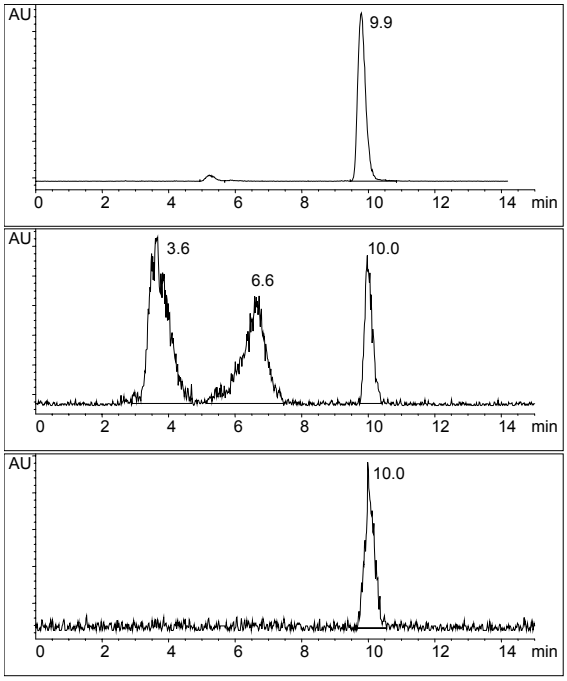

Fig. 2. RadioHPLC of the tracer before injection, plasma 10 min *p.i.* and brain homogenate (striatum + thalamus) 60 min *p.i.* (from top).

References

[1] Suehiro, M. *et al.*, J. Nucl. Med. 34 (1993) 120-127.
[2] Zessin, J. *et al.*, J. Labelled Compd. Radio-pharm. 46 (2003) S146.

Animal PET Studies with [^{11}C]SMe-ADAM

R. Bergmann, J. Zessin

Biodistribution of [^{11}C]SMe-ADAM was studied by animal PET and showed suitable characteristics for imaging SERT in the living brain.

Introduction

The serotonin transporter (SERT) regulates the entire serotoninergic system and its receptors via modulation of extracellular fluid serotonin concentrations. Differences in SERT expression and function show associations with multiple human disorders and with side effects during treatment with antidepressant SERT antagonists, namely, the serotonin reuptake inhibitors (SRIs). Therefore, the in vivo distribution and kinetics of specific SERT binding radiotracers could give important information about the functional expression of the SERT. The biokinetics of the SERT binding radiotracer [^{11}C]SMe-ADAM was studied in rat brain to evaluate the potential of this compound to image the SERT in vivo.

Biodistribution and microPET imaging studies

Kinetic biodistribution studies were done in male Wistar rats by tail vein injection of [^{11}C]SMe-ADAM followed by brain dissection and tissue counting.
PET imaging was performed with a microPET® P4 primate model scanner (CTI Concorde Microsystems Inc. Knoxville, TN). No correction for recovery and partial volume effects was applied.
The brain distribution of the radiotracer showed a increasing specific accumulation in the striatum and thalamus, as regions with high SERT concentrations (Table 1, Fig. 1).

Table 1. Regional brain uptake and specific binding of the radiotracer [^{11}C]SMe-ADAM in male Wistar rats [a]

Time (min)	Striatum	Thalamus
5	3.16 ± 0.51	3.59 ± 0.41
	(1.72 ± 0.10)	(1.94 ± 0.73)
10	2.43 ± 0.39	3.04 ± 0.58
	(1.81 ± 0.30)	(2.28 ± 0.19)
30	2.41 ± 0.48	3.58 ± 0.40
	(2.73 ± 0.27)	(4.03 ± 1.50)
60	1.78 ± 0.30	2.86 ± 0.20
	(4.15 ± 0.17)	(6.74 ± 0.95)

[a] Regional brain uptake is represented as %ID/g (mean ± SD, 3 animals per group); specific binding (in parentheses) is expressed as ratio of activity in the tissues to that of the cerebellum.

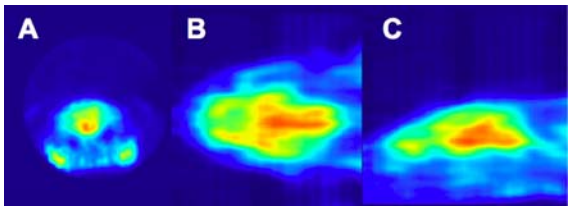

Fig. 1. Coronal (A), sagittal (B), and transversal (C) images of rat brain at 30 min after injection of 11 MBq of [^{11}C]SMe-ADAM (15 min acquisition).

The corresponding time-activity curves describing the kinetics of [^{11}C]SMe-ADAM binding in thalamus and cerebellum are presented in Fig. 2.

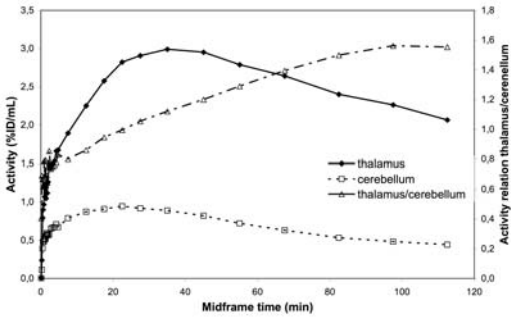

Fig. 2: Representative time activity curves of the [^{11}C]SMe-ADAM distribution in the rat brain measured with microPET®. Points represent the activities measured in the thalamic region (open circles), in the cerebellum (open triangles) and the activity relation between thalamus and cerebellum (closed squares) in one experiment.

The radioactivity concentration in the SERT-rich region thalamus increased during the first 25 min, peaked between 30 and 50 min, and decreased slowly after this time. The specific binding of [^{11}C]SMe-ADAM expressed as the ratio of radioactivity concentration in the SERT rich region thalamus and the reference region cerebellum increased up to 90 min to a plateau of 1.5 thereafter remains constant. This suggests a saturable specific binding of [^{11}C]SMe-ADAM, which is a favourable feature for quantitative analysis of PET images. Additionally, as the metabolism analysis showed, the measured activity was identical with the [^{11}C]SMe-ADAM compound, so that estimations of the SERT *in vivo* should be possible.

References

[1] Pawelke, B. *et al., this report*, p. 36.

Evaluation of ^{18}F-Labelled Annexin V: Apoptosis Imaging in Mice

R. Bergmann, C. Hultsch, B. Pawelke, J. Pietzsch, S. Bergmann[1], S. Zijlstra[2], J. Gunawan[2], W. Burchert[2], J. van den Hoff

[1]Universitätsklinikum Dresden, [2]Herz- und Diabeteszentrum Bad Oeynhausen

The biodistribution of ^{18}F-labelled annexin V and ^{18}F-labelled albumin in mice was analysed and compared in a model system of apoptosis. The distribution of both proteins in apoptotic regions was similar. Only at high liver destruction the accumulation of ^{18}FB-annexin was higher than that of ^{18}FB-albumin.

Apoptosis imaging with PET plays an increasing role in various medical fields like oncology, cardiology, transplant rejection, and inflammation, but the radiotracer distribution in the tissues is influenced by various mechanisms. In this study a recombinant annexin-V derivative and human serum albumin (HSA) were radiolabelled using N-succinimidyl-4-^{18}F-fluorobenzoate (SFB) [1], and characterised. Mechanism and specificity of both ^{18}F-annexin-V and ^{18}F-HSA biodistribution and accumulation were examined in rodents.

Recombinant annexin-V derivative and HSA were radiolabelled using SFB and the products were confirmed by size exclusion chromatography and SDS-PAGE. The radiotracer distributions in animals were studied in rats and mice *ex vivo* by organ extraction, autoradiography, and *in vivo* with animal PET. For apoptosis imaging, ^{18}F-annexin-V or ^{18}F-HSA were intravenously applied in 4 groups of mice that received either intraperitoneal 100 µl Anti-Fas antibody in 200 µl isotonic NaCl or 200 µl isotonic NaCl 2 hours before the radiotracer. The degree of liver apoptosis was characterised by plasma (Alanine-Amino-Transferase) ALAT and (Aspartat-Amino-Transferase) ASAT activity measurements.

The radiochemical yield was in the range of 10 to 30 % (corrected for decay) with a specific activity of more than 20 GBq/µmol.
The accumulation of ^{18}F-annexin-V and ^{18}F-HSA, respectively in the apoptotic livers (4–16 %ID/g) were correlated to the ASAT and increased up to 4 times in comparison to control. The biodistribution of the tracers were comparable except for the renal elimination of ^{18}F-annexin-V, which was up to 3 times higher than of ^{18}F-HSA.

The blood clearance of ^{18}F-annexin-V was faster than the elimination of ^{18}F-HSA from the blood.

^{18}F-annexin-V seems to be a PET-tracer for apoptosis imaging. The increasing accumulation of ^{18}F-HSA (Fig. 1) with increasing liver destruction in the used model could be interpreted as a degradation of the blood vasculature in the acute apoptosis, induced by the anti-Fas antibodies. Thus, in PET measurements of apoptosis, using ^{18}F-annexin V tissue reactions should be taken into account.

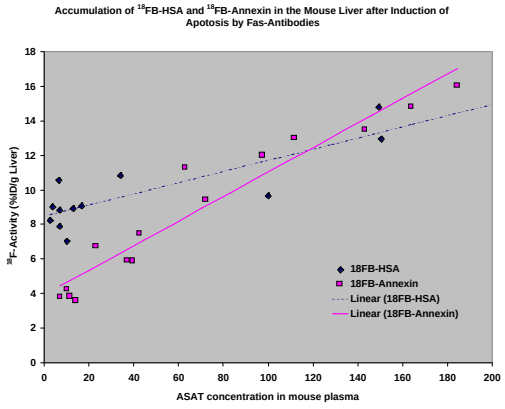

Fig. 1. Accumulation of ^{18}FB-HAS and ^{18}FB-annexin in the mouse liver after induction of apoptosis by Fas-antibodies.

References

[1] Mäding *et al.*, *this report*, p. 26.

Molecular and Biochemical Characterisation of Neurotensin Receptor-1 (NTR-1) in Different Tumour Cell Lines

C. Haase, R. Bergmann

The enhanced expression of Neurotensin Receptor-1 (NTR-1) mRNA in different tumour cell lines could be used as a specific diagnostic marker, e.g. in pancreatic cancer. The functional expression of the NTR-1 was studied on the mRNA and protein level in HT-29 and FaDu cells by RT-PCR and 2D-electrophoresis followed by Western blot.

Introduction

The human NTR-1 consists of 418 amino acids and belongs to a large superfamily of receptors coupled to G-proteins with seven transmembrane spanning regions (Fig. 1). The increasing interest for peptide receptors in cancer is the possibility of receptor targeting. It has already be shown that these receptors are only overexpressed in cancer, in comparison to their expression in normal tissue. To achieve better insight into the disease mechanism, it is important to better understand the molecular characteristics of pancreatic cancer [1, 2].

Fig. 1. Schematic drawing of the NTR in the three-dimensional space. Blue: helix 1; light blue: helix 2 + extracellular loop 1 + helix 3; red: helix 4 + extracellular loop 2 + helix 5; brown: helix 6 + extracellular loop 3 + helix 7.

Results and Discussion

For preparation of total RNA from HT29/WiDr (colorectal adenocarcinoma) and FaDu (squamous cell carcinoma) cells, an RNA isolation kit was used. The purity and integrity of RNA were analysed by measuring the absorbance ratio at A_{260}/A_{280} as well as by electrophoresis on a 1 % agarose gel. RT-PCR was performed with mRNA as template and 5´and 3´PCR primer specific for the human NTR-1 sequence. Products were analysed on a 1,5 % agarose gel.

As shown in Fig. 2, the 893-bp product resulting from primers against NTR-1 sequence was amplified from FaDu (1), HT29 (2) and WiDr cells (3). All three cell lines express the NTR sequence at high level. With the use of these two primers no more possible isoforms could be detected. Further studies will be done for RNA quantification in these cells and in different tumour mouse models.

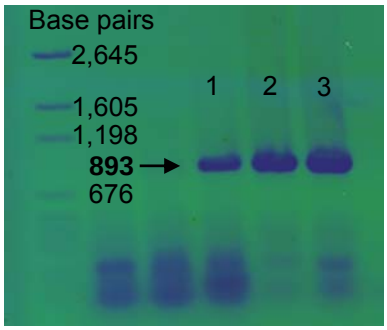

Fig. 2. RT-PCR with human specific NTR-1 primers (1 FaDu cells, 2 HT29 cells and 3 WiDr cells)

For Western blot and 2D-gel electrophoresis membrane proteins were extracted from FaDu, HT29 and WiDr cells by detergent based protein extraction utilizing the selective solubilisation of proteins afforded by detergents.

Immunoblot analysis of NTR-1 expression with human polyclonal NTR-1 antibody was detectable in all three cell lines with a molecular range of 48-50 kDa. The analysis of 2D-elctrophoresis (Fig. 3a) with following immunoblot (Fig. 3b) resulted in two apparent spots (Fig. 2).

For further studies of the protein structure (splice forms [3] or protein modifications) the spots from membrane were used for MALDI-MS analysis.

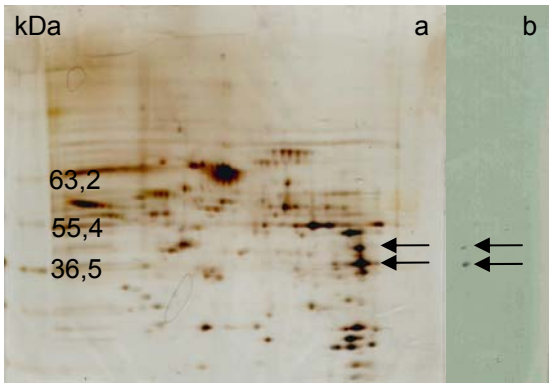

Fig. 3. 2D-gel and Western blot analysis of HT29 cells

References

[1] Reubi, J. C., Endocrine Rev. 24 (2003) 389-427.

[2] Pettibone, D. J. *et al.*, JPET 300 (2002) 305-313.

[3] Heymann, S. *et al.*, *this report*, p. 40.

Prediction of Alternative Spliceforms of the Neurotensin Receptor-1

S. Heymann[1], R. Bergmann
[1]*Humboldt University Berlin, Institute of Computer Science*

Possible alternative spliceforms of the neurotensin receptor-1(NTR-1) were predicted and an extracellular peptide sequence was identified, which could be important in receptor function regulation.

Introduction

Pancreatic cancer is an extremely aggressive malignant disorder with a definitely poor prognosis. The clinical characteristics of pancreatic cancer are much influenced by many different mechanisms and signals, like growth factors, growth factor receptors, apoptosis-inhibiting genes. Neurotensin is a neurotransmitter, which can also induce growth stimulation mediated via NTR. Autoradiographic binding analysis in resected pancreatic cancer revealed the presence of high levels of NTR-1 binding sites in 75 % of pancreatic cancers, suggesting that gastrointestinal hormones and neurotransmitters might also be involved in the regulation of pancreatic cancer cell behaviour [1]. It seems to be surprising that by NTR-1 autoradiography, only pancreatic cancer samples and not chronic pancreatitis (CP) samples exhibited increased NT binding. Wang [1] discussed, that it is probable that in CP NTR-1 mRNA is not translated into protein, which may result in low NTR-1 binding capacity, and alternatively, it is possible that in CP, most of the NTRs are occupied and thereby masked by endogenous NT, which is increased in the serum, and that this does not happen in pancreatic cancer, in which the serum levels of NT are lower.
We hypothesized that the discrepancy between mRNA and functional NTR-1 could be also a result of alternative spliceforms of the NTR-1. In this project, possible alternative spliceforms of the NTR-1 were predicted using a protein domain homology method [2].

Method

Alternative splicing can yield manifold different mature mRNAs from primary transcripts. Numerous studies revealed that alternative splicing occurs much more often than previously assumed. In particular, various protein sequences obtained from cDNA libraries of malignant tissues turned out to be aberrant spliceforms [3]. Computerized *alternative spliceform simulation* aims at biological knowledge acquisition [2], addressing a protein diversity problem. Applied to NTR-1, putative spliceforms were screened for effects on ligand binding. The yellow peptide in Fig. 2 is common to known and aberrant spliceforms, but differentially affected (Fig. 1) by a distant domain.
Fig. 1 illustrates how sensitive a hormone receptor responds to the loss of a small portion due to alternative splicing: Because of this loss, the important disulphide bridge could not be formed.

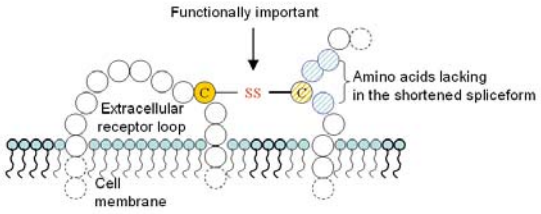

Fig. 1. Alternative spliceform prediction for cell surface protein studies

Results

The analysis of the NTR-1 genes showed a splicing sensitive peptide sequence (Fig. 2), which could be used as signal in further functional analysis of the NTR-1 using receptor binding assays, aptamers, 2D-electrophoresis and MALDI-MS [4].

Fig. 2. Target peptide sequence on NTR-1

References

[1] Wang, L. et al., Clin. Cancer Res. 6 (2000) 566-571.
[2] Hiller, M. et al., In silico Biology 4 (2004) 0017.
[3] Xu, Q. & Lee, C., Nucl. Ac. Res. 31 (2003) 5635-5643.
[4] Haase, C. *et al., this report*, p. 39.

Preparation of [^{86}Y]YCl_3 Solution for Labelling of Functionalised Biomolecules

S. Seifert, St. Preusche, J. Schlesinger, U. Schwarz[1], F. Wüst
[1]AEA Technology QSA GmbH, Braunschweig

The metallic positron emitter ^{86}Y has been produced using the solid target system at the Rossendorf CYCLONE 18/9 cyclotron. A separation protocol was developed to obtain ^{86}Y suitable to meet the high quality standard for labelling appropriately functionalised biomacromolecules like proteins and peptides.

Introduction

^{86}Y is a potentially better suited radionuclide than ^{111}In for the estimation of an absorbed dose in ^{90}Y therapy. The positron emitter ^{86}Y ($T_{1/2}$ = 14.7 h) is produced via the ^{86}Sr(p,n)^{86}Y nuclear reaction using enriched $^{86}SrCO_3$ as the target material. Two of the most crucial aspects for successful application of radiometals in any targeted radiotherapy or imaging application are related to the radionuclear and chemical purity of the radioisotope. The presence of metal contamination diminish labelling efficiencies, which may even lead to a complete radiolabelling failure of chelate conjugated biomolecules. Thus, elaboration of a simple, rapid, and highly efficient purification method is of paramount importance. To meet these requirements, we have established a separation/purification method developed in collaboration with AEAT. Moreover, a recycling procedure for sufficient target material recovery was elaborated.

Results and Discussion

In 2004 a total number of 18 irradiations of $^{86}SrCO_3$ were performed. Using 70 mg of the enriched target material pressed into a Pt target holder (Fig. 1), a 14 MeV proton beam with a beam current of 8 µA, and an irradiation time of 80 min, 1.7–1.8 GBq of ^{86}Y could be produced at EOB.

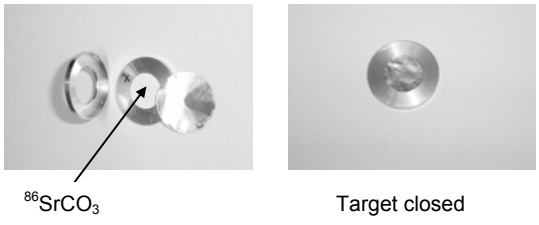

Fig. 1. Pt target holder with $^{86}SrCO_3$

After dissolution of the irradiated target material in hydrochloric acid, the separation of yttrium from the strontium solution is achieved by a chromatographic material supplied by AEAT. About 40 % of the starting ^{86}Y activity can finally be recovered in 1 N HCl. The solution is evaporated, and the residue is heated up to 400 °C in a heating block. After cooling the ^{86}Y activity is re-dissolved in 500 µl of 0.04 N HCl.

The final solution is analysed for chemical and radionuclear impurities by ICP-MS, γ-spectrometry, and a DTPA binding test.

It could be shown that ^{86}Y solutions of high purity are obtained when ultrapure chemicals, carefully purified vials and other devices are used to prevent any metal contamination. The found M^{3+} impurities (Al^{3+}, Fe^{3+}) are in the range of 20 - 25 µg/l when the irradiated target material $^{86}SrCO_3$ is removed from the Pt target holder using a special “dry” ejection method which circumvents the contact of the Pt target holder with hydrochloric acid.

The low M^{3+} concentrations are confirmed by positive results of the DTPA binding test, which was developed by AEAT. The test is performed with 0.1 ml each of two concentrations of DTPA (10 µg/ml and 0.1 µg/ml) in neutral solution buffered with potassium acetate. The radiolabelling yield is determined by TLC [silicagel//0.1 M potassium acetate pH 6/10 % ammonia (50/50)]. The ^{86}Y-DTPA complex moves with the solvent front while non-bound ^{86}Y remains at the origin. The final [^{86}Y]YCl_3 solution exhibits DTPA-binding of >95 % when 0.1 ml of DTPA solution (0.1 µg/ml) is used.

The results of γ-spectrometric analyses show that only 0.04 % of the long-lived isotop ^{88}Y are formed under the irradiation conditions mentioned above.

^{86}Y ($t_{1/2}$ = 0.608 d): 98.20 %
^{87}Y ($t_{1/2}$ = 3.346 d): 0.48 %
^{87m}Y ($t_{1/2}$ = 0.583 d): 1.31 %
^{88}Y ($t_{1/2}$ = 106.63 d): 0.04 % (n = 5)

The costly target material $^{86}SrCO_3$ has to be recycled. That succeeds by precipitation of the strontium chloride solutions with ammonium carbonate. We found that high concentrations of ammonium chloride in the strontium solution may prevent sufficient precipitation of $SrCO_3$. For that reason the strontium carbonate precipitation should be performed seperately from each eluate. Thus, too high amounts of ammonium chloride, which are obtained by pooling the eluates, can be avoided.

Yttrium-86 Labelling of Neurotensin(8-13) Derivatives

J. Schlesinger, R. Bergmann, F. Wüst

Several ^{86}Y complexes with functionalised neurotensin NT(8-13) derivatives were prepared. The radiochemical yield was determined dependent on the amount of functionalised peptide used.

Introduction

The application of appropriately radiolabelled neurotensin(8-13) derivatives should open an innovative approach for diagnosis and therapy of pancreas carcinomas, for 75 % of all pancreas tumours were found to overexpress the neurotensin receptor [1]. For radiolabelling the β^--emitter yttrium-90 and the β^+-*emitter* yttrium-86 represent an interesting "*matched pair*" enabling both, therapy and diagnosis, respectively.

The present work is aimed at acquiring basic radiochemical knowledge on labelling of several functionalised neurotensin(8-13) derivatives with cyclotron-produced n.c.a. yttrium-86 [2]. In this report we describe the fuctionalisation of neurotensin(8-13) (NT(8-13)) with DTPA and DOTA as suitable chelators for forming stable complexes with yttrium and subsequent radiolabelling with yttrium-86.

Results and Discussion

Preparation of DOTA- and DTPA-functionalised NT(8-13) derivatives (Fig. 1)

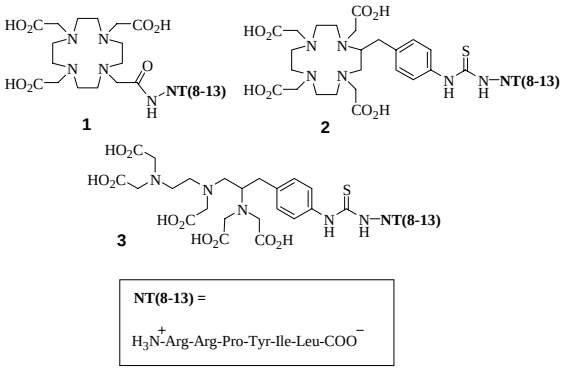

Fig. 1. DOTA- and DTPA-functionalised neurotensin(8-13) derivatives.

The preparation of DOTA-NT(8-13) **1** was carried out by the reaction of DOTA(Bu^t)$_3$ with NT(8-13) in the presence of HATU as activating agent providing DOTA-NT(8-13) conjugate **1** in 31 % yield. Significantly higher yields were obtained when bifunctional chelating agents p-SCN-bz-DOTA and SCN-bz-DTPA were linked to NT(8-13) via formation of a thiourea functionality, being 49 % (DOTA-bz-NT(8-13) **2**) and 92 % (DTPA-bz-NT(8-13) **3**), respectively. However, in contrast to compound **1** compounds **2** and **3** were shown to be fairly unstable under acidic conditions due to EDMAN degradation.

The IC_{50} values of non-radioactive yttrium complexes toward the neurotensin receptor 1 were determined to be 4.7 nM for complex **4** and 4.3 nM for complex **5** using a radiometric binding assay with ^{3}H-labelled NT(8-13) as tracer (IC_{50} ^{3}H-NT(8-13): 0.7 nM). Complexes Y-DOTA-NT(8-13) **4** und Y-DOTA-bz-NT(8-13) **5** were prepared in 68 % and 73 % yield after HPLC-purification (Fig. 2).

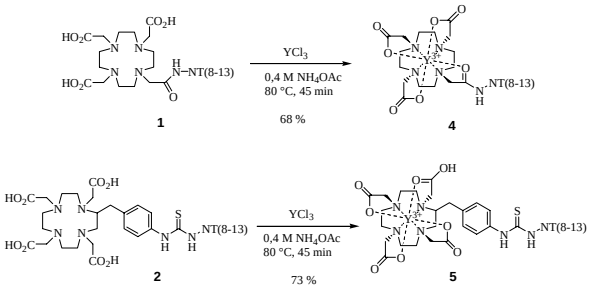

Fig. 2. Synthesis of yttrium-complexes **4** and **5**.

^{86}Y-labelling

The radiolabelling of DOTA- and -DTPA functionalised NT(8-13) derivatives **1**, **2** and **3** with n.c.a. yttrium-86 was studied using different amounts of chelator. The radiochemical yields (RCYs) strongly depend on the amount of DOTA-NT(8-13) **1**, DOTA-bz-NT(8-13) **2** and DTPA-bz-NT(8-13) **3**, which were subjected to the radiolabelling procedure (0.4 M NH_4OAc buffer, 95 °C, 25 min.). The RCYs were determined by means of radio-TLC using RP-18 plates and MeOH/10 % NH_4OH (9:1) as eluent. The RCYs were 91-100 % for [^{86}Y]Y-DOTA-NT(8-13) when 35-250 µg of DOTA-NT(8-13) **1** were used. Lower RCYs were found in the case of thiourea conjugates **2** and **3**, being 65-70 % (25-250 µg of DOTA-bz-NT(8-13) **2**) and 48-95 % (40-330 µg of DTPA-bz-NT(8-13) **3**), respectively.

References

[1] Reubi, J. C. *et al.*, Gut 42 (1998) 546-550.
[2] Preusche, S. *et al.*, *this report*, p. 62.

Technetium and Rhenium Complexes with Modified Fatty Acid Ligands 7. Synthesis and Biological Evaluation of a New Type of Technetium-Labelled Fatty Acids for Myocardial Metabolism Imaging

M. Walther, C. M. Jung, R. Bergmann, J. Pietzsch, K. Rode, W. Kraus[1], H.-J. Pietzsch, H. Spies

[1]*Bundesanstalt für Materialforschung und –prüfung, Berlin*

Technetium-99m '4+1' fatty acid complexes were synthesised and investigated in vivo.

Introduction

To develop technetium-labelled fatty acid analogues for myocardial metabolism imaging, rhenium model complexes and their ^{99m}Tc analogues were synthesised according to the '4+1' mixed-ligand approach and investigated *in vitro* and *in vivo*.
To estimate the diagnostic value of the ^{99m}Tc-labelled fatty acids the compounds were investigated in cell-uptake experiments and in biodistribution studies using male Wistar rats (5–6 weeks old, body weight 151±15 g).

Results and Discussion

The formation of the rhenium models was accomplished by ligand exchange reactions using different pre-formed rhenium precursors.
The rhenium model complexes were completely characterised by NMR, IR, MS, EA and by single crystal X-ray analyses for the C_{15}-derivative in order to determine the geometrical impact of the chelate unit on the fatty acid structure (Fig. 1).

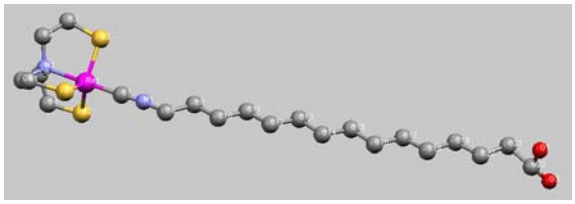

Fig.1. Molecular structure of the $ReNS_3C_{15}$-fatty acid.

The new fatty acid tracers contain the metal core in the oxidation states +3, well-wrapped in a trigonal-bipyramidal coordination moiety which is attached at the omega position of a fatty acid chain. The compounds differ in their chain lengths with 10 or 11 methylene groups and in the insertion of a sulphur atom into the chain. This structural feature is considered to be a good imitate of the well-established iodinated phenyl fatty acids.
Noticable heart uptake of the ^{99m}Tc tracers being in the order of 3.7 % ID/g 5' p.i. and accompanied by a good heart to blood ratio (Fig. 2) confirms the remarkably results of the perfused heart experiments [1].

While the tracers are superior to other described Tc-fatty acid imitates [2, 3] with regard to good heart to blood ratios, heart to liver ratio has to be improved.
For this, chemical modifications will be performed at the chelating part as well as at the alkyl chain.

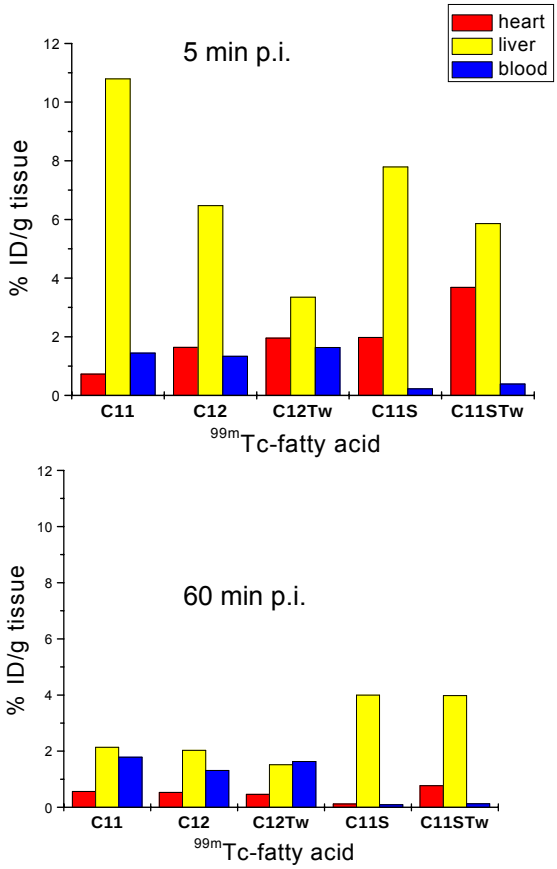

Fig. 2. Heart, liver and blood uptake of selected Tc-fatty acids in Wistar rats, with comparison of experiments under addition of Tw = TWEEN 80.

References

[1] Walther, M. *et al., this report*, p. 35.
[2] Jung, C. M. *et al., Annual Report 2001*, FZR-340, pp. 51-53.
[3] Jung, C. M. *et al., Annual Report 2002*, FZR-363, p. 51 and literature cited therein.

Technetium and Rhenium Complexes with Modified Fatty Acid Ligands
8. Myocardial Extraction of a New Type of Technetium-Labelled Fatty Acids

M. Walther, C. M. Jung, S. Stehr[1], A. Heintz[1], G. Wunderlich[1], H.-J. Pietzsch, J. Kropp[1], A. Deussen[1], H. Spies

[1]*TU Dresden, Medizinische Fakultät Carl Gustav Carus*

Technetium-99m '4+1' fatty acid complexes and well-known iodine labelled fatty acids like IPPA were compared concerning their heart uptake on perfused guinea pig heart studies.

Introduction

Newly developed technetium-labelled fatty acid analogues are promising agents for myocardial metabolism imaging.

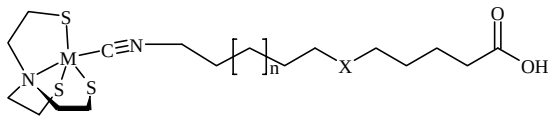

M = Re, ^{99m}Tc, X = C, S, n = 1 -7

The myocardial extraction of eight ^{99m}Tc analogues of rhenium model complexes synthesised according to the '4+1' mixed-ligand approach [1] have been tested in a guinea pig heart-LANGENDORFF model.

Results and Discussion

All substances showed extraction rates in the region of 5 to about 40 %. In particular, experiments with fatty acid analogues C_{11} (39.8 %), but also C_{12} (14.8 %) and $C_{11}S$ (17.1 %) showed values superior to that of '3+1' Tc-fatty acid derivatives described before [2].

When compared with extraction rates for [^{123}I]iodophenylpentadecanoic acid (IPPA) determined with the same set-up, extraction for the C_{11} and $C_{11}S$ compounds is 3 fold and 1.3 fold, respectively (Fig. 1).

These results confirm our hypothesis that the "4+1" Tc(III) chelate unit is a promising tool for the Tc-labelling of fatty acids. Further experiments with different species are planned to elucidate exact myocardial uptake mechanisms.

Derivatives that show high extraction rates in the isolated constant-flow-perfused guinea pig heart model will be involved to characterise *in vivo* patterns in mice and guinea pigs.

References

[1] Walther, M. *et al., this report*, p. 34.

[2] Jung, C. M. *et al., Annual Report 2001*, FZR-340, p. 51 and literature cited therein.

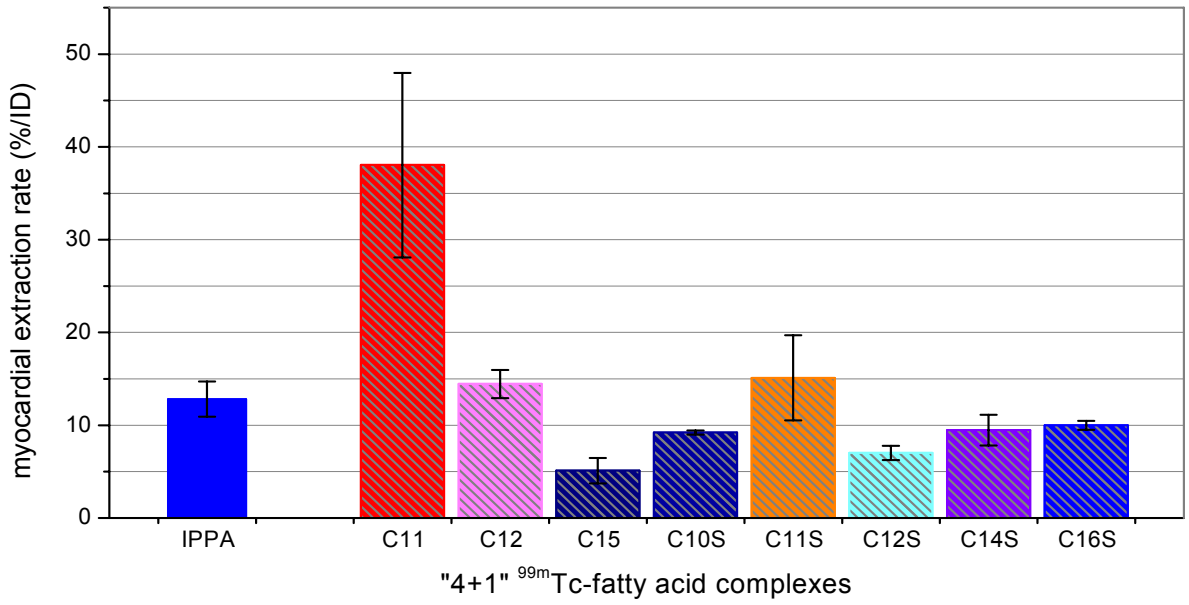

Fig. 1. Extraction rates of the new '4+1' mixed-ligand Tc complexes in comparison with IPPA.

^{99m}Tc-Labelled RGD-Peptide Using the "4+1" Mixed-Ligand Chelate System

J.-U. Kuenstler, S. Seifert, R. Bergmann, H.-J. Pietzsch

A new ^{99m}Tc-labelling method for the RGD-peptide c(RGDyK) via a "4+1" mixed-ligand complex is described, enabling labelling of about 0.1 mg peptide with 1 GBq in a yield of 70 %. For identity confirmation of the ^{99m}Tc-labelled RGD-peptide the analogous Re compound was prepared. Biodistribution studies with ^{99m}Tc-labelled c(RGDyK) were performed.

Introduction

Radiolabelled RGD-derived compounds showing a large potential for imaging of tumour-induced angiogenesis have already been described and studied *in vivo* with a large variety in both the labelling system and the RGD-motive [1].
In this report we present a new ^{99m}Tc-labelling procedure for the RGD-peptide c(RGDyK) according to the "4+1" mixed-ligand approach [2]. The ^{99m}Tc-labelled c(RGDyK) is investigated in biodistribution studies.

Results and Discussion

The RGD-peptide c(RGDyK) was modified by introducing an isocyanide group using the bifunctional coupling agent CN-BFCA [3]. This reacted with the ε-amino group of lysine to give **CN-c(RGDyK)**. A two-step procedure was performed to obtain the ^{99m}Tc-labelled compound **^{99m}Tc(NS$_3$)(CN-c(RGDyK)** (Fig. 1). At first ^{99m}Tc-EDTA was formed, which reacted in a second step with CN-c(RGDyK) and the tetradentate ligand N(CH$_2$CH$_2$SH)$_3$ [3]. This procedure enabled ^{99m}Tc-labelling of 0.1 mg CN-c(RGDyK) with up to 1 GBq and a radiochemical yield of 70 %. To verify the identity of the ^{99m}Tc-labelled c(RGDyK) an analogous "4+1" Re compound **Re(NS$_3$)(CN-c(RGDyK)** (Fig. 1) was synthesised. The obtained compounds were characterized by RP-HPLC (Fig. 2) and ESI-MS.

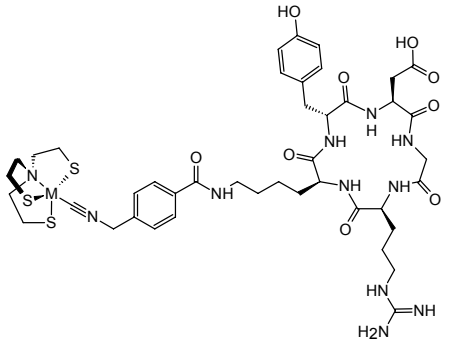

Fig. 1. Prepared "4+1" complex bearing RGD-peptide,
M = ^{99m}Tc: ^{99m}Tc(NS$_3$)(CN-c(RGDyK),
M = Re: Re(NS$_3$)(CN-c(RGDyK).

Biodistribution studies of **^{99m}Tc(NS$_3$)(CN-c(RGDyK)** in rats and tumour-bearing mice exhibited a high liver and kidney uptake (Table 1). The tumour uptake was relatively low, reflecting the lack of specific receptor ($\alpha_v\beta_3$) uptake. The receptor state of the tumour is not known.

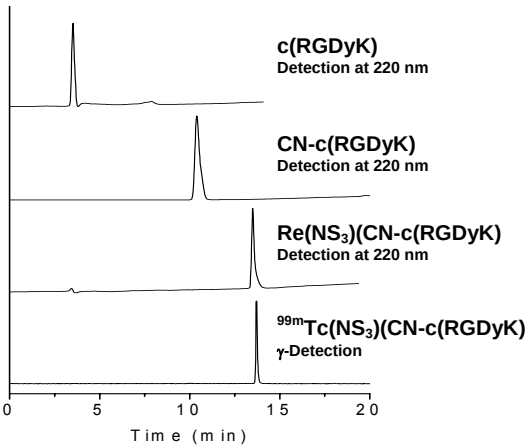

Fig. 2. Chromatograms (HPLC, RP-18, MeCN/H_2O/TFA) of prepared compounds.

Table 1. Biodistribution of **^{99m}Tc(NS$_3$)(CN-c(RGDyK)** in Wistar rats and nude mice bearing MDA-MB-468 tumour (% ID/g tissue/100 g BW, mean ± S.D., n = 3) 60 min after i.v. injection .

Organ	Rat	Mouse
Blood	0.32 ± 0.04	0.56 ± 0.28
Muscle	0.12 ± 0.04	0.13 ± 0.03
Brain	< 0.05	< 0.05
Pancreas	0.18 ± 0.03	0.18 ± 0.13
Spleen	1.41 ± 0.30	0.74 ± 0.16
Adrenals	0.33 ± 0.10	0.99 ± 0.17
Kidney	2.78 ± 0.39	1.19 ± 0.10
Heart	0.19 ± 0.05	0.37 ± 0.05
Lungs	0.54 ± 0.09	1.62 ± 0.44
Liver	3.49 ± 0.29	3.84 ± 0.38
Femur	0,23 ± 0.04	0.19 ± 0.04
Tumour		0.22 ± 0.03

The described method allows the ^{99m}Tc-labelling of c(RGDyK) via "4+1" complexes. Structural variations to reduce the kidney and liver uptake as well as receptor binding studies to clarify the influence of the coupled "4+1" complex should be performed.

References

[1] Haubner, R. *et al.*, Curr. Pharm. Design 10 (2004) 1439-1455.
[2] Pietzsch, H.-J. *et al.*, Bioconjugate Chem. 12 (2001) 538-544.
[3] Seifert, S. *et al.*, Bioconjugate Chem. 15 (2004) 856-863.

Metabolic Stability and Biodistribution of Model Compounds Based on the ^{99m}Tc "4+1" Mixed-Ligand Chelate System

B. Pawelke, S. Seifert, R. Bergmann

The metabolic stability of model compounds bearing a Tc(III) NS_3/isonitrile mixed-ligand chelate unit was investigated in rats and discussed in connection with biodistribution examinations.

Introduction

Trigonal-bipyramidal "4+1" Tc complexes containing the NS_3/isonitrile ligand system have been developed as versatile building blocks for labelling of biomolecules. A number of these complexes have been investigated and reported to be stable against ligand exchange in glutathione challenge experiments as well as *in vitro* in whole blood and plasma of rats.[1] Therefore, they are considered promising candidates for further development. Recently, an improved procedure for their preparation was introduced [2]. In order to evaluate the behaviour *in vivo* we investigated the biodistribution and metabolic pattern of the model compounds **1-4** in Wistar rats.

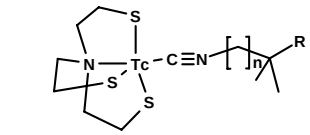

1: n=1, R=OMe
2: n=0, R=Me

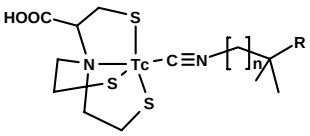

3: n=1, R=OMe
4: n=0, R=Me

Results and Discussion

Metabolic stability

Arterial blood samples, urine, organ homogenates and content of intestine of rats were analysed after *i.v.* injection of ^{99m}Tc labelled compounds **1-4**. For compounds **3** and **4** bearing a carboxyl group, the presence of a hydrophilic main metabolite was stated in plasma, organ homogenates as well as in rinsing fluid of intestine (for an example, see Fig. 1). The compounds without carboxyl group did not show a comparably consistent metabolic pattern in the different samples but instead a considerably increased amount of activity bound to plasma proteins. It was concluded that the metabolic attack at compounds **3** and **4** occurs mainly at the carboxyl group. Compounds **1** and **3** show a more complex degradation mechanism compared to **2** and **4**, respectively, which is attributed to a higher metabolic susceptibility of the monodentate ligand (not shown in detail).

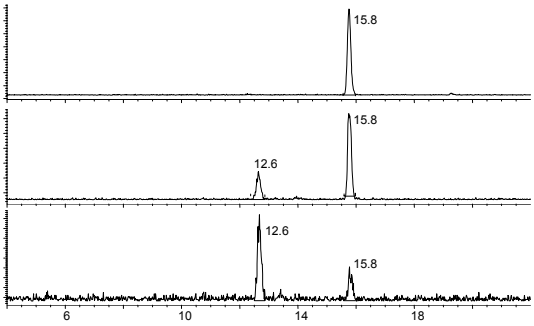

Fig. 1. Radiochromatograms of compound **4** in rats: injected compound, plasma and liver homogenate 60 min *p.i.* (from top).

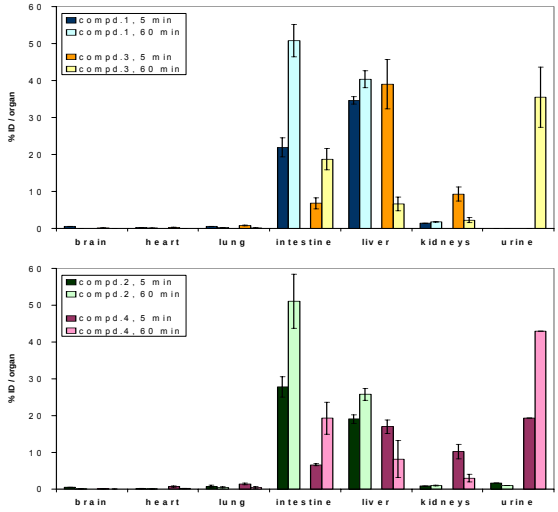

Fig. 2. Biodistribution of compounds **1-4** in rats (n = 4).

Biodistribution

A higher accumulation in liver and intestine was observed for compounds **1** and **2** whereas **3** and **4** seem to undergo mainly renal excretion (Fig. 2). The lower accumulation in liver and intestine of compounds **3** and **4** may be discussed in terms of a lower lipophilicity of the parent compounds with carboxyl group themselves as well as of the influence of the hydrophilic metabolites described above.

References

[1] Pietzsch, H.-J. *et al.*, Bioconjugate Chem. 12 (2001) 538-544.
[2] Seifert, S. *et al.*, Bioconjugate Chem. 15 (2004) 856-863.

Inhibition of Thymidine Phosphorylase as one Approach in Tumour Chemotherapy

M. Grote, St. Noll, B. Noll

Thymidine phosphorylase (TP, EC 2.4.2.4) is one of the key enzymes involved in the salvage biosynthesis pathway and catabolism of pyrimidine 2'-deoxynucleosides. Several new pyrimidine derivatives were tested concerning their inhibitory effect on E. coli TP.

The enzyme thymidine phosphorylase (TP) converts thymidine (dT) to thymine and α-D-2-deoxy-ribose-1-phosphate in a reversible reaction. TP expression is enhanced in several types of human tumour tissues (e.g. in mamma, ovarian or colon carcinomas) [1].
To clarify the role TP is playing in this process inhibitors are necessary to prevent this enzymatic activity. Specific inhibitors will disturb the salvage pathway and diminish the clearance of thymidine and 2'-deoxynucleosides leading to cell death. The monitoring of this process requires suitable radiotracers acting as inhibitors.
A first step of this approach was to study whether a number of novel acyclic nucleoside derivatives [2] (Fig. 1) are potential inhibitors of thymidine phosphorylase, derived from *E. coli*. The sequences of this enzyme correspond to about 70 % with human TP.

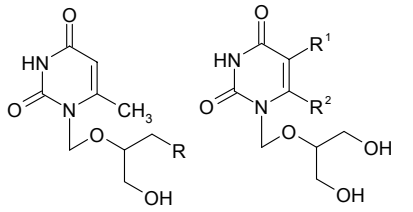

1. R = OH
2. R = F

3. R^1 = I, R^2 = H
4. R^1 = I, R^2 = CH_3
5. R^1 = OH, R^2 = H
6. R^1 = H, R^2 = H

Fig. 1.

The inhibition assays contained 250 µM ^{3}H-thymidine, 10 mM Tris*HCl pH 7.4, 2 mM KH_2PO_4 and 1 % HSA in a final volume of 15 µl [3]. The inhibitory effect was tested with various amounts of inhibitor. Aliquots of 2 µl were withdrawn at several time points and spotted to a TLC plate to determine the enzyme reaction. Plates were developed in CH_2Cl_2/MeOH (10:1) and scanned with a TLC scanner. The inhibition of TP was expressed as ratio of ^{3}H-thymine formed without and with the respective compound (Table 1).

Table 1. Inhibition of thymidine phosphorylase by uracil derivatives.

Comp.	Conc. [µM]	% inhibitory 5 min	10 min	15 min
1	1000	45	35	32
	500	18	15	14
2	1000	30	24	22
	500	24	19	18
3	1000	83	76	74
	500	26	21	19
4	1000	38	36	45
	500	15	8	12
5	1000	30	67	76
	500	19	36	46
6	1000	59	62	60
	500	47	45	52

All substances tested offer a more or less inhibitory effect on TP. Particularly compounds **3** and **5** revealed a significant inhibition and appear to be capable for further more experiments with isolated human TP and with human cell lines.

References

[1] Matsushita, S. *et al.*, Cancer Res. 59 (1999) 1911.
[2] Noll, St. *et al., Annual Report 2003*, FZR-394, p. 20.
[3] Esteban-Gamboa, A. *et al.*, J. Med. Chem. 43 (2000) 971.

Synthesis and ^{18}F-Labelling of Novel Acyclic Purine Nucleosides

B. Noll, St. Noll

The synthesis and ^{18}F-labelling of two novel acyclic purine nucleosides for monitoring gene expression of herpes simplex virus type 1 thymidine kinase gene (HSV1-tk) is described.

Introduction

Monitoring thymidine kinase expression should be possible by using ^{18}F-labelled nucleosides. Thus, two new precursors have been synthesised followed by ^{18}F-labelling to get new potential substrates **1** and **3** for monitoring gene expression of herpes simplex virus type 1 thymidine kinase gene (HSV1-tk).

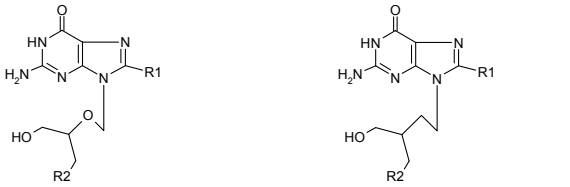

1: R1 = Br, R2 = ^{18}F
2: R1 = H, R2 = OH
5: R1 = Br, R2 = OH

3: R1 = Br, R2 = ^{18}F
4: R1 = H, R2 = OH
6: R1 = Br, R2 = OH

Synthesis

To brominate the acyclonucleosides ganciclovir **2** and penciclovir **4** a standard procedure was used yielding **5** and **6** [1]. For that **2** and **4** were dissolved in 0.5 M sodium acetate buffer. A saturated solution of bromine-water was then added and the reaction mixture was allowed to stir at 22 °C for several hours. The brominated compounds were purified by column chromatography on Sephadex G10 and water as eluent.

Our strategy to label the nucleosides at the acyclic side chain with ^{18}F requires the protection of the second hydroxyl group and of the amino group at position 2. Therefore 8-bromoganciclovir **5**, and 8-bromo-penciclovir **6** were treated with p-anisyl-chlorodiphenyl-methane in dimethyl formamide. Triethylamine and traces of dimethylamino pyridine were added and the mixture was allowed to react for 2 hours at 55 °C. Thus, the protected compounds **7** and **8** were formed in a yield of about 65 %.

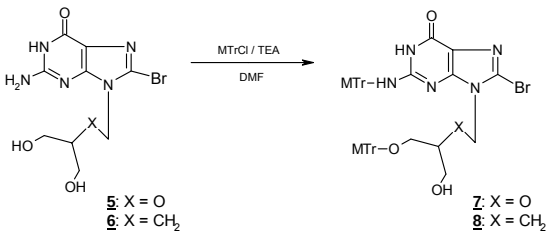

5: X = O
6: X = CH_2

7: X = O
8: X = CH_2

The once-tritylated and the threefold tritylated compounds being occurred as by-products in the synthesis were separated by column chromatography on silica gel and dichloromethane/methanol 10:1 as eluent.

The introduction of the p-toluenesulphonyl group into **7** and **8** as leaving group for the fluorination was carried out with p-toluenesulphonyl chloride in a five-fold molar excess in anhydrous pyridine for 6 hours at room temperature. The precursors **9** and **10** were purified by column chromatography on silica gel and dichloromethane/methanol 15:1 as eluent of about 55 %.

All substances synthesised were identified by elemental analysis and ^{1}H NMR spectroscopy.

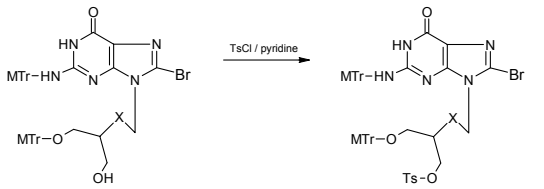

7: X = O
8: X = CH_2

9: X = O
10: X = CH_2

^{18}F-Labelling

An [^{18}F]KF/K2.2.2 complex was received after azeotropic distillation with acetonitrile, kryptofix 2.2.2 and potassium carbonate. This complex was allowed to react with the precursors **9** and **10** (5 mg), dissolved in acetonitrile, for 25 min at 160 °C. Then, the reaction mixture was given over a silica Sep-pak cartridge and eluted with dichloromethane/methanol (85/15 v/v). The cartridge holds back K_2CO_3, kryptand and non-converted [^{18}F]KF whereas the desired [^{18}F]F-labelled tracers **1** and **3** were eluted.

The labelling yield amounted to about 55 % (50 min reaction time). HPLC analysis (Phenomenex C18, PBS/MeCN 80:20) of the reaction mixture after Si Sep-pak elution yielded a radiochemical purity >98 %.

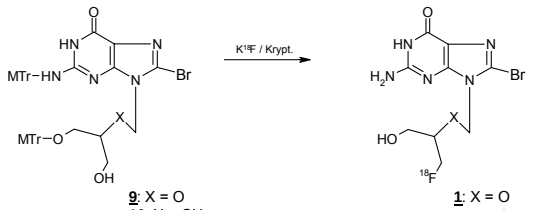

9: X = O
10: X = CH_2

1: X = O
3: X = CH_2

References

Rokos, H. *et al.*, Chem. Ber. 108 (1975) 2872.

Biodistribution of ^{18}F-Labelled Acyclic Guanosine and Thymine Derivatives

B. Noll, St. Noll, M. Grote, R. Bergmann

The biodistribution of ^{18}F-labelled acyclic guanine and thymine derivatives has been studied in Wistar rats concerning their behaviour as potential substrates of HSV-1 thymidine kinase for monitoring gene therapy.

Recently the syntheses of novel acylic pyrimidine nucleosides [1], acyclic purine nucleosides [2] and the corresponding precursors have been reported. The ^{18}F-labelled acyclic guanine and thymine derivatives were developed as potential substrates of the HSV1 TK to monitor gene expression. The labelling with fluorine-18 was carried out according to an optimised procedure with variation in reaction time and temperature. The general procedure is described in [2].
All tracers were purified by HPLC on RP18 column and water/ethanol (90/10 up to 97/3) as eluent. The biodistribution in male Wistar rats 5 and 120 min after i.v. injection is depicted in Figs. 1 and 2 as % dosis/organ.
The following ^{18}F-labelled compounds **1**-**4** were tested.

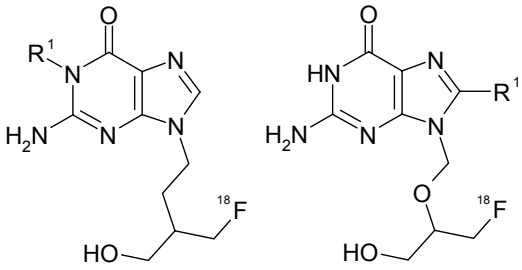

1. R^1 = H, FHBG
2. R^1 = CH_3, FMHBG
3. R^1 = H, FHPG
4. R^1 = Br, BrGCV

As acyclic thymidine derivatives the ^{18}F-labelled tracers **5**-**7** were taken into account:

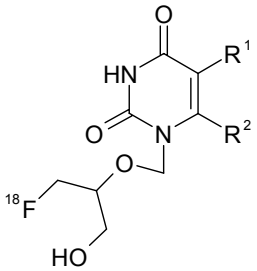

5. R^1 = I, R^2 = H, Iodacyclur
6. R^1 = I, R^2 = CH_3, Iodmetacyclur
7. R^1 = H, R^2 = H, Acyclur

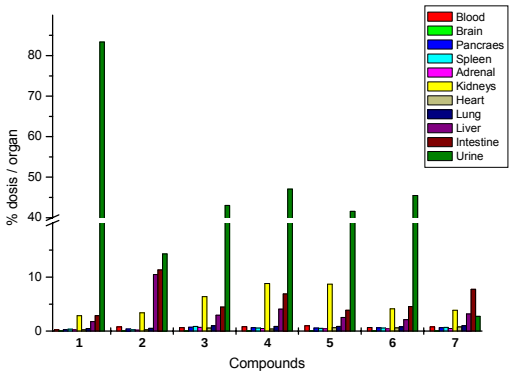

Fig. 1. Biodistribution of acyclic nucleosides in Wistar rats after 5 min.

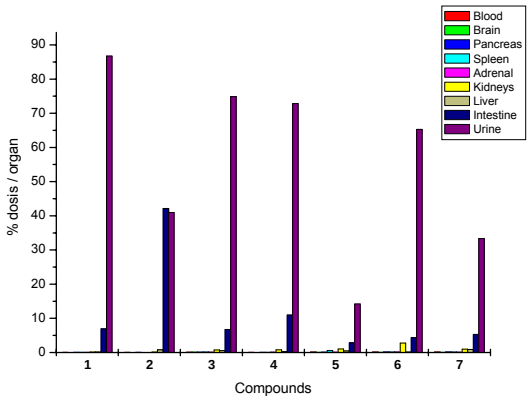

Fig. 2. Biodistribution of acyclic nucleosides in Wistar rats after 120 min.

References

[1] Noll, B. *et al.*, *Annual Report 2003*, FZR-394, p. 19.
[2] Noll, B. *et al.*, *this report*, p. 39.

Biodistribution of ^{18}F-Labelled Acyclic Guanine and Uracile Derivatives

B. Noll, St. Noll, M. Grote, R. Bergmann

The biodistribution of ^{18}F-labelled acyclic guanine and uracile derivatives has been studied in Wistar rats concerning their behaviour as potential subtrates of HSV-1 thymidine kinase for monitoring gene therapy.

Recently, the syntheses of novel acylic pyrimidine nucleosides [1], acyclic purine nucleosides [2] and the corresponding precursors have been reported. The ^{18}F-labelled acyclic guanine and uracile derivatives were developed as potential substrates of the HSV-1 TK to monitor gene expression. The labelling with fluorine-18 was carried out according to an optimised procedure with variation in reaction time and temperature. The general procedure is described in [2].
All tracers were purified by HPLC on RP18 column and water/ethanol (90/10 up to 97/3) as eluent. The biodistribution in male Wistar rats 5 and 120 min after single i.v. injection is depicted in figures 1 and 2 as % injected dose/organ.

The following ^{18}F-labelled compounds **1**-**5** were tested.

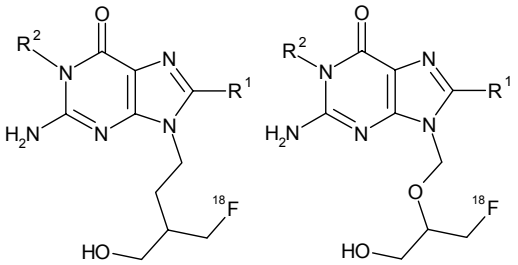

1. R^1 = H, R^2 = H FHBG
2. R^1 = CH_3, R^2 = H FMHBG
3. R^1 = Br, R^2 = H BrGCV
4. R^1 = H R^2 = H FHPG
5. R^1 = Br, R^2 = H BrPCV

As acyclic uridine derivatives the ^{18}F-labelled tracers **6**-**8** were taken into account:

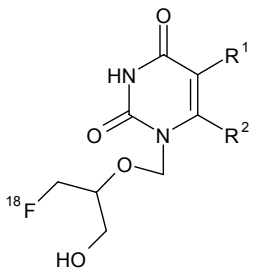

6. R^1 = I, R^2 = H, Iodacyclur
7. R^1 = I, R^2 = CH_3, Iodmetacyclur
8. R^1 = H, R^2 = H, Acyclur

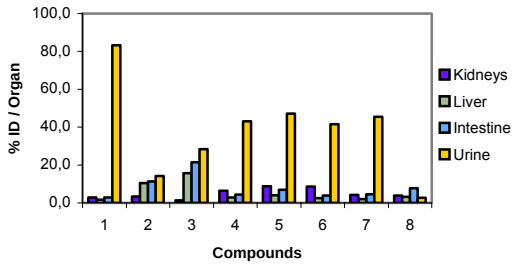

Fig. 1. Biodistribution of acyclic nucleosides in Wistar rats 5 min p.i..

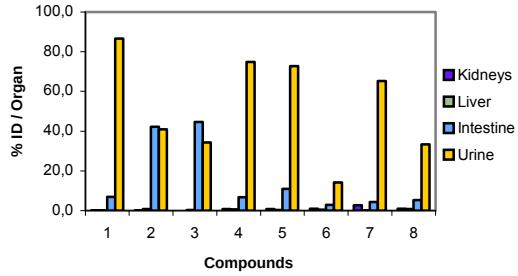

Fig. 2. Biodistribution of acyclic nucleosides in Wistar rats 120 min p.i..

As expected, all compounds showed a fast blood clearance. The biliary elimination was correlated with the lipophilicity of the compounds tested. After 60 min most of the activity was found in intestine and urine. The fast excretion of the tracer seems to be a prerequisite for high target/non target ratio for monitoring gene expression.

References

[1] Noll, B. *et al*., *Annual Report 2003*, FZR-394, p.19.
[2] Noll, B. *et al., this report*, p. 39.

RADIOMETAL THERAPEUTICS

Hydrophilic Rhenium-188 Complexes for Attaching the Metal to Biomolecules 4. Synthesis and Characterisation of Hydroxymethyl Phosphine Containing '4+1' Complexes

E. Schiller, W. Kraus[1], H.-J. Pietzsch, H. Spies
[1]*Bundesanstalt für Materialforschung und –prüfung, Berlin*

A synthetic route for the preparation of hydroxymethyl phosphines is presented. Model complexes of these ligands were prepared to evaluate their use in the design of '4+1'-type complexes.

Introduction

Synthesis of hydrophilic species is an important aim in the development of rhenium-188 complexes of the '4+1' mixed ligand approach [1]. Katti and co-workers reported on water-soluble tetradentate ligands containing phosphines with hydroxymethyl substituents [2]. Sulfur or nitrogen heteroatoms in the phosphine's backbone are responsible for their high stability against oxidation. These phosphines are considered as appropriate synthons in the design of radiopharmaceuticals of favourable biodistribution. We wanted to adapt the published synthesis strategy to the development of monodentate ligands for the '4+1' approach.

Results and Discussion

Hydroxymethyl phosphonium salts were synthesised according to Scheme 1. Resulting PN and PS phosphonium salts **3** and **4**, respectively, can be converted to their corresponding tertiary phosphines by addition of triethylamine.

Scheme 1. Syntheses of hydroxymethyl-functionalised PN (**3**) and PS (**4**) ligands.

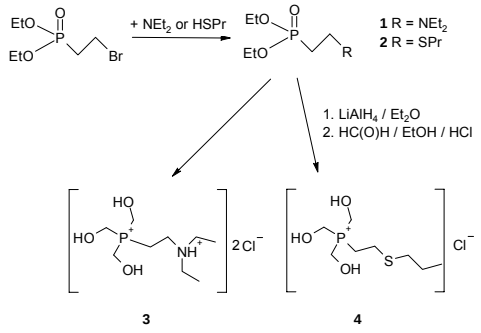

First diethylamine or 1-propanethiol was alkylated with commercial available diethyl 2-bromoethyl phosphonate. Then the phosphonates **1** and **2** were reduced with $LiAlH_4$. The resulting primary phosphines were reacted without isolation with formaldehyde in acidic solution, yielding the phosphonium salts as colorless viscous oils.
'4+1' complexes **Re1** and **Re2** were prepared by heating a methanol/triethylamine solution of $[Re(tu)_6]Cl_3$ (tu = thiourea) and equimolar amounts of the phosphine ligand and tris(2-mercaptoethyl)amine (NS_3) for two hours under reflux.
Phosphonium salts as well as the '4+1' complexes were characterized by means of multinuclear NMR and elemental analysis. Complexes were additionally investigated by UV/vis spectroscopy and X-ray structure analysis. Crystal structures are displayed in Fig. 1.

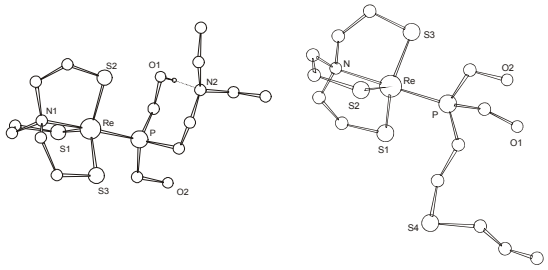

Fig. 1. Crystal structures of **Re1** (left) and **Re2** (right).

Re1 showed high stability in organic solvents at room temperature whereas **Re2** was converted to a more hydrophilic species under these conditions. The final product of this conversion (**Re3**) was isolated by column chromatography. Mass spectrometry, IR spectroscopy and X-ray structure analysis (Fig. 2) indicated the oxidation of the sulfur atom in the phosphine's backbone to the corresponding sulfoxide. Therefore only PN ligands are investigated furtherly [3].

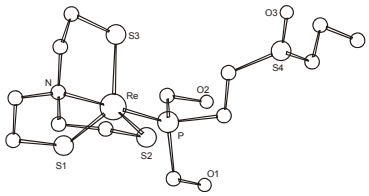

Fig. 2. Crystal structure of **Re3**.

References

[1] Schiller, E. *et al., Annual Report 2003*, FZR-394, p. 44.
[2] Katti, K. V. *et al.*, Acc. Chem. Res. 32 (1999) 9.
[3] Schiller, E. *et al., this report*, p. 46.

Hydrophilic Rhenium-188 Complexes for Attaching the Metal to Biomolecules
5. Determination of *in Vitro* Stabilities

E. Schiller, S. Seifert, F. Tisato[1], F. Refosco[1], H.-J. Pietzsch
[1]*ICIS-CNR, Padova, Italy*

Looking for suitable candidates for the development of rhenium-188 radiotherapeutics we determined in vitro stabilities of various complexes with tetradentate/monodentate ('4+1') coordination. Influences of the nature of the ligands on the in vitro stability are discussed.

Introduction

According to the so-called '4+1' approach [1] we have synthesised a series of rhenium-188 model complexes using a method recently described by Seifert and co-workers [2]. We determined in vitro stabilities of these compounds by incubating 2-3 MBq of each complex in phosphate buffer, human plasma and rat plasma, followed by checking the amount of $^{188}ReO_4^-$ formed after 1 h, 24 h and 48 h by thin layer chromatography.

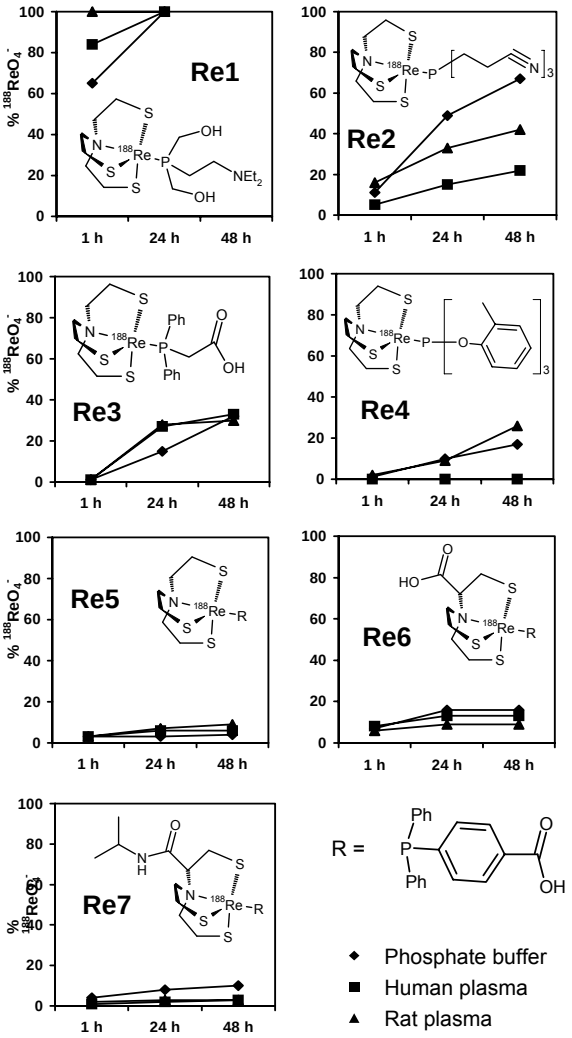

Fig. 1. In vitro stabilities of ^{188}Re complexes **Re1–Re7**.

Results and Discussion

In vitro stabilities of rhenium-188 '4+1' complexes were found to be strongly dependent on the nature of the monodentate phosphorus(III) ligands (see **Re1** – **Re5** in Fig. 1). The most hydrophilic complex bearing a hydroxymethyl phosphine [3] **Re1** was not stable giving large amounts of perrhenate. Conversely, more lipophilic compounds **Re4** and **Re5** were found to produce only little amounts of perrhenate.

Obviously, only complexes bearing a bulky phosphorus co-ligand which generates along with the three thiolate sulfurs of the NS_3 ligand a lipophilic area around the rhenium are of high in vitro stability. This lipophilic area prevents the Re(III) center from hydrolysis and re-oxidation to perrhenate.

The initial aim to develop hydrophilic rhenium-188 complexes of high in vitro stability can be achieved by preserving the lipophilic core in the inner coordination sphere and introduction of hydrophilic functional groups either at the NS_3 framework and/or at the monodentate ligand. Therefore, complexes having a carboxyl group containing tetradentate NS_3 ligand [2, 4] or a derivative thereof are an appropriate approach. Complexes of this formulation (**Re6**, **Re7**) exhibited higher hydrophilicity (**Re6** >> **Re7** > **Re5**) but comparable in vitro stability than their unsubstituted analogue **Re5**. Therefore we consider these agents as promising candidates for the development of rhenium-188 radiopharmaceuticals.

References

[1] Spies, H. *et al.*, Inorg. Chim. Acta 240, (1995), 465.
[2] Seifert, S. *et al.*, Bioconj. Chem. 15, (2004), 856.
[3] Schiller, E. *et al., this report*, p. 45.
[4] Schiller, E. *et al.*, *Annual Report 2003*, FZR-394, p. 45.

^{188}Re-EDTA – a Suitable Precursor for Preparing ^{188}Re(V) Complexes

S. Seifert

The ^{188}Re(III) complex with ethylene diamine tetraacetic acid (EDTA) was found to be a suitable precursor for preparing ^{188}Re complexes of the same or higher oxidation states. That was tested by ligand exchange reactions with ligands forming Re(V)oxo complexes like ECD, EC, another N_2S_2 ligand, or DMSA.

Introduction

^{99m}Tc(III)-EDTA and the analogue ^{188}Re complex has been successfully used to prepare '4+1' complexes containing the tetradentate NS_3 ligand and a phosphine or isonitrile as the monodentate ligand [1]. The reduction of Tc(VII) or Re(VII) to the oxidation state 3+ succeeds at room temperature, also in the case of perrhenate generator eluate and allows the gently preparation of M(III) complexes. Considering the tendency of carrier-free ^{188}Re complexes of lower oxidation states to re-oxidise in solution, it should be possible to prepare ^{188}Re complexes of higher oxidation states by ligand exchange reaction of ^{188}Re-EDTA with ligands forming such kinds of complexes. Therefore, corresponding studies were performed using tetradentate N_2S_2 ligands like ECD, its acid form EC, KET 397 or dithiol ligands like DMSA (Fig. 1).

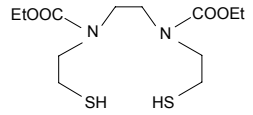

L,L-ECD (*L,L*-ethylene dicysteine diethyl ester)

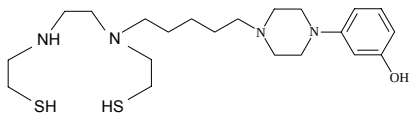

KET 397

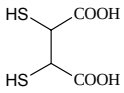

DMSA

Fig. 1. Ligands used for re-oxidation studies

Results and Discussion

The preparation of ^{188}Re(V) complexes was carried out in two steps. At first, the ^{188}Re-EDTA was prepared by reconstitution of a kit containing 5 mg EDTA, 5 mg mannitol, and 1 mg $SnCl_2$ with 2–5 ml of acidic perrhenate eluate as described in [1]. In a second step, 1 ml of the ^{188}Re-EDTA solution was added to the aqueous/ethanolic solution of 0.5–1.0 mg of the appropriate ligand. After slight heating to 40–50 °C for 30 min the desired Re(V) complexes were formed with yields of 50–80 % of the starting activity (reaction conditions were not optimised up to now). Generally, the reaction succeeds in a neutralised ^{188}Re-EDTA solution. Fig. 2 shows as an example the re-oxidation of ^{188}Re-EDTA in an ECD solution. The comparison of retention times of the formed ^{188}Re-ECD complex and a "kit-like" ^{99m}Tc-ECD preparation confirms the identity of the final complex.

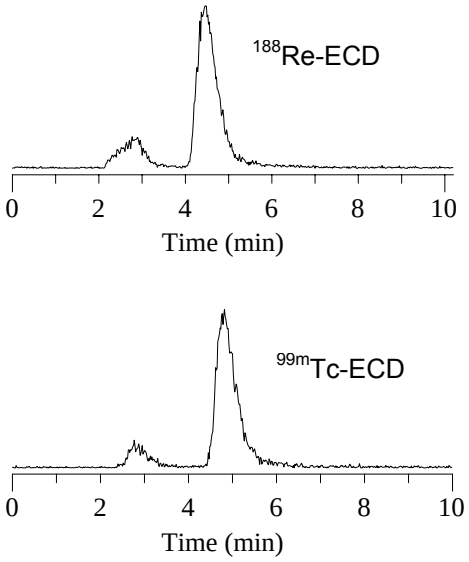

Fig. 2. Comparison of HPLC analyses of ^{188}Re-ECD and a "kit-like" ^{99m}Tc-ECD preparation.

In Table 1 the results of the presented studies are summarised.

Table 1. Yields and reaction conditions for the preparation of ^{188}Re(V) complexes

Complex formed	Yield [%]	Reaction conditions
^{188}Re-ECD	80	1 mg ligand, rt, 45 min
^{188}Re-KET 397	50	same
^{188}Re-DMSA	56	30 min

References

[1] Seifert, S. *et al.*, Bioconjugate Chem. 15 (2004) 856-863.

In Vitro Stability of ^{188}Re Complexes

S. Seifert, C. Jentschel

The in vitro stability of ^{188}Re complexes of various oxidation states and coordination spheres was studied in phosphate buffer, rat plasma and human plasma.

Introduction

The aim of this study was to determine the rate of re-oxidation of various ^{188}Re(III) and ^{188}Re(V) complexes to perrhenate in phosphate buffer and plasma solutions. The influence of chemical nature of the monodentate ligand in '4+1' ^{188}Re(III) complexes of the type [^{188}Re(NS_3)(isonitrile)] was investigated using *tert*. butylisonitrile (TBI), cyclohexylisonitrile (CHI), and triphenylmethylisonitrile (TPMI).The stabilities were compared with those of ^{188}Re(V)-MAG_3 and ^{188}Re(V)-DMSA.

Results and Discussion

The '4+1' ^{188}Re(III) complexes were prepared according to the described method using the two-step procedure via ^{188}Re-EDTA [1]. ^{188}Re(V)-MAG_3 was prepared according to [2] and for the preparation of ^{188}Re(V)-DMSA a commercial kit was reconstituted at 100 °C with 1.0 ml of perrhenate eluate [3].

For stability studies the preparations were purified by semi-preparative HPLC and 0.1 ml of the complex solution (2-5 MBq) were added to 0.4 ml of 0.01 M phosphate buffer of pH 7.4, a mixture of 0.2 ml buffer and 0.2 ml human plasma, as well as a mixture of 0.2 ml buffer and 0.2 ml rat plasma. The yield of perrhenate formed by incubation at room temperature was determined by TLC [RP-18//acetonitrile/water (80/20)] at three times (after 1, 24, and 48 h). The results are presented in Figs. 1 and 2.

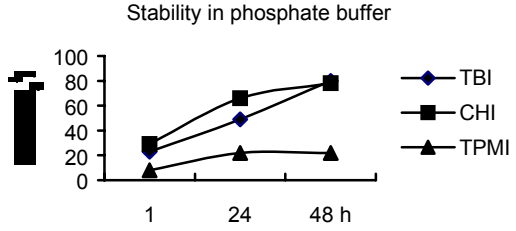

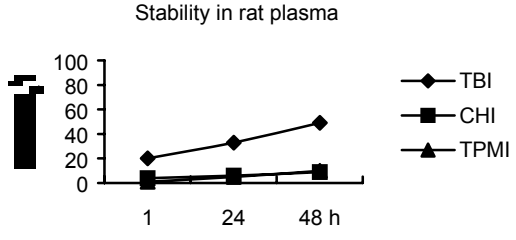

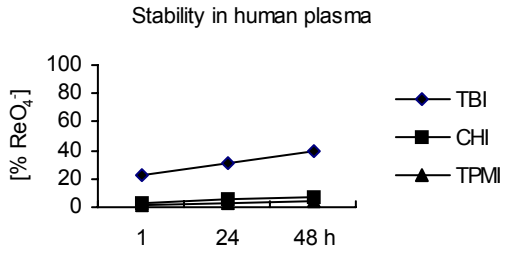

Fig. 1. Stabilities of '4+1' ^{188}Re complexes

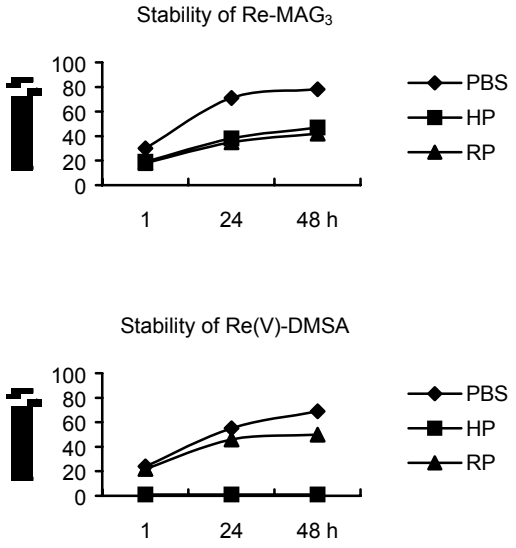

Fig. 2. Stabilities of ^{188}Re-MAG_3 and ^{188}Re(V)-DMSA in phosphate buffer (PBS), human plasma (HP), and rat plasma (RP).

The remarkable high stability of the '4+1' complex [^{188}Re(NS_3)(TPMI)] confirms results obtained with various phosphine ligands [3]. Obviously, '4+1' complexes with a phenyl-groups bearing monodentate ligand are well-shielded and more stable against re-oxidation. Such types of ^{188}Re(III) complexes are much more stable than ^{188}Re(V) complexes. The high stability of ^{188}Re(V)-DMSA in human plasma was also found by Blower *et al.* [4].

References

[1] Seifert, S. *et al.*, Bioconjugate Chem. 15 (2004) 856.
[2] Oh, S. J. *et al.*, Appl. Radiat. Isot. 59 (2003) 225.
[3] Schiller, E. *et al.*, *this report*, p. 46.
[4] Blower, P. J. *et al.*, Eur. J. Nucl. Med. 25 (1998) 613.

Novel and Efficient Preparation of Precursor $[^{188}Re(OH_2)_3(CO)_3]^+$ for the Labelling of Biomolecules

S. H. Park[1], S. Seifert, H.-J. Pietzsch
[1]Division of Radioisotope Production and Application, Korea Atomic Energy Research Institute, Daejeon, Republic of Korea

A novel and efficient method for preparing $^{188}Re(I)$ tricarbonyl precursor $[^{188}Re(OH_2)_3(CO)_3]^+$ has been developed by reacting [^{188}Re]perrhenate with Schibli's kit in the presence of borohydride exchange resin (BER) as an additional reducing agent. The precursor was produced in more than 90 % yield by reacting 3 mg BER, 3 mg $BH_3{\cdot}NH_3$, and 3 mg $K_2[BH_3CO_2]$, dissolved in saline, with a solution of $Na^{188}ReO_4$ and concentrated phosphoric acid (85 %, 8 µl) at 60 °C for 15 min.

Introduction

The $^{99m}Tc(I)$ and $^{188}Re(I)$ tricarbonyl precursors $[M(OH_2)_3(CO)_3]^+$ have been shown to be excellent starting materials for the synthesis of further $^{99m}Tc(I)$ and $^{188}Re(I)$ tricarbonyl complexes as well as radiolabelling of target specific biomolecules [1]. Recently, a user-friendly kit formulation (IsoLink™) was developed using potassium boranocarbonate, $K_2[BH_3CO_2]$, for preparation of the ^{99m}Tc precursor complex. This solid reagent serves both as a source of CO as well as a reductant for technetium. It was also used by Schibli and co-workers for the preparation of the corresponding ^{188}Re precursor complex [2]. [^{188}Re]perrhenate eluate (1 ml) was reduced in neutral solution with 3 mg $K_2[BH_3CO_2]$ and 5 mg $BH_3{\cdot}NH_3$ by incubation at 60 °C for 15 min. The amount of reducing agents and acid (concentrated phosphoric acid) was carefully balanced, to avoid fast hydrolysis of the boranes and to maintain a sufficient low pH to stabilize reduced rhenium intermediates. The preparations resulted in yields >85 % of the desired precursor complex, remaining perrhenate (7±3 %), colloidal $^{188}ReO_2$ (<5 %), and a by-product of unknown composition.

To overcome the moderate yields we used the recently described borohydride exchange resin (BER) as an additional reducing agent [3]. For preparation of BER the chloride-form resin (Amberlite® ion exchange resin, 12.5 g) was slurry-packed with water into a 30 ml fritted glass funnel mounted on a filter flask. Then, an aqueous sodium tetrahydroborate solution (200 ml, 0.25 M) was slowly passed through the resin over a period of 30 min. After washing with distilled water and ethanol, the tetrahydroborate-form anion exchange resin was partially air-dried by removing ethanol on the surface of the BER.

Results and Discussion

Optimal yields of the precursor complex were obtained using the following preparation conditions: To a vial containing a mixture of 3 mg $K_2[BH_3CO_2]$, 3 mg $BH_3{\cdot}NH_3$, and 3 mg BER, 1.0 ml of [^{188}Re]perrhenate eluate and 8 µl phosphoric acid (85 %) were added. The vial was incubated at 60 °C for 15 min. Pressure from the evolving H_2 gas was balanced with a 20 ml syringe. 90–95 % of the desired $[^{188}Re(OH_2)_3(CO)_3]^+$ complex were found by HPLC and TLC analyses. The assay for the formation of the $^{188}Re(I)$ tricarbonyl precursor, reduced-hydrolyzed ^{188}Re, and [^{188}Re]perrhenate was achieved by investigating their positions using an instant thin-layer chromatography (silicagel//MeOH/HCl (95/5). $^{188}Re(I)$ tricarbonyl precursor: 90-95 % (R_f = 0.4); reduced-hydrolyzed ^{188}Re: less than 3 % (origin); [^{188}Re]perrhenate ion: 5-8 % (R_f = 0.8). The identity of the precursor was confirmed by reaction with histidine. The retention time of $^{188}Re(I)$ tricarbonyl histidine was compared to that of $^{99m}Tc(I)$ tricarbonyl histidine and found to be identical.

According to the present study, employing the borohydride exchange resin (BER) as a novel reducing agent, $^{188}Re(I)$ tricarbonyl precursor having high radiochemical purity as well as high labelling efficiency can be prepared without nitrogen gas flushing and ice bath cooling. The BER is advantageous in terms of being stable over a wide range of pH (2-11) and applicable to biologically active molecules, as well as being easily removable through filtration when being administrated.

Acknowledgements

This work was supported by the Mid- and Long-term Nuclear R & D Program of the Korean Ministry of Science and Technology and the Technical Cooperation Program of the International Atomic Energy Agency (ROK 03002).

References

[1] Alberto, R. *et al.*, J. Am. Chem. Soc. 120 (1998) 7987.
[2] Schibli, R. *et al.*, Bioconjugate Chem. 13 (2002) 750.
[3] Park, S. H. *et al.*, J. Labelled Compd. Radiopharm. 47 (2004) 683.

Biological Evaluation of ^{64}Cu-Labelled Tetrapropionitrile Derivatized Macrocyclic Ligands

P. McQuade[1], M. Wüst[1], M. Welch[1], F. Wüst
[1]Mallinckrodt Institute of Radiology, Washington University School of Medicine, St. Louis

Three tetrapropionitrile-containing azamacrocycles have been labelled with ^{64}Cu. Biological evaluation of the ^{64}Cu complexes comprised in vitro uptake studies in EMT-6 cells and biodistribution studies on BALB/c mice bearing EMT-6 tumours.

Introduction

The positron-emitting isotope ^{64}Cu has found use as both a diagnostic agent by utilizing the high sensitivity of PET imaging, and also as a radiotherapy agent. As a result alternative approaches to targeted radiotherapy may be developed from studies on novel ^{64}Cu-labelled derivatized macrocyclic ligands, by improving on the efficiency and clearance properties of known radiopharmaceuticals.
One such family of macrocyclic ligands containing propionitrile groups have been shown to cause DNA damage in P388 and BEL-7404 cell lines [1].

Results and Discussion

Macrocyclic ligands containing nitrile groups have been synthesised by the Michael addition of acrylonitrile to the corresponding macrocycle to give cyclen-N,N',N'',N'''-tetrapropionitrile (**Cyclen-TPN**), cyclam-N,N',N'',N'''-tetrapropionitrile (**Cyclam-TPN**) and cyclo15-N,N',N'',N'''-tetrapropionitrile (**Cyclo15-TPN**) (Fig. 3).

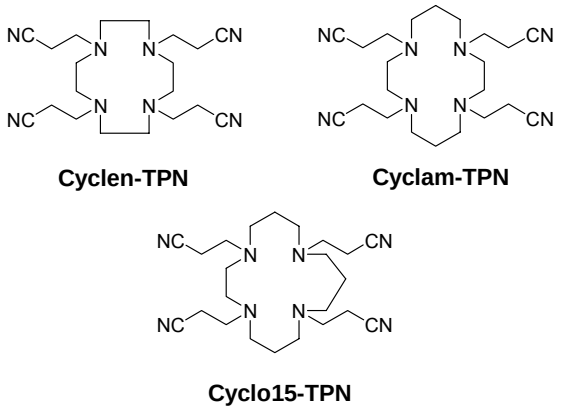

Fig. 1: Macrocycles Cyclen-TPN, Cyclam-TPN and Cyclo15-TPN.

Labelling of these compounds with ^{64}Cu was achieved at 85 °C at pH 5.5 (0.1 M NH_4OAc) for 60 minutes, with specific activities of 500 mCi/mg typically being obtained. All three Cu(II) complexes are hydrophilic with log P values of -1.47±0.1, -2.17±0.1 and -0.71±0.05, and were shown to be stable in vitro by incubating at 37 °C in rat serum for 2 h. The in vitro uptake of these complexes in EMT-6 cells was investigated. **^{64}Cu(II)-Cyclen-TPN** had an uptake of 6.67±0.81 % after 15 minutes, which then increased to around 20 % after 2 h, before reaching a plateau. Both complexes **^{64}Cu(II)-Cyclam-TPN** and **^{64}Cu(II)-Cyclo15-TPN** showed similar uptake in this cell line.
Biodistribution studies on these complexes have also been obtained on BALB/c mice bearing EMT-6 tumours. **^{64}Cu(II)-Cyclen-TPN** had a tumor uptake of 3.96±0.56 %ID/g after only 5 minutes, which increased to 4.72±0.74 after 4 h. **^{64}Cu(II)-Cyclam-TPN** and **^{64}Cu(II)-Cyclo15-TPN** had a tumour uptake of 4.80±0.30 %ID/g and 2.11±0.29 %ID/g after 5 min, respectively. Tumour uptake of **^{64}Cu(II)-Cyclam-TPN** dropped to 2.18±0.29 %ID/g after 4 h, whereas an increased uptake of 3.28±0.36 %ID/g was found for **^{64}Cu(II)-Cyclo15-TPN**. The tumour uptakes are summarized in Table 1.

Table 1. Tumour (T) uptake for ^{64}Cu-labelled Cyclen-TPN, Cyclam-TPN and Cyclo15-TPN in BALB/c mice implanted with EMT-6 tumours. *(Data presented as %ID/g ± sd (n=4). Tumour/Blood (T/B) and Tumour/Muscle (T/M) ratios ± sd.)*

	Cyclen-TPN		Cyclam-TPN		Cyclo15-TPN	
	5 min	4 h	5 min	4 h	5 min	4 h
T	3.96±0.60	4.72±0.74	4.80±0.30	2.18±0.29	2.11±0.29	3.28±0.36
T/B	0.70±0.19	1.37±0.16	0.71±0.22	1.37±0.16	1.16±0.09	1.83± .29
T/M	1.68±0.34	4.44±0.98	1.79±0.14	5.14±0.69	3.80±0.57	4.70±0.97

Conclusion

In vivo studies on these tetrapropionitrile ligands show that tumour uptake is observed and that compounds of this type may be of use as both a diagnostic or radiotherapy agent.

References

[1] Kong, D. *et al.*, Polyhedron 19 (2000) 217.

Formation of Stable Cu(II)-Complexes with Dendritic Oxybathophenanthroline Ligands

H. Stephan, G. Geipel[1], G. Bernhard[1], U. Hahn[2], F. Vögtle[2]
[1]Institut für Radiochemie, [2]Universität Bonn

Hydrophobic dendritic oxybathophenanthroline ligands (generation 0 to 4) have been synthesised. The complexation behaviour towards Cu(II) has been studied using liquid-liquid extraction experiments and time-resolved laser-induced fluorescence spectroscopy (TRFLS). The formation of 1:3 complexes (metal:ligand) having high stability has been proven in organic media.

Introduction

Derivatives of 1,10-phenathroline and their metal complexes are of considerable interest in bioinorganic chemistry, biology and medicine [1]. In this nexus, dendritic modification (Scheme 1) is gaining in importance opening the way of tailoring complexation and solubility behaviour. Ruthenium(II) complexes containing dendritic 4,7-bis(benzyloxy)-1,10-phenanthroline show interesting luminescence and redox properties [2]. Octahedral assemblies can be obtained by coordination of phenanthroline ligands having branched units in the 3,8-position with certain metal ions [3]. Recently, bischelates of dendritic 2,9-disubstituted phenanthroline derivatives with copper(I) have been described [4].

Scheme 1. Suitable positions for dendritic modification of 1,10-phenanthroline

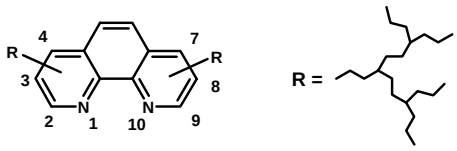

Here we want to report the complexation behaviour of dendritic oxybathophenanthroline ligands towards copper(II).

Results and Discussion

Dendritic oxybathophenanthroline ligands from zero to the fourth generation (cf. Scheme 2; only generation 1 is shown) were synthesised by addition of 2 equiv. of the corresponding dendritic benzylbromides to 1 equiv. deprotonated 4,7-bis(4´-hydroxyphenyl)-1,10-phenanthroline (NaH) dissolved in DMF.

Scheme 2. Dendritic oxybathophenanthroline ligand (generation 1)

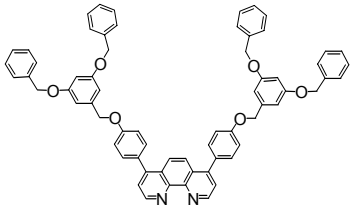

Liquid-liquid extraction studies in the system $Cu(NO_3)_2$/MES-NaOH buffer (pH = 5.3)//ligand/$CHCl_3$ using ^{64}Cu for the determination of copper concentration have been performed. The higher the generation of the dendritic ligand the higher the extraction efficiency of Cu(II) clearly indicating a dendritic effect. The results obtained from liquid-liquid extraction point to fast kinetics of complexation and the formation of 1:3 complexes (Cu(II):ligand) in the organic phase. This finding has been corroborated by spectroscopic investigations using TRLFS experiments. Spectroscopic titration of dendritic ligands with copper(II) gives the evidence of clear 1:3 complex formation for all dendritic ligands investigated. It can be seen from Fig.1 that the intensity of the emitted fluorescence signal of the dendritic ligand (excitation wavelength: 266 nm) is reduced with increasing copper concentration. At the stoichiometry of 1:3 (Cu(II):ligand) the fluorescence of the ligand is almost disappeared and clearly visible in a spectral shift. This points to the formation of highly stable Cu(II) complexes in the organic media.

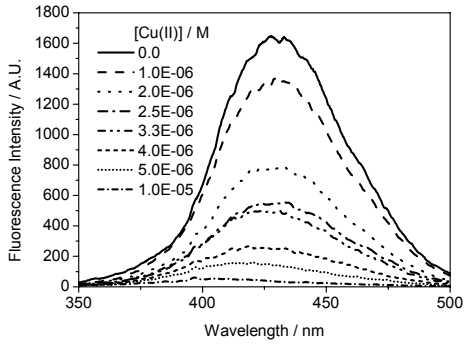

Fig. 1. Time resolved fluorescence spectra of oxybathophenanthroline ligand (generation 1) in dependence of $Cu(CF_3SO_3)_2$ concentration in $CHCl_3$.

The results obtained for the copper complexation with hydrophobic dendritic ligands have encouraged us to develop water-soluble analogues having PEG arms as branching units in view of binding the diagnostically and therapeutically relevant radioisotopes ^{64}Cu and ^{67}Cu.

References

[1] Luman, C. R., Castellano, F. N., in: Comprehensive Coord. Chem. 2004, vol. 1, pp. 25-39.
[2] Serroni, S. *et al.*, Gazz. Chim. Ital. 124 (1994) 423.
[3] Tor, Y., C. R. Chimie 6 (2003) 755.
[4] Gumienna-Kontecka, E. *et al.*, Inorg. Chem. 43 (2004) 3200-3209.

Remarkable Enhancement of Cell Uptake for $[Ti_2W_{10}PO_{40}]^{7-}$ in the Presence of Chitosan

H. Stephan, R. Bergmann, K. Rode, A. Röllich, W. Kraus[1], K. Inoue[2], L. Jelínek[3], Z. Matějka[3]
[1]BAM Berlin, [2]Saga University, Japan, [3]Institute of Chemical Technology Prague

The Keggin type metal oxygen anion cluster $[Ti_2W_{10}PO_{40}]^{7-}$ forms stable particles of defined stoichiometry with the polysaccharide chitosan. Cell uptake studies with $[Ti_2W_{10}PO_{40}]^{7-}$ using the tumour cell line HT-29 showed that the tungsten amount inside the cells is remarkably enhanced in the presence of chitosan.

Introduction

Certain polyoxometalates (POMs) have been recognized to efficiently penetrate into tumour cells and to act as anti-tumour agents [1]. However, many derivatives have a poor hydrolytic stability under physiologically relevant conditions leading to non-reproducible results. $K_7[Ti_2W_{10}PO_{40}]$ has been found as a very stable compound even at higher pH [2]. Thus, this tungsten oxygen cluster has been chosen for cell uptake experiments.

Results and Discussion

$K_7[Ti_2W_{10}PO_{40}]$ was prepared according to [3]. This polyoxotungstate has a high water solubility (>0.05 M), and it crystallizes from aqueous solution as $K_4H_3[Ti_2W_{10}PO_{40}]\cdot 15H_2O$ having a tetragonal structure (Fig. 1).

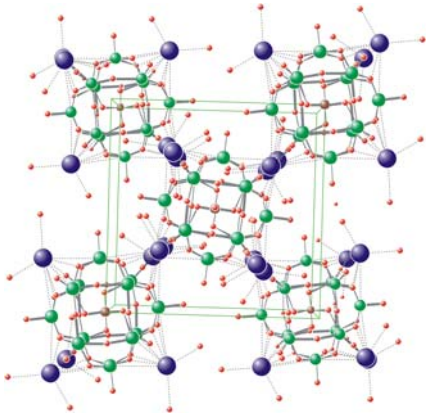

Fig. 1. Crystal packing of $K_4H_3[Ti_2W_{10}PO_{40}]\cdot 15H_2O$

The polyanion is surrounded by potassium cations and water molecules that form a hydrogen bond network with terminal and point-bridged oxygens from the cluster anion leading to a highly symmetric structure. Knowing that aminosaccharides can form stable complexes with metal oxoanions [4], the potassium cation was replaced by glucosamine and water-soluble chitosan (M_r ~ 10.000 g/mol; Fig. 2), respectively.

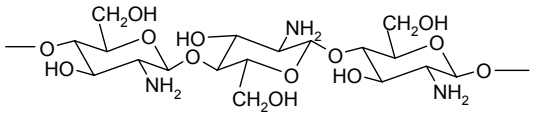

Fig. 2. Chemical structure of chitosan

After mixing an aqueous solution of $K_7[Ti_2W_{10}PO_{40}]$ (c = 10^{-4} M) with chitosan (0.5…2 g/l), the formation of stable nanometer-sized particles has been observed [5]. Interestingly, the stoichiometry of the particles formed of chitosan and $[Ti_2W_{10}PO_{40}]^{7-}$ in the pH-range = 5.0…7.6 was always 1:5 independently from the initial chitosan concentration.

Cell uptake studies of $[Ti_2W_{10}PO_{40}]^{7-}$ has been performed using HT-29 cell line (adenocarcinoma). Thus, ~$5\cdot 10^4$ HT-29 cells were incubated for 24 h at 37 °C under 5 % CO_2 using McCoy's 5A medium (24-well plates, 4 replicates for each concentration) in the presence of various $[Ti_2W_{10}PO_{40}]^{7-}$ concentrations (0–500 µM). In order to study the influence of aminosaccharides on the cell uptake of the polyoxotungstate two additional test series in the presence of glucosamine (10^{-4} M) and chitosan (1 g/l) have been carried out. Glycolysis studies using ^{18}F-labelled FDG point to a low toxicity of $[Ti_2W_{10}PO_{40}]$ and $[Ti_2W_{10}PO_{40}]$/glucosamine mixtures in the HT-29 cell line. On the other hand, glycolysis activity is remarkably decreased in the case of applying $[Ti_2W_{10}PO_{40}]$/chitosan particles. This finding may be explained on the basis of a considerably higher tungsten content found in cells contacted with nanoparticles formed of $[Ti_2W_{10}PO_{40}]^{7-}$ with chitosan (Table 1).

Table 1. Tungsten content in HT-29 cells

Conditions	µg W / mg cell protein
100 µM $[Ti_2W_{10}PO_{40}]$	1.3± 0.7
100 µM $[Ti_2W_{10}PO_{40}]$ + 100 µM glucosamin	1.3± 0.8
100 µM $[Ti_2W_{10}PO_{40}]$ + 1 g/l chitosan	**30.5± 2.9**

References

[1] Rhule, J. T. *et al.*, Chem. Rev. 98 (1998) 327-357.
[2 Stephan, H. *et al.*, *Annual Report 2003,* FZR-394, p. 50.
[3] Domaille, P. J. *et al.*, Inorg. Chem. 22 (1983) 818-822.
[4] Matějka, Z. *et al.*, J. Ion Exch. 14 (Suppl.) (2003), 237.
[5] Richter, W. *et al.*, *this report*, p. 53.

Colloid-Chemical Characterisation of Nanoparticles Formed by $[Ti_2W_{10}PO_{40}]^{7-}$ and Chitosan

W. Richter[1], H. Zänker[1], P. Krotká[2], Z. Matějka[2], A. Röllich, H. Stephan
[1]Institut für Radiochemie, [2]Institute of Chemical Technology Prague

Nanoparticles formed of the Keggin type cluster anion $[Ti_2W_{10}PO_{40}]^{7-}$ with the polysaccharide chitosan have been characterised by photon correlation spectroscopy, scanning electron microscopy, filtration and centrifugation experiments. Experiments reveal that the size of the particles formed are in the range of 40 to 300 nm.

Introduction

Organic modification of polyoxometalates (POMs) appears highly attractive to develop metallic drugs [1]. Thus, starch and liposome encapsulated POMs show suitable biocompatibility, enhanced chemical stability and improved antitumoural activity [2, 3]. Recently, we found that $[Ti_2W_{10}PO_{40}]$/chitosan associates have been efficiently taken up into tumour cells [4]. Chitosan is a linear polysaccharide composed of randomly distributed ß-(1-4)-linked D-glucosamine (deacetylated unit) and N-acetyl-D-glucosamine (acetylated unit). Low molecular weight chitosan is well-soluble in water. But when $K_7[Ti_2W_{10}PO_{40}]$ (POM1) is added, nanoparticles may be formed. In this paper, we want to report the colloid-chemical characterization of these particles.

Experimental

Chitosan (YC-100, M_r ~ 10.000 g/mol) was supplied by YDC company (Seoul, South Korea). The experiments were done with two solutions: solution A (50 mg/l chitosan and $1 \cdot 10^{-4}$ M POM1) and solution B (500 mg/l chitosan and $1 \cdot 10^{-4}$ M POM1). Both solutions were diluted with water in the ratio 1:10. These solutions were investigated with the following techniques: photon correlation spectroscopy (PCS), filtration, centrifugation, and scanning electron microscopy. The centrifugates, filtrates and filter cakes were analysed by ion chromatography and ICP-MS.

Results and Dicussion

The filtration experiments of the solutions suggested that all particles are smaller than 1 µm. Fig. 1 shows an SEM micrograph of the deposits on a 100-nm filter confirming the existence of particles in the 100-nm size range. PCS measurements in the solution revealed the presence of colloid particles of 40 to 300 nm in diameter. Fig. 2 shows the particle size distribution from solution A received by PCS measurement analysed by CONTIN method [5]. Centrifugation experiments have been performed with both solutions: Solution A with an excess of POM1 and solution B with an excess of chitosan. As can be seen from Table 1, comparable size distribution of particles has been found. This finding points to the formation of well-defined associates between chitosan and POM1.

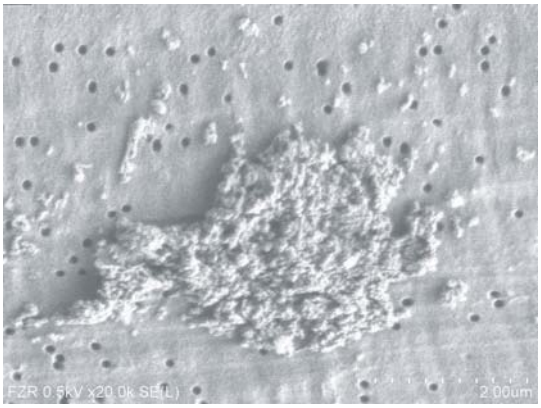

Fig. 1. Scanning electron micrograph of $[Ti_2W_{10}PO_{40}]$/ chitosan associates (filter pores = 100nm)

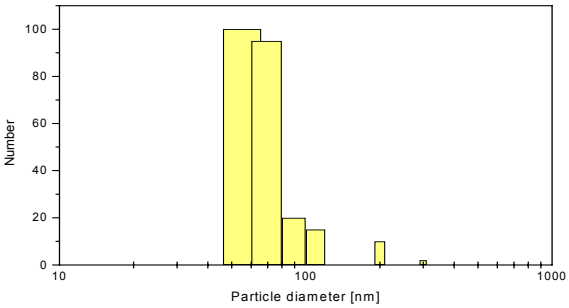

Fig. 2. Particle size distribution as obtained by photon correlation spectroscopy (PCS) for solution A

Table 1. Particle size distribution as obtained by centrifugation (average density of the particles = 1,1 g/cm^3)

Particle size [nm]	Solution A	Solution B
>370	0,8 %	2,1 %
370 ... 224	9,7 %	2,4 %
224 ... 132	18,1 %	18,2 %
132 ... 52	25,6 %	37,3 %
<52	45,8 %	40,0 %

References

[1] Rhule, J. T. *et al.*, Chem. Rev. 98 (1998) 327-357.
[2] Wang, X. *et al.*, Dalton Trans. (2003) 957-960.
[3] Yang, Y. *et al.* Trans. Metal Chem. 29 (2004) 96-99.
[4] Stephan, H. *et al.*, *this report*, p. 52.
[5] Provencher, S. W., Makromol. Chem. 180 (1979) 201-209.

Estimation of Partition Coefficient (log P) with Molecular Modelling of Rhenium and Technetium Complexes

K. Yoshizuka[1], H. -J. Pietzsch, H. Stephan
[1] *University of Kitakyushu, Japan*

A novel molecular modelling method for Re and Tc complexes combined with the molecular mechanics and the molecular dynamics has been developed for estimating log P of these complexes between water and 1-octanol.

Introduction

Lipophilicity of ^{99m}Tc and ^{188}Re tracers is an important parameter for the prediction of absorption and distribution of these tracers in biosystems.
We are now developing an estimation method of log P of Re and Tc complexes combined with the molecular mechanics (MM) and the molecular dynamics (MD). In this paper, we describe the MM and the MD in binary system of water/1-octanol of Re- and Tc-DMSA model complexes as shown in Fig. 1.

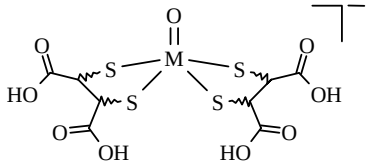

Fig. 1. Re- and Tc-DMSA complexes (mixtures of isomeres)

Calculation methods

The MM calculations were performed with the strain minimization program MOMEC97 [2]. Within the molecular mechanics frame work, the structure of a molecule is modified in order to minimize its total strain energy (U_{total}) consisting of bond length deformation (E_b), valence angle deformation (E_θ), torsion angle deformation (E_ϕ) and non-bonded interaction (E_{nb}), as expressed by eq.(1).

$$U_{total} = \Sigma(E_b + E_\theta + E_\phi + E_{nb}) \qquad (1)$$

No symmetry restrictions were imposed on the local coordination sphere, and non-bonded interactions involving the metal center were neglected. Input coordinates were obtained from X-ray crystal structure data in literatures. The constant values of force field parameters were adjusted until an optimal agreement between calculated and observed structures was obtained throughout the entire range of available structures.
The MD simulations were performed using the MD program WinMASPHYC Pro. The potential parameters for MD calculations were transferred from those of MM described above.

Results and Discussion

Fig. 2 illustrates RMS overlays of the calculated lowest energy structures of Re-DMSA calculated by MOMEC97 with crystal structure cited in Cambridge Structure Database. Since both structures are in good agreement with corresponding (RMS = 0.24 Å), we consider that this force field parameters are also adaptable in order to obtain the calculated structures of these complexes.

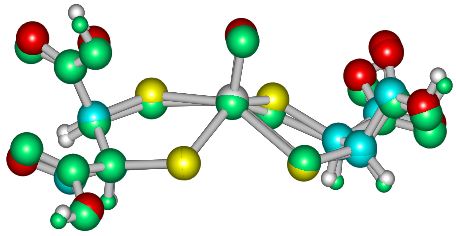

Fig. 2. Overlay of computed MOMEC and X-ray structures of Re-DMSA.

Fig. 3 shows the MD snap shot of Re-DMSA in water/1-octanol binary system (1.5×1.5×6 nm) after 100 ps. Using the calculated internal energies of the binary systems of both the complex in 1-octanol (U_o) and that in water (U_a), the energy difference ($\Delta U = U_o - U_a$) can be obtained. Since ΔU directly reflects the energy difference between non-bonded interaction of the complex and solvent, we are attempting the quantitative structure-property relationship (QSPR) between ΔU and experimental values of log P.
Both experimental and calculated values pointed to a higher lipophilicity of the Tc complexes in comparison with the Re analogues.

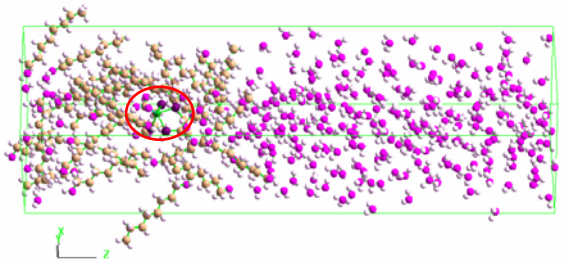

Fig. 3. MD simulation of Re-DMSA complex in water/ 1-octanol binary system

References

[1] Seifert, S. *et al.,* Appl. Radiat. Isot 48 (1997) 1051-1057.
[2] Yoshizuka, K. Ronbunshu 26 (2000) 517-522.

PET IN DRUG AND FOOD RESEARCH

Biodistribution and Catabolism of ^{18}F-Labelled Amadori Product Fructoselysine

C. Hultsch, M. Hellwig[1], R. Bergmann, B. Pawelke, T. Henle[1]
[1]Institute of Food Chemistry, TU Dresden

After synthesis of an ^{18}F-labelled analogue of fructoselysine by conjugation with N-succinimidyl-4-[^{18}F]fluorobenzoate, biodistribution and catabolism of this labelled compound were studied.

Introduction

Amadori products are formed in food via Maillard reaction. This reaction takes place when components like reducing sugars and amino acids or proteins react together. It occurs in most foods during heating. Thereby up to 50 % of the lysyl moieties may be modified because the ε-amino group of lysine is especial susceptible to reactions with sugars [1].
Therefore one of the most important Amadori products is fructoselysine. Several studies concering bioavailability of fructoselysine show that at most 1 to 3 % of alimentary administered fructoselysine is excreted to the urine. Because recovery in faeces is also only 1 to 2 %, the fate of 95 % fructoselysine remains unclear [2]. For this reason, biodistribution, catabolism and elimination of ^{18}F-labelled fructoselysine were investigated.

Results and Discussion

N-succinimidyl-4-[^{18}F]fluorobenzoate was used to modify fructoselysine at its α-amino group. The coupling reaction resulted in the respective 4-[^{18}F]fluorobenzoylated derivative (Fig. 1), which was separated by semipreparative HPLC.

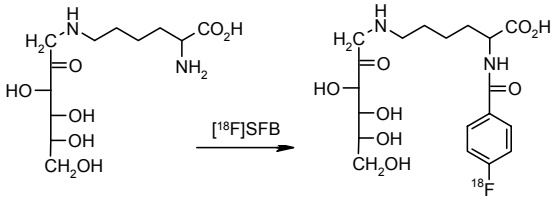

Fig. 1. Conjugation of fructoselysine with [^{18}F]SFB

Firstly *in vitro* testings were accomplished. Thereby the [^{18}F]fluorobenzoylated fructoselysine remained almost unchanged in all examined tissue homogenates (brain, liver, kidney, pancreas, heart and spleen from male Wistar rats) as well as in plasma and whole blood. Only in lysed whole blood the formation of a metabolite (m_1) could be observed. The formation of this metabolite could be inhibited by addition of 1-deoxy-1-morpholinofructose, a specific inhibitor of the enzyme fructosamine 3-kinase [3]. Furthermore, the metabolite m_1 was completely transformed to [^{18}F]fluoro-benzoylated fructoselysine after addition of the enzyme alkaline phosphatase. Therefore m_1 should be a phosphate ester which is formed by a fructosamine kinase.
In *in vivo* experiments the metabolite m_1 was also found. In plasma the appearance of m_1 could not be observed till 60 min p.i.. Then 10 % of total radioactivity were derived from m_1. In urine 60 min p.i. a second metabolite (m_2) could be found. m_2 was identified as [^{18}F]fluorobenzoylated lysine. However, altogether m_1 and m_2 represented less than 8 % of the total radioactivity. Furthermore, 60 min p.i. in the kidney sample 16 % of unmodified [^{18}F]fluorobenzoylated fructoselysine were left. The portion of m_1 was about 82 %. m_2 was found to 2 %.
Moreover, biodistrubtion of the fructoselysine derivative was investigated. The results are presented in Figs. 2 and 3. For comparison the biodistribution results of [^{18}F]fluorobenzoylated lysine are also shown.

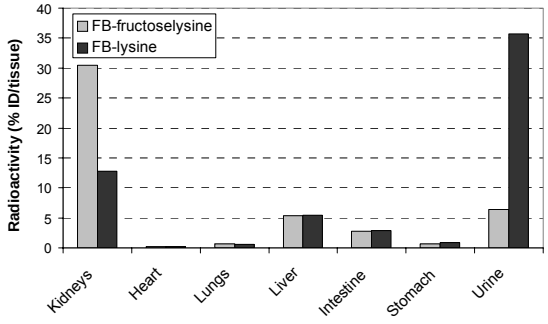

Fig. 2. Biodistributions (5 min p.i.)

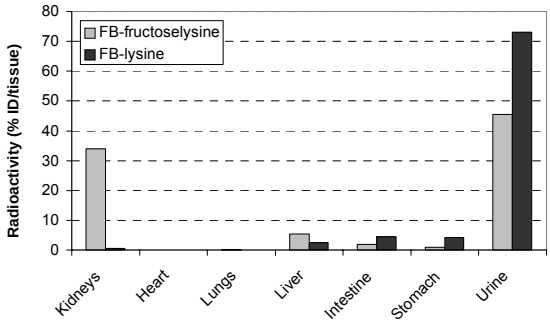

Fig. 3. Biodistributions (60 min p.i.)

After intravenous application the [^{18}F]fluorobenzoylated fructoselysine was fast taken up into the kidneys. 5 min p.i. over 30 % of the administered dose could be found in the kidneys. Also 60 min p.i. still more than 30 % of

whole radioactivity were localised in the kidneys. However, in comparison to [^{18}F]fluorobenzoylated lysine the [^{18}F]fluorobenzoylated fructoselysine showed a stronger accumulation in the kidneys and a delayed excretion into the urine.
Because the studies of the *in vivo* stability showed the existence of large amounts of m_1 – a phosphate ester of [^{18}F]fluorobenzoylated fructoselysine – in the kidneys, the accumulation of radioactivity seems to result from this phosphate ester. Recapitulatory, it should be noticed that amost half of the administered [^{18}F]fluorobenzoylatedfructose lysine was excreted to the urine nearly unchanged within 60 min p.i..
Consequently, the main part of the lysine, which was fructosylated during food processing, remains unusable in spite of the activity of renal fructosamine kinase.

References

[1] Belitz, H. D., Grosch, W., Schieberle, P. (2001) Lehrbuch der Lebensmittelchemie, Springer Verlag, Berlin.
[2] Erbersdobler, H. F. *et al*., Dev. Food Sci. 13 (1986) 503-508.
[3] Delpierre, G. *et al*., Biochem. J. 352 (2000) 835-839.

Radiolabelled Flavonoids and Polyphenols
III. Synthesis of an ^{18}F-Labelled Resveratrol Derivative

S. Gester, J. Pietzsch, F. Wüst

*The Wittig-Horner-Emmons carbonyl olefination was employed as the key step in the synthesis of 5-[(E)-2-(4-[^{18}F]fluorophenyl)ethenyl]-1,3-benzenediol (3,5-dihydroxy-4'-[^{18}F]fluoro-trans-stilbene) **[^{18}F]-1**. In a typical experiment, starting from 5.75 GBq [^{18}F]fluoride, 215 MBq of **[^{18}F]-1** could be obtained within a total synthesis time of 120-130 min.*

Introduction

As reported earlier we set up a synthesis of ^{18}F-labelled resveratrol derivative 5-[(*E*)-2-(4-[^{18}F]fluorophenyl)ethenyl]-1,3-benzenediol **[^{18}F]-1** to evaluate the radiopharmacological profile by means of PET [1]. However, the use of methoxy groups as protecting groups in the ^{18}F-labelled stilbene compound proved to be not suitable due to low yields observed in the deprotecting step. Therefore we now describe a modified synthesis of 5-[(*E*)-2-(4-[^{18}F]fluorophenyl)ethenyl]-1,3-benzenediol **[^{18}F]-1** using MOM-ether protecting groups.

Results and Discussion

The syntheses of novel labelling precursor **4c** and reference compound **1** are given in Fig. 1.

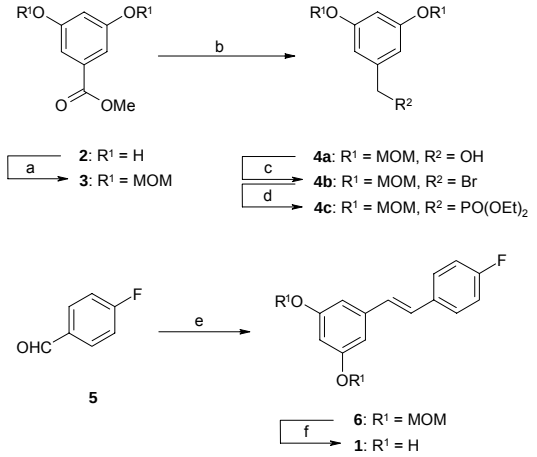

Reagents and conditions: (a) MOMCl, DIPEA, THF, reflux, 100 %; (b) $LiAlH_4$, Et_2O, 0°C-RT, 92 %; (c) NBS, PPh_3, DMF, 60 °C, 56 %; (d) $P(OEt)_3$, 160 °C, 65 %; (e) **4c**, KO^{t}Bu, DMF, 100 %; (f) MeOH, HCl, 93 %.

Fig. 1. Synthesis of the labelling precursor **4c** and reference compound **1**

The labelling precursor **4c** was obtained in four steps starting from commercially available methyl 3,5-bis(methoxymethoxy)benzoate **2**. The phenolic OH-groups in **2** were protected as MOM-ether groups, and MOM-ether **3** was reduced with $LiAlH_4$ to give [3,5-bis-(methoxymethoxy)phenyl]methanol **4a** in 92 % yield according to Sun *et al.* [2]. Subsequent bromination of the benzyl alcohol **4a** with NBS/PPh_3 in DMF gave 1-(bromomethyl)-3,5-bis(methoxymethoxy)benzene **4b** in 56 % yield [3]. Finally, a Michaelis-Arbuzov reaction of the bromide **4b** with an excess of triethyl phosphite at 160 °C gave diethyl-[3,5-bis-(methoxymethoxy)benzyl]phosphonate **4c** in 65 % yield. The Wittig-Horner-Emmons carbonyl olefination of the phosphonate **4c** with 4-fluorobenzaldehyde **5** under basic conditions (KO^{t}Bu, DMF) led to the formation of 1-[(*E*)-2-(4-fluorophenyl)-ethenyl]-3,5-bis(methoxymethoxy)benzene **6** in quantitative yield. Treatment of MOM-ether **6** with HCl provided reference compound **1** in 93 % yield.

The radiosynthesis of **[^{18}F]-1** was carried out by coupling phosphonic acid diester **4c** in the presence of KO^{t}Bu with readily available 4-[^{18}F]fluorobenzaldehyde **[^{18}F]-5** according to a Wittig-Horner-Emmons carbonyl olefination protocol (Fig. 2).

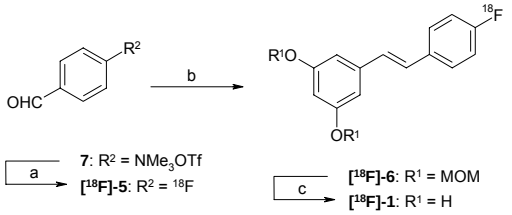

Reagents and conditions: (a) [^{18}F]F$^-$, K_2CO_3/Kryptofix$_{222}$, DMF, 120 °C, 15 min; (b) **4c**, KO^{t}Bu, DMF, 60 °C, 15 min; (c) 3 N HCl, 60 °C, 20 min.

Fig. 2. Synthesis of ^{18}F-labelled resveratrol derivative **[^{18}F]-1**

The resulting coupling product **[^{18}F]-6** was treated with 3 N HCl to remove MOM-ether protecting groups. Subsequent final semi-preparative HPLC purification gave compound **[^{18}F]-1** in decay-corrected radiochemical yield of 9 % and at a specific activity of 90 GBq/µmol within 120-130 min. The radiochemical purity exceeded 95 %. The radiopharmacological evaluation of **[^{18}F]-1** is currently in progress.

References

[1] Gester, S. *et al.*, *Annual Report 2003*, FZR-394, p. 29.
[2] Sun, W. Y. *et al.*, Synthesis 11 (1998) 1619-1622.
[3] Wüst, F. *et al.*, Radiochim. Acta 92 (2004) 349-353.

CYCLOTRON OPERATION

Operation of the Rossendorf PET Cyclotron "CYCLONE 18/9" in 2004

St. Preusche, F. Wüst

Routine operation

The radionuclides produced in routine operation in 2004 were F-18, C-11, O-15 available as $[^{18}F]F^-$, $[^{18}F]F_2$, $[^{11}C]CO_2$, and $[^{15}O]H_2O$. There were no demands for production of ^{13}N. The production of the non-standard radionuclide ^{86}Y became routine operation in 2004. Table 1 gives an overview of the 2004 radionuclide production.

Due to an increasing demand of radiopharmaceuticals (FDOPA, OMFD) and radiotracers the daily operating time of the CYCLONE 18/9 increased by 30 % with regard to the maximum value of 2001 and varied now between three and five hours. It is the first time that the number of deuterons beam hours exceeds those of the protons significantly.

Table 1. Radionuclide production in 2004

RN	Radionuclide production	
	Number of Irradiations	$SumA_{EOB}$ GBq
$[^{18}F]F^-$	274	9002
$[^{18}F]F_2$	303*)	1837
^{11}C	106	2900
^{15}O	88	1940
^{86}Y	18	20.1
^{56}Co	4	0.002

*) including pre-irradiations

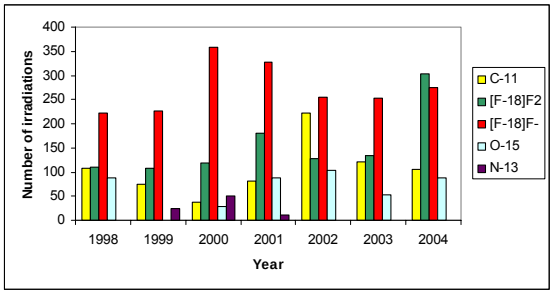

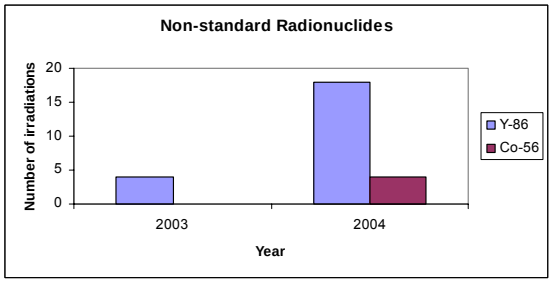

Fig 1a, b. Number of irradiations of radionuclides produced.

Fig. 1 shows the number of irradiations of our radionuclides and Fig. 2 the total amount of activity produced over the last seven years (1998 to 2004).

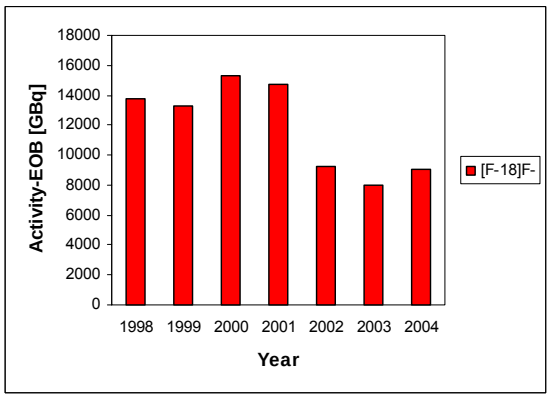

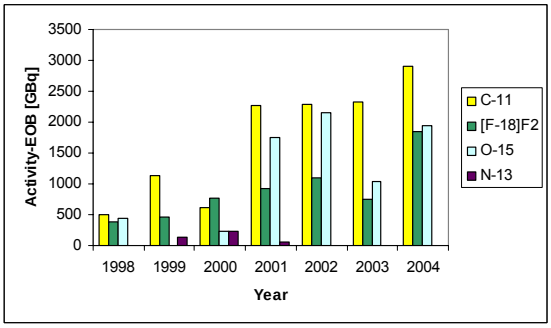

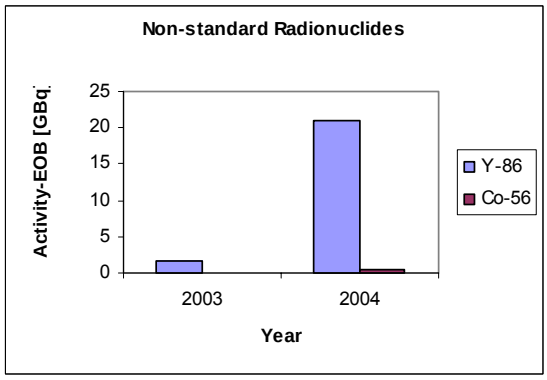

Fig. 2a, b, c. Total amount of activity produced.

Improvements at the cyclotron

An improved version of the Rossendorf solid target system [1, 2] was designed, assembled and tested. Thus, the yield of ^{86}Y produced could be increased by 50 % using similar irradiation conditions.

Maintenance and service

- Stripper foils
Serious problems with the carbon stripper foils occurred in 2004 and led to a number of cyclotron openings that exceeded the average annual value by a factor of 3. The stripper foils tore at the front edge of the fork or at any other edges and curled. Thus, stable extraction conditions were not possible any more. We also observed this effect with stripper foils that were not in the ion beam. Comprehensive investigations were carried out and led to the result that these effects could be explained by the bad quality of the stripper foils. Since the end of 2004 we have tested carbon foils of other suppliers.

- Cathodes for the ion sources
Since 2004 the cathodes for both ion sources are manufactured in the FZR (Dept. of Research Technology). With the new Ta cathodes the ion sources need less arc current to achieve a certain ion beam current and work more stable over period of use.

- Annual check of the cyclotron
The annual check of the CYCLONE 18/9 facility by the TÜV Sachsen organization (TÜV = Association for Technical Inspection) under § 66 (2) of the Radiation Protection Regulation was carried out in the second half of September. There were no objections to the further operation of the cyclotron.

Radiation protection

- Emission of radionuclides with the exhaust air
The emission of radionuclides with the exhaust air is routinely monitored. As shown in Table 2, it is well below the limit of 2.0E11 Bq.

Table 2. Emission of radionuclides with the exhaust air in 2004 as a result of cyclotron operation

Radionuclide	Emission [Bq/a]
^{41}Ar	1.7E10
^{18}F	6.3E09
Sum	2.3E10
Percentage of the annual limit	11.7

- Exposure to radiation of the cyclotron staff
The cyclotron staff belong to category A of occupational exposed persons. The average exposure to radiation of the cyclotron staff over the years is shown in Table 3. The increase in 2004 is due to the strongly increased number of cyclotron openings to replace destroyed stripper foils and to more maintenance work as result of an increased number of beam hours and related to it an increased wear.

Table 3. Average exposure to radiation of the cyclotron staff

Year	Exposure [mSv]
1997	1.8
1998	2.9
1999	3.5
2000	6.2
2001	4.6
2002	1.7
2003	2.6
2004	5.2

References

[1] Preusche, St. *et al.*, *Annual Report 2002*, FZR-363, p. 69.
[2] Preusche, St., *et al., this report*, p. 63.

Improved Version of the Rossendorf Solid Target System

St. Preusche, N. Dohn, H. Roß

An improved version of the Rossendorf solid target system was designed, assembled and tested.

Introduction

Originally, the Rossendorf solid target system (STS) [1, 2] consisted of an irradiation chamber to irradiate targets with rectangular shape (*rectangle targets*) and a module connected to the chamber to irradiate targets with circular shape (*disk targets*).
During the test period of STS in 2003 it became obvious that very sensitive target materials will not be used in the next future and thus there will be no reasons for using the irradiation chamber with the rectangle targets.
The focus of interest changed to the use of the disk target system only.

Technical feature

The irradiation chamber was completely removed from STS and new adapter flanges to match the disk target system to the external beam transport line were designed, manufactured and tested.
Fig. 1 shows the new disk target system.

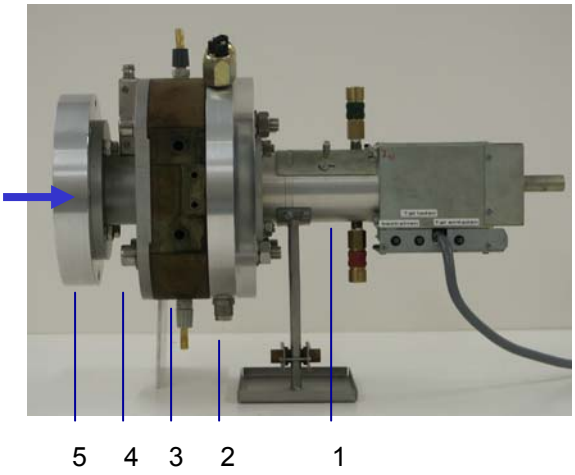

Fig. 1. New disk target system; 1 - target unit with insulating flange, 2 - He cooling flange, 3 - collimator flange with vacuum window, 4 - adapter flange, 5 - adapter flange to ISO DN 100 (external beam transport line)
Arrow: ion beam direction.

The disk target holder with the target is electrically driven from the load position into the irradiation position and there it is fixed by a spring. The target holder is water cooled at the rear, the target surface is He cooled by a special nozzle inside the He cooling flange (see Fig. 1, position 2) and in this way the vacuum window is also cooled. The collimator insert (see Fig. 1, position 3) is water cooled.

Water and He interlocks for the disk target are connected to the cyclotron's internal interlock system. They act only in the case when the vacuum valve of the external beam transport line is open.

Results

The new disk target system has been working for half a year in the predicted way. Without the long irradiation chamber and its low He overpressure inside there are less energy losses of the ion beam on the target resulting in higher production yields of e.g. ^{86}Y. With comparable irradiation parameters it is now possible to achieve 50 % more ^{86}Y activity [3].

References

[1] Preusche, St. *et al.*, *Annual Report 2002*, FZR-363, p. 69.
[2] Preusche, St. *et al.*, *Annual Report 2003*, FZR-394, p. 59.
[3] Preusche, St. *et al.*, *this report*, p. 64.

Production of ^{86}Y and ^{56}Co at the Rossendorf PET Cyclotron "CYCLONE 18/9"

St. Preusche, F. Wüst, K.D. Schilling[1], N. Dohn, H. Roß
[1]FZR, Institut für Kern- und Hadronenphysik

Additional to the routine production of ^{18}F, ^{15}O, ^{13}N and ^{11}C the positron emitting radionuclides ^{86}Y and ^{56}Co are produced using the Rossendorf solid target system.

Introduction

The number of radionuclides produced at the Rossendorf CYCLONE 18/9 cyclotron was increased in 2004. Additional to the routine production of ^{18}F, ^{15}O, ^{13}N and ^{11}C the positron emitting radionuclides ^{86}Y ($T_{1/2}$ = 14.7 h) and ^{56}Co ($T_{1/2}$ = 77.3 d) are produced using the Rossendorf solid target system [1, 2].
^{86}Y as potentially better radionuclide than ^{111}In for the estimation of an absorbed dose in ^{90}Y therapy is produced via the ^{86}Sr(p,n)^{86}Y nuclear reaction using enriched $^{86}SrCO_3$ as target material [3].
^{56}Co is produced via the ^{56}Fe(p,n)^{56}Co nuclear reaction using natural Fe as target material. The Institut für Kern- und Hadronenphysik of the FZR uses ^{56}Co as a very convenient gamma calibration source for HPGe detectors applied in measurements of characteristic γ-radiation in nuclear resonance fluorescence [4] and photo-activation [5] experiments at the Rossendorf ELBE Radiation Source.

Results and Discussion

^{86}Y

The enriched target material (70 mg) is pressed into a platinum target holder and covered by a thin platinum foil for protection.
Typical irradiation parameters are:
Ion beam on the target: (6.5 – 8) µA
Irradiation time: (80 – 110) min

With these parameters (1.3 – 2.2) GBq of ^{86}Y could be achieved at end of bombardment (EOB).
In 2004 18 irradiations of $^{86}SrCO_3$ were carried out and a total amount of 21 GBq of ^{86}Y activity (EOB) was produced.
The results of γ-spectrometric analyses show that only 0.04 % of the long-lived radionuclide ^{88}Y ($T_{1/2}$ = 106.6 d) are formed under the irradiation parameters mentioned above [3].

^{56}Co

The first tests to find suitable irradiation parameters for the production of ^{56}Co were carried out with a target area of 12 mm in diameter (natural Fe: ^{54}Fe/5,8 %, ^{56}Fe/91,7 %, ^{57}Fe/2.2 %, ^{58}F/0.3 %). Using an ion beam on the target of (1 – 2) µA and irradiation times of (2 – 20) min (0.08 – 1.8) MBq of ^{56}Co could be achieved at EOB.
The results of γ-spectrometric analyses show that less than 1 % of the long-lived radionuclides ^{57}Co ($T_{1/2}$ = 271.8 d) and ^{58}Co ($T_{1/2}$ = 70.8 d) are formed under these irradiation parameters [6].
The ^{56}Co activity of 80 kBq had to be reduced due to the very sensitive detector systems. A new target design became necessary: a removable Fe insert of only 16 mm^2 in cross section as target surface is now fixed in the target holder disk.
Using an ion beam current of 1 µA on the target and irradiation times of (2 – 3) min 12.5 – 15.7 kBq of ^{56}Co could be achieved at EOB.
These ^{56}Co activities enable an effective calibration of the HPGe detectors.

References

[1] Preusche, St. *et al.*, *Annual Report 2003*, FZR-394, p. 59.
[2] Preusche, St. *et al.*, *this report*, p. 63.
[3] Seifert, S. *et al.*, *this report*, p. 32.
[4] Schwengner, R., *Annual Report 2003*, FZR-398, p. 24.
[5] Erhard, M. *et al.*, *Annual Report 2003*, FZR-401, p. 13.
[6] Kaden, M., *private information.*

II. PUBLICATIONS, LECTURES, PATENTS AND AWARDS OF THE INSTITUTE AND THE PET-CENTRE ROSSENDORF

PUBLICATIONS

Ahl, B.; Weissenborn, K.; van den Hoff, J.; Fischer-Wasels, D.; Köstler, H.; Hecker, H.; Burchert, W.
Regional differences in cerebral blood flow and cerebral ammonia metabolism in patients with cirrhosis.
Hepatology 40 (2004) 73-79.

Anton, M.; Wittermann, C.; Haubner, R.; Simoes, M.; Reder, S.; Essien, B.; Wagner, B.; Henke, J.; Erhardt, W.; Noll, S.; Hackett, N. R.; Crystal, R. G.; Schwaiger, M.; Gansbacher, B.; Bengel, F. M.
Coexpression of herpesviral thymidine kinase reporter gene and VEGF gene for noninvasive monitoring of therapeutic gene transfer: an in vitro evaluation.
J. Nucl. Med. 45 (2004) 1743-1746.

Baumann, M.; Krause, M.; Eicheler, W.; Petersen, C.; Zips, D.; Beuthien-Baumann, B.; Kotzerke, J.; Laniado, M.; Herrmann, T.
Mikromilieu und Hypoxie im Bild.
Nova Acta Leopoldina NF 89, Nr. 337, (2004) 119-225.

Bergmann, R.; Pietzsch, J.; Füchtner, F.; Pawelke, B.; Beuthien-Baumann, B.; Johannsen, B.; Kotzerke, J.
3-O-methyl-6-^{18}F-fluoro-L-dopa, a new tumor imaging agent: investigation of transport mechanism in vitro.
J. Nucl. Med. 45 (2004) 2116-2122.

Bolzati, C.; Benini, E.; Cazzola, E.; Jung, C.; Tisato, F.; Refosco, F.; Pietzsch, H.-J.; Spies, H.; Uccelli, L.; Duatti, A.
Synthesis, characterization, and biological evaluation of neutral nitrido technetium(V) mixed ligand complexes containing dithiolates and aminodiphosphines. A novel system for linking technetium to biomolecules.
Bioconjugate Chem. 15 (2004) 628-637.

Bredow, J.; Kretzschmar, M.; Wunderlich, G.; Dörr, W.; Pohl, T.; Franke, W.-G.; Kotzerke, J.
Therapy of malignant ascites in vivo by ^{211}At-labelled microspheres.
Nuklearmedizin 43 (2004) 63-68.

Brogsitter, C.; Wonsak, A.; Würl, K.; Kotzerke, J.
Peritoneal strumosis.
Eur. J. Nucl. Med. Mol. Imaging 31 (2004) 1057-1058.

Brust, P.; Vorwieger, G.; Walter, B.; Füchtner, F.; Stark, H.; Kuwabara, H.; Steinbach, J.; Bauer, R.
The influx of neutral amino acids into the porcine brain during development: a positron emission tomography study.
Developmental Brain Research 152 (2004) 241-253.

Brust, P.; Walter, B.; Hinz, R.; Füchtner, F.; Müller, M.; Steinbach, J.; Bauer, R.
Developmental changes in the activity of aromatic amino acid decarboxylase and catechol-*O*-methyl transferase in pigs: a positron emission tomography study.
Neuroscience Letters 364 (2004) 159-163.

Bühler, P.; Just, U.; Will, E.; Kotzerke, J.; van den Hoff, J.
An accurate method for correction of head movement in PET.
Trans. IEEE. Med. Imag. 23 (2004) 1179-1185.

Drews, A.; Heimbold, I.; Pietzsch, H.-J.; Johannsen, B.
Design and biological evaluation of Tc-99m ligands derived from WAY 100635 for serotonin 5-HT$_{1A}$ receptor binding.
in: Development of Tc-99m Agents for Imaging Central Neural System Receptors
IAEA Technical Reports Series no. 426, Vienna, 2004.

Fernandes, C.; Knieß, T.; Gano, L.; Seifert, S.; Spies, H.; Santos, I.
Synthesis and biological evaluation of silylated mixed-ligang ^{99m}Tc complexes with the [PNS/S] donor atom set.
Nucl. Med. Biol. 31 (2004) 785-793.

Grote, M.; Noll, S.; Noll, B.; Johannsen, B.
Syntheses of novel modified acyclic purine and pyrimidine nucleosides as potential substrates of herpes simplex type-1 thymidine kinase for monitoring gene expression.
Can. J. Chem. 82 (2004) 513-523.

Holthoff, V. A.; Beuthien-Baumann, B.; Zündorf, G.; Triemer, A.; Lüdecke, S.; Winiecki, P.; Koch, R.; Füchtner, F.; Herholz, K.
Changes in brain metabolism associated with remission in unipolar major depression.
Acta Psychiatr. Scand. 110 (2004) 184-194.

Kopprasch, S.; Pietzsch, J.; Grässler, J.
The protective effects of HDL and its constituents against neutrophil respiratory bust activation by hypochlirite-oxidized LDL.
Mol. Cell. Biochem. 258 (2004) 121-127.

Kopprasch, S.; Pietzsch, J.; Westendorf, T.; Kruse, H.-J.; Grässler, J.
The pivotal role of scavenger receptor CD36 and phagocyte-derived oxidants in oxidized low density lipoprotein-induced adhesion to endothelial cells.
Int. J. Biochem. Cell Biol. 36 (2004) 460-471.

Lange, S.; Viergutz, T.; Simkó, M.
Modifications in cell cycle kinetics and in expression of G1 phase-regulating proteins in human amniotic cells after exposure to electromagnetic fields and ionizing radiation.
Cell Prolif. 37 (2004) 337-349.

Miyagawa, M.; Anton, M.; Haubner, R.; Simoes, M. S.; Städele, C.; Erhardt, W.; Reder, S.; Lehner, T.; Wagner, B.; Noll, S.; Noll, B.; Grote, M.; Gambhir, S. S.; Gansbacher, B.; Schwaiger, M.; Bengel, F. M.
Positron emission tomography of cardiac transgene expression - comparison of two approaches based on herpesviral thymidine kinase reporter gene.
J. Nucl. Med. 45 (2004) 1917-1923.

Naumann, R.; Beuthien-Baumann, B.
Can [F^{18}]FDG positron emission tomography replace bone marrow biopsy in staging of patients with malignant lymphoma?
Clin. Lymphoma 5 (2004) 127.

Naumann, R.; Beuthien-Baumann, B.; Reiß, A.; Schulze, J.; Hänel, A.; Bredow, J.; Kühnel, G.; Kropp, J.; Hänel, M.; Laniado, M.; Kotzerke, J.; Ehninger, G.
Substantial impact of FDG PET imaging on the therapy decision in patients with early-stage Hodgkin's lymphoma.
Br. J. Cancer 90 (2004) 620-625.

Noll, B.; Hilger, C. S.; Leibnitz, P.; Spies, H.
Neutral oxorhenium(V) and oxotechnetium(V) complexes with novel amide thioether dithiolate ligands derived from cysteine.
Radiochim. Acta 92 (2004) 271-276.

Palma, E.; Correia, J.; Domingos, A.; Santos, I.; Alberto, R.; Spies, H.
Rhenium and technetium tricarbonyl complexes anchored by 5-HT_{1A} receptor-binding ligands containing P,O/N donor atom sets.
J. Organomet. Chem. 689 (2004) 4811-4819.

Pietzsch, J.; Bergmann, R.
Analysis of 6-hydroxy-2-aminocaproic acid (HACA) as a specific marker of protein oxidation: The use of N(O,S)-ethoxycarbonyl trifluoroethyl ester derivatives and gas chromatography/mass spectrometry.
Amino Acids 26 (2004) 45-51.

Pietzsch, J.; Bergmann, R.; Wüst, F.; van den Hoff, J.
Proteinoxidation und Krankheit
FZR-Jahresbericht 2003, FZR-398 (2004) pp. 52-61.

Pietzsch, J.; Bergmann, R.; Kopprasch, S.
Analysis of non-protein amino acids as specific markers of low density lipoprotein apolipoprotein B-100 oxidation in human atherosclerotic lesions: the use of N(O,S)-ethoxycarbonyl trifluoroethyl ester derivatives and GC-MS.
Spectroscopy 18 (2004) 177-183.

Roch, B.; Kopprasch, S.; Pietzsch, J.; Schröder, H.
Oxidativ modifizierte Lipoproteine und deren Antikörper bei Patienten mit Aniphospholipid-Syndrom.
Z. Rheumatol. 63 (2004) 331-337.

Saidi, M.; Kretzschmar, M.; Seifert, S.; Bergmann, R.; Pietzsch, H.-J.
Cyclopentadienyl tricarbonyl complexes of ^{99m}Tc for the in vivo imaging of the serotonin 5-HT_{1A} receptor in the brain.
J. Organomet. Chem. 689 (2004) 4739-4744.

Schreiber, A.; Krause, M.; Zips, D.; Dörfler, A.; Richter, K.; Vettermann, S.; Petersen, C.; Beuthien-Baumann, B.; Thümmler, D.; Baumann, M.
Effect of the hypoxic cell sensitizer isometronidazole on local control of two human squamous cell carcinomas after fractionated irradiation.
Strahlenther. Onkol. 180 (2004) 375-382.

Seifert, S.; Künstler, J.-U.; Schiller, E.; Pietzsch, H.-J.; Pawelke, B.; Bergmann, R.; Spies, H.
Novel procedures for preparing ^{99m}Tc(III) complexes with tetradentate/monodentate coordination of varying lipophilicity and adaptation to ^{188}Re analogues.
Bioconjugate Chem. 15 (2004) 856-863.

Siegel, G.; Malmster, M.; Pietzsch, J.; Schmidt, A.; Buddecke, E.; Michel, F.; Ploch, M. Schneider, W.
The effect of garlic on arteriosclerotic nanoplaque formation and size.
Phytomedicine 11 (2004) 24-35.

Stephan, H.; Gloe, K.; Kraus, W.; Spies, H.; Johannsen, B.; Wichmann, K.; Chand, D. K.; Bharadwag, P. K.; Müller, U.; Müller, W. M.; Vögtle, F.
Binding and extraction of pertechnetate and perrhenate by azacages.
In: Fundamentals and applications of anion separation, R. P. Singh, B. A. Moyer (Eds.), Kluwer, New York (2004) pp. 151-168.

Tisato, F.; Refosco, F.; Porchia, M.; Bolzati, C.; Bandoli, G.; Dolmella, A.; Duatti, A.; Boschi, A.; Jung, C. M.; Pietzsch, H.-J.; Kraus, W.
Stereochemistry of the substitution-inert $[M(N)(PXP)]^{2+}$ metal-fragment: the crucial role of the diphosphine heteroatom X in the stabilization of the nitrido moiety (M = Tc, Re; PXP = diphosphine ligand).
Inorg. Chem. 43 (2004) 8617-8625.

Walter, B.; Brust, P.; Füchtner, F.; Müller, M.; Hinz, R.; Kuwabara, H.; Fritz, H.; Zwiener, U.; Bauer, R.
Age-dependent effects of severe traumatic brain injury on cerebral dopaminergic activity in newborn and juvenile pigs.
J. Neurotrauma 21 (2004) 1076-1089.

Weissenborn, K.; Bokemeyer, M.; Ahl, B.-R.; Fischer-Wasels, D.; Giewekemeyer, K.; Van Den Hoff, J.; Köstler, H.; Berding, G.
Functional imaging of the brain in patients with liver cirrhosis.
Metabolic Brain Disease 19 (2004) 269-280.

Wüst, F.; Knieß, T.
No carrier added synthesis of ^{18}F-labelled nucleosides using Stille cross-coupling reactions with 4-[^{18}F]fluoroiodobenzene.
J. Labelled Compd. Radiopharm. 47 (2004) 457-468.

Wüst, F.; Müller, M.; Bergmann, R.
Synthesis of 4-([^{18}F]fluoromethyl)-2-chlorophenylisothiocyanate: A novel bifunctional ^{18}F-labelling agent.
Radiochim. Acta 92 (2004) 349-353.

Zöphel, K.; Kotzerke, J.
Is ^{11}C-choline the most appropriate tracer for prostate cancer?
Eur. J. Nucl. Med. Mol. Imaging 31 (2004) 756-759.

ABSTRACTS

Beuthien-Baumann, B.; Zündorf, G.; Lüdecke, S.; Triemer, A.; Schierz, K.; Herholz, K.; Holthoff, V.
Einfluss von klinischen Charakteristika auf den regionalen cerebralen Glukosestoffwechsel bei der unipolaren Depression.
Nuklearmedizin 43 (2004) A82.

Brust, P.; Walter, B.; Füchtner, F.; Müller, M.; Hinz, R.; Kuwabara, H.; Steinbach, J.; Bauer, R.
Schweres Schädel-Hirn-Trauma löst im unreifen Gehirn eine Erhöhung der dopaminergen Aktivität aus.
Nuklearmedizin 43 (2004) A97.

Bühler, P.; Langner, J.; Kotzerke, J.; van den Hoff, J.
Einfluss unvermeidbarer Patientenbewegungen auf PET-Hirnuntersuchungen.
Nuklearmedizin 43 (2004) V196.

Graessler, J.; Westendorf, T.; Kopprasch, S.; Pietzsch, J.; Schroeder, H. E.
Effect of low density lipoproteins (LDL) isolated from subjects with normal and impaired glucose tolerance on the gene expression of CD36, SR-BI, and PPARγ.
Atherosclerosis 5 (2004) (Suppl. 1) 83.

Herting, B.; Holthoff, V. A.; Triemer, A.; Poetrich, K.; Herholz, K.; Beuthien-Baumann, B.; Reichmann, H.
Depressive symptoms and regional cerebral glucose metabolism in patients with MSA and PSP.
J. Neurol. Sciences (2004) (Abstracts).

Höhne, A.; Bergmann, R.; Wüst, F.
Synthese eines Fluor-18 markierten COX-2.
Nuklearmedizin 43 (2004) V173.

Holthoff, V. A.; Herholz, K.; Perani, D.; Sorbi, S.; Beuthien-Baumann, B.; Kalbe, E.
Depression and regional cerebral glucose metabolism in early dementia.
Eur. J. Neurol. (2004) (Suppl.) 172.

Hultsch, C.; Wüst, F.; Pawelke, B.; Bergmann, R.
Mikro-PET-Untersuchungen zu Bioverteilung und Metabolismus von F-18-fluorbenzoylierten Aminosäuren und Dipeptiden in den Nieren.
Nuklearmedizin 43 (2004) P40.

Julius, U.; Pietzsch, J.;
Increased LDL apolipoprotein B-100 oxidation in IGT and overt Type 2 diabetes.
Diabetes 53 (2004) A231.

Just, U.; Pötzsch, C.; Bühler, P.; Beuthien-Baumann, B.; van den Hoff, J.
Atemtriggerung zur Verbesserung der Darstellung und Abgrenzbarkeit von intrathorakalen Raumforderungen in der PET.
Nuklearmedizin 43 (2004) V192.

Kühnel, G.; von Ruthendorf-Przewoski, J.; Naumann, R.; Beuthien-Baumann, B.; Reiß, A.; Kotzerke, J.; Laniado, M.
Konventionelles Staging und Staging mit FDG-PET bei Patienten mit Morbus Hodgkin unter Berücksichtigung der Therapieentscheidung.
Fortschr. Röntgenstr. 176 (2004) S249.

Langner, J.; Bühler, P.; Pötzsch, C.; van den Hoff, J.
Nutzung von Mehrprozessorsystemen für den routinefähigen Einsatz listmode-basierter Bewegungskorrektur in der PET.
Nuklearmedizin 43 (2004) V189.

Mäding, P.; Zessin, J.; Pleiß, U.; Wüst, F.
Synthesis of a ^{11}C-labelled taxan derivative by [1-^{11}C]acetylation.
J. Labelled Compd. Radiopharm. 47 (2004) 263-265.

Oehme, L.; Hoinkis, C.; Appold, S.; Beuthien-Baumann, B.; Pötzsch, C.; Baumann, M.; Kotzerke, J.
Integration nuklearmedizinischer Bilder in die Bestrahlungsplanung des nichtkleinzelligen Bronchialkarzinoms.
Nuklearmedizin 43 (2004) A130.

Pietzsch, J.; Bergmann, R.; Wuest, F.; Pawelke, B.; van den Hoff, J.
Assessment of metabolism of native and oxidized low density lipoprotein in vivo: insights from animal positron emission tomography (PET) studies.
Atherosclerosis 5 (2004) (Suppl. 1) 43-144.

Pietzsch, J.; Bergmann, R.; Kopprasch, S.
Rheumatoid arthritis synovial fluid LDL induce monocyte chemotaxis and adhesion
Atherosclerosis (2004) 5 (Suppl. 1):16

Pietzsch, J.; Bergmann, R.; Wuest, F.; Pawelke, B.; van den Hoff, J.
Assessment of metabolism of native and oxidized low density lipoprotein in vivo: insights from high resolution animal positron emission tomography studies.
Nuklearmedizin 43 (2004) A77.

Pietzsch, J.; Knop, K.; Rode, K.; Wüst, F.; Bergmann, R.; van den Hoff, J.
Synthesis and biological characterization of fluorinated N-benzoylpolyamines as substrates for tissue transglutaminase.
Nuklearmedizin 43 (2004) A78.

Spirling, S.; Lüdecke, S.; Kalbe, E.; Beuthien-Baumann, B.; Lenz, O.; Zündorf, G.; Herholz, K.; Holthoff, V. A.
Early Alzheimer's disease with apathy or depression: Differences in regional brain metabolism.
APA 2004 New Res. Prog. NR663.

Stephan, H.; Bergmann, R.; Lange, S.; Röllich, A.; Sawatzki, A.-K.; Inoue, K; Jelinek, L.; Parschova, H.; Matejka, Z.
Binding and in vitro transport behaviour of polyoxotungstates in the presence of aminosaccharides.
Chem. Listy 98 (2004) s35-36.

Weck, A.; Julius, U.; Pietzsch, J.
Insulinresistenz (IR) und Lipoprotein (Lp)-subfraktionen (Sf) bei verschiedenen Graden der Glukosetoleranz (GT)
Diabetes und Stoffwechsel 13 (2004) 117.

Wüst, F.
Carbon-11 labelled compounds in the development of pharmaceuticals.
J. Labelled Compd. Radiopharm. 47 (2004) 261-262.

Wüst, F.; Kniess, T.; Bergmann, R.
Synthesis of a ^{11}C-labelled nonsteroisal glucocorticoid receptor ligand as potential radiotracer for imaging brain glucocorticoid receptors with positron emission tomography (PET).
J. Labelled Compd. Radiopharm. 47 (2004) 1051-1052.

LECTURES AND POSTERS

Lectures

Beuthien-Baumann, B.
PET in clinical oncology and research.
European Master Course in Radiobiology, University College London and Gray Laboratory, London, U. K., 30.01.2004.

Beuthien-Baumann, B.; Zündorf, G.; Lüdecke, S.; Triemer, A.; Schierz, K.; Herholz, K.; Holthoff, V.
Einfluss von klinischen Charakteristika auf den regionalen cerebralen Glukosestoffwechsel bei der unipolaren Depression.
42. Jahrestagung der Deutschen Gesellschaft für Nuklearmedizin, Rostock, 21.-24.04.2004.

Beuthien-Baumann, B.
Früh- und Differentialdiagnose von Parkinsonsyndromen: Teilgebiet Nuklearmedizinische Diagnostik.
Klinische Visite Parkinson, Dresden, Universitätsklinikum Carl Gustav Carus, 03.09.2004.

Brust, P.; Walter, B.; Füchtner, F.; Müller, M.; Hinz, R.; Kuwabara, H.; Steinbach, J.; Bauer, R.
Schweres Schädel-Hirn-Trauma löst im unreifen Gehirn eine Erhöhung der dopaminergen Aktivität aus.
42. Jahrestagung der Deutschen Gesellschaft für Nuklearmedizin, Rostock, 21.-24.04.2004,.

Brust, P.; Walter, B.; Hinz, R.; Müller, M.; Kuwabara, H.; Füchtner, F.; Bauer, R.; Steinbach, J.
Brain trauma elicits increased AADC acticity in newborn piglets.
Neuroreceptor Mapping 2004 Meeting.

Bühler, P.; Langner, J.; Kotzerke, J.; van den Hoff, J.
Einfluss unvermeidbarer Patientenbewegungen auf PET-Hirnuntersuchungen.
42. Jahrestagung der Deutschen Gesellschaft für Nuklearmedizin, 21.-24.04.2004, Rostock.

Fedorov, V.; Mironov, Y.; Shestopalov, M.; Brylev, K.; Yarovoi, S.; Spies, H.; Pietzsch, H.-J.; Stephan, H.; Kraus, W.
Octahedral rhenium cluster complexes with organic ligands as new preparations for medical applications.
Topical Meeting of the European Ceramic Society “Nanostuctures & Nanocomposites”, St. Petersburg, Russia, 05.-07.07.2004.

Füchtner, F.; Preusche, S.; Mäding, P.; Steinbach, J.
Factors affecting the specific activity of [^{18}F]fluoride from a water target.
10th Workshop on Targetry and Target Chemistry, Madison, USA, 13.-15.08.2004.

Gester, S.; Pietzsch, J.; Wüst, F.
Synthese und radiopharmakologische Untersuchung eines ^{18}F-markierten Resveratrolderivates
12. Jahrestagung der AG Radiochemie/Radiopharmazie, Walberberg, 23.-25.09.2004.

Gester, S.
Radiomarkierung von Polyphenolen und Flavonoiden mit PET-Radionukliden.
1. Workshop Positronen-Emissions-Tomographie in der Lebensmittelforschung, Dresden, 17.05.2004.

Grote, M.
Synthese und Untersuchung von Substraten der viralen Thymidinlkinase und Fluor–18 Markierung geeigneter Verbindungen zum Monitoring der Genexpression.
Forschungszentrum Jülich, 16.12.2004.

Grote, M.; Noll, St.; Noll, B.
Syntheses of ^{18}F-labeled acyclic purine and pyrimidine nucleosides intended for monitoring gene expression.
6th International Conference on Nuclear and Radiochemistry, Aachen, 29.08.-03.09.2004.

Grote, M.; Noll, St.; Noll, B.
Syntheses of ^{18}F-labeled acyclic purine and pyrimidine nucleosides intended for monitoring gene expression.
European Symposium on Radiopharmacy and Radiopharmaceuticals, Gdansk, Poland, 09.-12.09.2004.

Heinrich, T.
Rhenium-188: Chemie eines therapeutisch interessanten Radionuklides.
Bundesanstalt für Materialforschung und –prüfung, Berlin, 19.03.2004 (invited).

Heinrich, T.
Neuartige Re-188-Komplexe abgeleitet von Dimercatobernsteinsäure.
12. Jahrestagung der AG Radiochemie/Radiopharmazie, Walberberg, 23.-25.09.2004.

Höhne, A.; Bergmann, R.; Wüst, F.
Synthese eines Fluor-18 markierten COX-2.
42. Jahrestagung der Deutschen Gesellschaft für Nuklearmedizin, Rostock, 21.-24.04.2004.

Hultsch, C.; Bergmann, R.; Pawelke, B.; Pietzsch, J.; Wüst, F.; Johannsen, B.; Henle, T.
Untersuchungen zur Bioverteilung und Elimination des Isopeptides N-ε-(γ-Glutamyl)-lysin mittels Positronen-Emissions-Tomographie.
14. Arbeitstagung der Lebensmittelchemischen Gesellschaft – Fachgruppe in der Gesellschaft Deutsche Chemiker Regionalverband Süd-Ost, Halle, 01.-02.04.2004.

Hultsch, C.; Wüst, F.; Pawelke, B.; Bergmann, R.
Mikro-PET-Untersuchungen zu Bioverteilung und Metabolismus von F-18-fluorbenzoylierten Aminosäuren und Dipeptiden in den Nieren.
42. Jahrestagung der Deutschen Gesellschaft für Nuklearmedizin, Rostock, 21.-24.04.2004.

Jelínek, L.; Krotká, P.; Burda, R.; Parschová, H.; Matejka, Z.; Sawatzki, A.-K.; Röllich, A.; Stephan, H.
Interaction of polyoxotungstates with aminosaccharide based sorbents: Sorption kinetics, complex stability and implications for the therapeutic application of polyoxotungstates.
XVIVth International Symposium “Ars Separatoria 2004”, Z. Potok, Poland, 10.-13.06.2004.

Julius, U.; Pietzsch, J.;
Increased LDL apolipoprotein B-100 oxidation in IGT and overt Type 2 diabetes.
64th Scientific Sessions of the American Diabetes Association (ADA), Orlando, USA, 04.-08.06.2004.

Just, U.; Pötzsch, C.; Bühler, P.; Beuthien-Baumann, B.; van den Hoff, J.
Atemtriggerung zur Verbesserung der Darstellung und Abgrenzbarkeit von intrathorakalen Raumforderungen in der PET.
42. Jahrestagung der Deutschen Gesellschaft für Nuklearmedizin, Rostock, 21.-24.04.2004.

Kopprasch, S.; Graessler, J.; Pietzsch, J.; Schröder, H. E.
Low level CRP increases adhesion of leukocytes to endothelial cells and decreases phagocyte respiratory burst activities.
15th International Symposium on Drugs Affecting Lipid Metabolism (DALM), Venice, Italy, 24.-27.10.2004

Kühnel, G.; von Ruthendorf-Przewoski, J.; Naumann, R.; Beuthien-Baumann, B.; Reiß, A.; Kotzerke, J.; Laniado, M.
Konventionelles Staging und Staging mit FDG-PET bei Patienten mit Morbus Hodgkin unter Berücksichtigung der Therapieentscheidung.
Deutscher Röntgenkongress, Wiesbaden, 20.-22.05.2004.

Langner, J.; Bühler, P.; Pötzsch, C.; van den Hoff, J.
Nutzung von Mehrprozessorsystemen für den routinefähigen Einsatz listmode-basierter Bewegungskorrektur in der PET.
42. Jahrestagung der Deutschen Gesellschaft für Nuklearmedizin, Rostock, 21.-24.04.2004.

Mäding, P.; Füchtner, F.; Hilger, C. S.; Halks-Miller, M.; Horuk, R.
^{18}F-Labelling of a potent nonpeptide CCR1 antagonist for the diagnosis of the Alzheimer´s disease.
12th Workshop of the Central European Division e. V. of the International Isotope Society, Bad Soden, 17.-18.06.2004.

Miyagawa, M.; Simoes, M. V.; Städele, C.; Haubner, R.; Reder, S.; Lehner, T.; Noll, S.; Noll, B.; Grote, M.; Gambhir, S. S.; Gansbacher, B.; Schwaiger, M.; Anton, M.; Bengel, F. M.
Comparison of two HSV1-tk-based approaches for PET of cardiac transgene expression.
51st Annual Meeting, Society of Nuclear Medicine, Philadelphia, USA, 19.-23.06.2004.

Oehme, L.; Hoinkis, C.; Appold, S.; Beuthien-Baumann, B.; Pötzsch, C.; Baumann, M.; Kotzerke, J.
Integration nuklearmedizinischer Bilder in die Bestrahlungsplanung des nichtkleinzelligen Bronchialkarzinoms.
42. Jahrestagung der Deutschen Gesellschaft für Nuklearmedizin, Rostock, 21.-24.04.2004.

Pietzsch, J.; Bergmann, R.; Wuest, F.; Pawelke, B.; van den Hoff, J.
Assessment of metabolism of native and oxidized low density lipoprotein in vivo: insights from animal positron emission tomography (PET) studies.
74th European Atherosclerosis Society Congress, Seville, Spain, 17.-20.04.2004.

Pietzsch, J.; Bergmann, R.; Wuest, F.; Pawelke, B.; van den Hoff, J.
Assessment of metabolism of native and oxidized low density lipoprotein in vivo: insights from high resolution animal positron emission tomography studies.
42. Jahrestagung der Deutschen Gesellschaft für Nuklearmedizin, Rostock, 21.-24.04.2004.

Pietzsch, J.
Metabolismus oxidierter Proteine in vivo: Einblicke mit Kleintier-PET-Untersuchungen.
1. Workshop “Positronen-Emissions-Tomographie in der Lebensmittelforschung“, Rossendorf, 17.05.2004.

Pietzsch, J.
In vino sanitas. Den Geheimnissen des Weines auf der Spur.
Vortrag zur “Langen Nacht der Wissenschaften“, Dresden, 25.06.2004.

Pietzsch, H.-J.; Schiller, E.; Seifert, S.; Künstler, J.-U.; Spies, H.
Tc and Re labelling of biomolecules according to the "4+1" mixed-ligand approach: switching from diagnostic to therapeutic radiopharmaceuticals.
2nd Research Co-ordination Meeting of the International Atomic Energy Agency's Co-ordinated Research Project on "Development of ^{99m}Tc based Small Bio Molecules Using Novel ^{99m}Tc Cores", IAEA-Hauptquartier Wien, Vienna, Austria, 15.-19.11.2004 (invited).

Röhrich, A.; Stephan, H.
Darstellung und Charakterisierung von Glycoclustern auf der Basis von PAMAM-Dendrimeren mit Cyclam-Core.
Institutsseminar, Universität Bonn, 01.12.2004.

Röllig, A.; Stephan, H.
Improved binding of polyoxotungstates by polysaccharides.
Institutskolloquium, Institute of Chemical Technology, Prague, Czech Republik, 27.05.2004.

Saidi, M.; Kretzschmar, M.; Seifert, S.; Bergmann, R.; Pietzsch, H.-J.
Cyclopentadienyl tricarbonyl complexes of ^{99m}Tc for the in vivo imaging of the serotonin 5-HT_{1A} receptor in the brain.
2. International Symposium on Bioorganometallic Chemistry (ISBOMC04), Zurich, Switzerland, 14.-19.07.2004. (invited).

Schiller, E.; Kraus, W.; Seifert, S.; Pawelke, B.; Bergmann, R.; Spies, H.; Pietzsch, H.-J.
Labelling of biomolecules using organometallic Tc(III) and Re(III) mixed-ligand complexes.
COST ACTION B12 “Radiotracers for in vivo assessment of biological function”, Lisbon, Portugal, 21.05.2004 (invited).

Schiller, E.
Rhenium-188-Gemischtligandkomplexe mit Phoshinliganden: Stabilitätsbetrachtungen
12. Jahrestagung der AG Radiochemie/Radiopharmazie; Walberberg, 23.-25.09.2004.

Schiller, E.; Kraus, W.; Seifert, S.; Pawelke, B.; Bergmann, R.; Spies, H.; Pietzsch, H.-J.
Labelling of biomolecules using organometallic Tc(III) and Re(III) mixed-ligand complexes.
European Symposium on Radiopharmacy and Radiopharmaceuticals; Gdansk, Poland, 09.-12.09.2004.

Schlesinger, J.; Bergmann, R.
^{86}Y-Markierung von Neurotensin(8-13)-Derivaten.
12. Jahrestagung der AG Radiochemie/Radiopharmazie, Walberberg, 23.-25.09.2004.

Seifert, S.; Künstler, J.-U.; Schiller, E.; Pietzsch, H.-J.; Pawelke, B.; Bergmann, R.; Spies, H.
^{99m}Tc and ^{188}Re mixed-ligand complexes at lower oxidation state.
Institutskolloquium, The Korea Atomic Energy Research Institute, Hanaro Application Research, Daejeon, Korea, 24.04.2004 (invited).

Seifert, S.; Künstler, J.-U.; Schiller, E.; Pietzsch, H.-J.; Pawelke, B.; Bergmann, R.; Spies, H.
^{99m}Tc and ^{188}Re mixed-ligand complexes at lower oxidation state.
19th KAIF/KNS Annual Conference, Seoul, Korea, 25.-27.04.2004 (invited).

Stephan, H.
Dendritic encapsulation of rhenium and copper.
Supraphone-Meeting, Xanten, 06.-08.05.2004 (invited).

Stephan, H.; Bergmann, R.; Lange, S.; Röllich, A.; Sawatzki, A.-K.; Inoue, K.; Jelínek, L.; Parschová, H.; Matejka, Z.
Binding and in vitro transport behavior of polyoxotungstates in the presence of aminosaccharides.
International Conference on Supramolecular Science & Technology, Prague, Czech Republik, 05.-09.09.2004.

van den Hoff, J.
Listmode based movement correction in PET.
Workshop on Physical and Chemical Aspects of PET Radiopharmaceuticals, Bratislava, Slovakia, 19.-22.09.2004 (invited).

Walther, M.; Jung, C. M.; Bergmann, R.; Pietzsch, J.; Rode, K.; Stehr, S.; Heintz, A.; Wunderlich, G.; Kraus, W.; Pietzsch, H.-J.; Kropp, J.; Deussen, A.; Spies, H.
Synthesis and biological evaluation of a new type of technetium-labelled fatty acids for myocardial metabolism imaging.
European Symposium on Radiopharmacy and Radiopharmaceuticals, Gdansk, Poland, 09.-12.09.2004.

Wüst, F.
Aspekte der PET-Radiochemie in der Lebensmittelchemie.
1. Workshop Positronen-Emissions-Tomographie in der Lebensmittelforschung, Dresden, 17.05.2004.

Wüst, F.
PET radiochemistry and the potential of PET in drug development and evaluation.
Boehringer Ingelheim, 07.04.2004 (invited).

Wüst, F.; Kniess, T.; Bergmann, R.
Synthesis of a ^{11}C-labelled nonsteroisal glucocorticoid receptor ligand as potential radiotracer for imaging brain glucocorticoid receptors with positron emission tomography (PET).
12th Workshop of the Central European Division e. V. of the International Isotope Society, Bad Soden, 17.-18.06.2004.

Wüst, F.
Positronen-Emissions-Tomographie (PET): Wie radioaktive Substanzen den Körper biochemisch transparent machen.
Tag der offenen Tür, FZ-Rossendorf, 18.09.2004.

Wüst, F.
Radiopharmaceutical chemistry at the PET Center Rossendorf.
Washington University, School of Medicine, St. Louis, USA, 08.10.2004 (invited).

Wüst, F.
Transition metal-mediated C-C and C-N bond forming reactions with the short-lived positron emitters ^{11}C and ^{18}F.
Washington University, School of Medicine, St. Louis, USA, 12.10.2004 (invited).

Posters

Graessler, J.; Westendorf, T.; Kopprasch, S.; Pietzsch, J.; Schroeder, H. E.
Effect of low density lipoproteins (LDL) isolated from subjects with normal and impaired glucose tolerance on the gene expression of CD36, SR-BI, and PPARγ.
74th European Atherosclerosis Society Congress, Seville, Spain, 17.-20.04.2004.

Heintz, A.; Stehr, S. N.; Wunderlich, G.; Walther, M.; Jung, C. M.; Bergmann, R.; Pietzsch, J.; Rode, K.; Kraus, W.; Pietzsch, H.-J.; Kropp, J.; Spies, H.; Deussen, A.
Myocardial extraction of a new type of technetium-labeled fatty acids
European Symposium on Radiopharmacy and Radiopharmaceuticals, Gdansk, Poland, 09.-12.09.2004.

Julius, U.; Pietzsch, J.;
Increased LDL apolipoprotein B-100 oxidation in IGT and overt Type 2 diabetes.
64th Scientific Sessions of the American Diabetes Association (ADA), Orlando, USA, 04.-08.06.2004.

Julius, U.; Pietzsch, J.
Lipoprotein kinetics as measured with stable isotopes in familial combined hyperlipidemia and impaired glucose tolerance.
15th International Symposium on Drugs Affecting Lipid Metabolism (DALM), Venice, Italy, 24.-27.10.2004.

Kraus, W.; Stephan, H.; Spies, H.; Reck, G.
Käfigstrukturen für die nuklearmedizinische Diagnostik.
Gemeinsame Jahrestagung DGK und DGKK, Jena, 15.-19.03.2004.

Oehme, L.; Hoinkis, C.; Appold, S.; Beuthien-Baumann, B.; Pötzsch, C.; Baumann, M.; Kotzerke, J.
Integration nuklearmedizinischer Bilder in die Bestrahlungsplanung des nichtkleinzelligen Bronchialkarzinoms.
42. Jahrestagung der Deutschen Gesellschaft für Nuklearmedizin, Rostock, 21.-24.04.2004.

Pietzsch, J.; Bergmann, R.; Wuest, F.; Pawelke, B.; van den Hoff, J.
Assessment of metabolism of native and oxidized low density lipoprotein in vivo: insights from animal positron emission tomography (PET) studies.
74th European Atherosclerosis Society Congress, Seville, Spain, 17.-20.04.2004.

Pietzsch, J.; Bergmann, R.; Kopprasch, S.
Rheumatoid arthritis synovial fluid LDL induce monocyte chemotaxis and adhesion
74th European Atherosclerosis Society Congress, Seville, 17.-20.04.2004

Seifert, S.; Künstler, J.-U.; Schiller, E.; Pietzsch, H.-J.; Pawelke, B.; Bergmann, R.; Spies, H.
Labelling of biomolecules using ^{99m}Tc(III) and ^{188}Re(III) mixed-ligand complexes.
ISBOMC'04, Second International Symposium on Bioorganometallic Chemistry, Zurich, Switzerland, 14.-17.07.2004.

Weck, A.; Julius, U.; Pietzsch, J.
Insulinresistenz (IR) und Lipoprotein (Lp)-subfraktionen (Sf) bei verschiedenen Graden der Glukosetoleranz (GT)
39. Jahrestagung der Deutschen Diabetes-Gesellschaft, Hannover, 19.-22.05.2004.

Westendorf, T.; Kopprasch, S.; Pietzsch, J.; Graessler, J.
LDL isolated from subjects with impaired glucose tolerance increase the expression of CD36 and PPARγ in macrophages.
15th International Symposium on Drugs Affecting Lipid Metabolism (DALM), Venice, Italy, 24.-27.10.2004.

PATENTS

Dinkelborg, L.; Blume, F.; Hilger, C.-S.; Heldmann, D.; Platzek, J.; Niedballa, U.; Miklautz, H.; Speck, U.; Duda, S.; Tepe, G.; Noll, B.; Görner, H.
Stents with a radioactive surface coating, processes for their production and their use for restenosis prophylaxis.
US 6709693

Hilger, C. S.; Johannsen, B.; Steinbach, J.; Mäding, P.; Halks-Miller, M.; Horuk, R.; Dinter, H.; Mohan, R.; Hesselgesser, J. E.
Radiopharmaceuticals for diagnosing Alzheimer´s disease.
US 6,676,926 B2

Spies, H.; Pietzsch, H.-J.; Jung, C.
Technetiummarkierte Fettsäuren und deren Verwendung für die Myokarddiagnostik sowie Verfahren zur Herstellung der technetiummarkierten Fettsäuren.
DE 103 16 965

AWARDS

Dr. P. Bühler, U. Just, J. Langner
Technologiepreis 2004 des Forschungszentrums Rossendorf:
List-mode basierte Verfahren zur Korrektur von Patientenbewegungen in der PET
16.12.2004

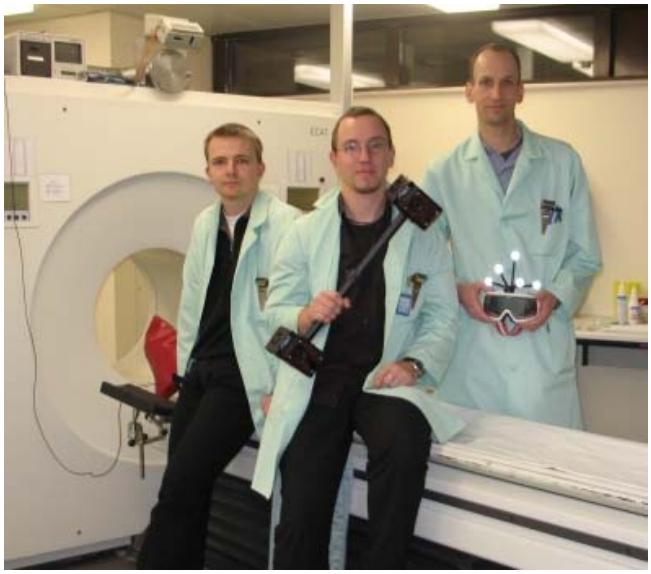

DIPLOMA

K. Knop
Entwicklung eines neuen Radiotracers zur Charakterisierung von Transglutaminasen in vivo.
Fachhochschule Zittau/Görlitz, 27.01.2004.

J. Langner
Development of a parallel computing optimised head movement correction method in positron emission tomography.
Hochschule für Technik und Wirtschaft Dresden, 19.02.2004

A. Höhne
Synthese von ^{18}F-markierten Cyclooxygenase-2-Inhibitoren als Radiotracer für die Positronen-Emissions-Tomographie.
Technische Universität Dresden, 30.06.2004.

J. Schlesinger
Yttrium-86 Markierung von Neurotensin (8-13)-Derivaten.
Technische Universität Dresden, 15.07.2004.

S. Juran
Synthese und Charakterisierung von Kupferkomplexen mit Bispidin-Liganden.
Fachhochschule Lausitz, Senftenberg, 10.12.2004.

PhD THESIS

J.-U. Künstler
Beitrag zur Präparation und Charakterisierung technetiummarkierter Antikörper und Peptide.
Technische Universität Dresden, 05.11.2004.

III. COLLABORATIONS, FUNDED PROJECTS AND FINANCIAL SUPPORT

COLLABORATIONS

The Institute sustains a number of valuable collaborations with other research institutions and is engaged in joint projects funded by federal and trans-national authorities and research initiatives as well as by the industry.

Naturally, the Technical University of Dresden continues to be an important partner in our cooperative relations. Cooperations exist with various groups in the Department of Chemistry and the Faculty of Medicine. Common objects of radiopharmacological and medical research link the Institute with the University Hospital in Dresden, above all with its Department of Nuclear Medicine (Prof. Kotzerke) which contributes to the staff of the jointly operated PET Centre Rossendorf. Application of the positron emission tomography technique has been successfully extended to new questions in collaboration with the Institute of Food Chemistry (Prof. Henle). Fruitful collaborations on the development of novel PET radiotracers have been established with the Institute of Organic Chemistry (Prof. Metz) and the Institute of Biochemistry (Prof. van Peè). Bioinorganic research activities are closely linked with the Department of Coordination Chemistry (Prof. Gloe).

On the national and international level, there exist a number of collaborations.

The identification of common objects in PET radiopharmacy has led to collaborative research with the Institute of Interdisciplinary Isotope Research at the University of Leipzig (Prof. Steinbach). Both institutes constitute an alliance of research in radiopharmaceutical sciences.

Cooperation in PET tracer chemistry and radiopharmacology has been established with the Turku Medical PET Center (Prof. Solin), Washington University, School of Medicine in St. Louis (Prof. Welch and Prof. Anderson), Harvard School of Medicine in Boston (Dr. Neumeyer), Northeastern University Boston (Prof. Hanson), University of Illinois in Champaign-Urbana (Prof. Katzenellenbogen) and the Instituto Tecnológico e Nuclear in Sacavèm (Dr. Santos).

Cooperation in the field of peptide chemistry and receptor research exists with the University of Leipzig (Prof. Beck-Sickinger) and the Free University of Brussels (Prof. Tourwe).

Cooperation in technetium and rhenium chemistry exists with the University of Ferrara (Prof. Duatti), CNR Padova (Dr. Tisato, Dr. Refosco), with the Korean Research Centre KAERI (Dr. Park), as well as with the University of Kitakyushu, Japan (Prof. Yoshizuka) and, more recently, the University of Missouri-Columbia (Dr. Smith). The Institute works with the University of Heidelberg (Prof. Comba) and with University Hospital Leipzig (Dr. Laub, Prof. Emmrich), on radioimmunoscintigraphy.

Very effective cooperation exists with the Federal Material Research Institute in Berlin (Dr. Reck, Mr. Kraus), whose staff members carried out X-ray crystal structure analysis of new technetium and rhenium complexes.

In the field of supramolecular chemistry, successful cooperation exists with the Kekulé Institute of Organic Chemistry and Biochemistry (Prof. Vögtle) of the University of Bonn.

PUBLIC FUNDED PROJECTS

The Institute is part of the Research Center Rossendorf, which is financed by the Federal Republic of Germany and the Free State of Saxony on a fifty-fifty basis.

The Institute participated in the following networks supported by Commission of the European Communities:

Radiotracers for *in vivo* assessment of biological function
COST B12
in collaboration with Sweden, Italy and Switzerland.
02/1999 – 04/2005.

Since 2004, the Institute is engaged in the SIXTH FRAMEWORK PROGRAMME PRIORITY 1 FP6-2002 LIFESCIHEALTH, in the project BioCare, Molecular Imaging for Biologically Optimized Cancer Therapy, Contract no.: 505785. The Institute contributes to the work packages: WP 3 - Molecular imaging of radiation therapy induced alteration of tumour cell proliferation and functional receptor expression, WP 4 - Aptamer based PET and SPECT tracers for molecular tumour imaging, together with partners from the Technical University of Dresden, Universitair Ziekenhuis Gasthuisberg, Université Catholique de Louvain, and University of Hamburg.
04/2004-10/2008.

The Institute further contributes to POL-RAD-PHARM (MARIE CURIE TRANSFER OF KNOWLEDGE FELLOWSHIP). Project full title: Chemical Studies for Design and Production of New Radiopharmaceuticals. The project aims at commencing and intensifying research in radiopharmaceutical chemistry – a new discipline for the host institution. For this purpose the host institution, located in Poland, has established partnership with other seven European laboratories.
The research part of the project includes:
(1) learning and/or mastering methods for obtaining novel potential radiopharmaceuticals labelled with ^{99m}Tc (diagnostic) and with ^{188}Re (therapeutic);
(2) developing a method for labelling biomolecules with ^{211}At by formation of stable heteroleptic complexes between astatide (At^-) and chelates of soft metal cations;
(3) developing methods for obtaining selected radionuclides of potential use in manufacturing radiopharmaceuticals, including metallic PET nuclides and alpha-emitters;
(4) developing analytical methods for purity control and stability studies of the novel radiopharmaceuticals.
07/2004-06/2008

On the national level, two research projects concerning tracer design, biochemistry and PET radiochemistry were supported by the Deutsche Forschungsgemeinschaft (DFG):

Molecular encapsulated ^{188}Re complexes: Development of robust and tunable radioactive rhenium complexes on the basis of novel chelators derived from dimercaptosuccinic acid (DMSA)
PI 255/5-1 (H.-J. Pietzsch) 12/2002 – 11/2004.

F-18 labelled corticosteroides as ligands for imaging brain glucocorticoid-receptors by means of PET
WU 340/1-1 (F. Wüst) 11/2004 – 10/2006.

The Sächsisches Staatsministerium für Wissenschaft und Kunst provided support for the following projects:

Development and characterization of nanoscale metal-based drugs targeting tumours
SMWK-No. 4-7531.50-03-0370-01/4, 06/2001 – 12/2004.

MeDDrive 2002
01/2004 – 12/2004

The Bundesministerium für Bildung und Forschung supported cooperation with

Czech Republic: Polyoxometallo compounds
WTZ, 08/2002 – 07/2005

Russia: Polynuclear metallo drugs
WTZ, 07/2003 – 09/2004

The Bundesministerium für Wirtschaft und Arbeit supported research projects on:

Preparation of ^{86}Y
08/2003 - 01/2005

Radioimmunodiagnostics of inflammation
05/2004 - 06/2007

Several laboratory visits were supported by the “Deutscher Akademischer Austauschdienst” (DAAD).

VIGONI-Project with Padova (Italy):
Labelling Dithiol Ligands with a TcN-Synthon
01/2005 – 12/2006

FINANCIAL SUPPORT BY THE INDUSTRY

The following projects were supported by cooperations with the industry:

ABX advanced biomedical compounds GmbH Dresden
Cooperation in functional diagnostics
04/2001 - 11/2004

ABX advanced biomedical compounds GmbH Dresden
Synthesis of precursors for PET radiopharmaceuticals
01/2003 – 12/2004

ABX advanced biomedical compounds GmbH Dresden
PET surrogate parameters
10/2003 - 06/2006

Apogepha Arzneimittel GmbH
Cooperation in pharmakokinetics and metabolism of propiverin
07/2003 – 03/2005

A.R.T. Hersching
Cooperation in movement tracking for PET
09/2002 – 12/2005

Bayer AG Leverkusen
Cooperation in drug development
05/2002 – 06/2005

Bruker BioSpin MRI GmbH
MPI/PET-Coupling
11/2003 – 12/2005

Nihon-Medi-Physics (Japan/USA)
Development and evaluation of technetium-99m-labelled fatty acids
01/2003 – 12/2005

ROTOP Pharmaka GmbH
Agent syntheses
06/2004 – 12/2006

Schering AG Berlin
Cooperation in drug development
1/2004 – 06/2005

Schering AG Berlin
Cooperation in nuclear diagnostics
07/1996 – 12/2004

Schering AG Berlin
Pharmaceutical research
01/2002 - 12/2006

Schering AG Berlin
Metal chelates
05/2003 - 12/2006

LABORATORY VISITS

Dr. F. Wüst
McLean Hospital, Boston, USA
16.-19.01.2004

Dr. S. Seifert
Korea Atomic Energy Research Institute (KAERI), HANARO, Div. of Radioisotope Production, Korea
21.-28.04.2004

A. Röllig
Institute of Chemical Technology, Prag, Czech Republik
23.-30.05.2004

E. Schiller
Forschungszentrum Padua, Italy
07.-16.07.2004

Dr. F. Wüst
School of Medicine, St. Louis, USA
23.09.-14.10.2004

T. Heinrich
Universität Ferrara, Italy
02.-26.11.2004

Dr. H.-J. Pietzsch
IAEA, Wien, Austria
14.-20.11.2004

GUESTS

S. Raji
Kwame Nkrumah University of Science and Technology, Kumasi
01.10.2003 – 28.03.2004

F. Aggrey
University of Cape Coast (U.C.C.)
15.10.2003 – 11.04.2004

Dr. R. Garcia
Instituto Technologico e Nuclear, Sacavem, Portugal
12.-30.01.2004

M. R. Zainol Abidin
University Malaya Medical Centre, Kuala Lumpur, Malaysia
01.03. – 26.03.2004

A. M. Zain
University Malaya Medical Centre, Kuala Lumpur, Malaysia
01.03. – 26.03.2004

Dr. S. Park
Korea Atomic Energy Research Institute, Daejeon, Korea
15.06. – 14.09.2004

X. Chen
Shanghai Jiao Tong University, China
19.07. – 18.09.2004

Prof. V. Fedorov
Siberian Branch of the Russian Academy, Novosibirsk, Russia
01.09. – 10.09.2004

Dr. T. Suzuki
University of Kitakyushu, Kitakyushu, Japan
01.09. – 11.10.2004

Prof. K. Yoshizuka
University of Kitakyushu, Japan
01.09. – 16.10.2004

Dr. Zhang Chunfu
Shanghai Institute of Applied Physics, China
04.10. – 29.10.2004

P. Krotka
Institute of Chemical Technology Prague, Czech Republic
16.10. – 31.10.2004

K. Brylev
Russian Academy of Science Siberian Branch, Novosibirsk, Russia
18.10.2004 – 16.12.2004

Prof. Z. Matejka
Institute of Chemical Technology Prague, Czech Republic
13.12. – 15.12.2004

P. Krotka
Institute of Chemical Technology Prague, Czech Republic
13.12. – 18.12.2004

MEETINGS ORGANIZED

1. Workshop “Positronen-Emissions-Tomographie in der Lebensmittelforschung”
Forschungszentrum Rossendorf/Technische Universität Dresden
17.05.2004

1. “List Mode User Meeting“
Forschungszentrum Rossendorf/Siemens Erlangen, CTI Knoxville, USA
18.05.2004

TEACHING ACTIVITIES

Summer term 2004

B. Johannsen, H.-J. Pietzsch
One term course on Metals in Biosystems (Introduction into Bioinorganic Chemistry)

J. Pietzsch
Lipoproteine and Atherogenese

Winter term 2004/2005

F. Wüst
One term course on Radiopharmaceutical Chemistry

IV. SEMINARS

TALKS OF VISITORS

Dr. N. Schramm, Forschungszentrum Jülich, Zentrallabor für Elektrotechnik
Erste Ergebnisse eines hochauflösenden Multi Pinhole Spect an Mäusen
02.03.2004

Prof. C. E. Müller, Universität Bonn, Pharmazeutisches Institut
Purinrezeptoren als Zielstrukturen in der Wirkstoff-Forschung
15.04.2004

Prof. K. Yoshizuka, University of Kitakyushu
Selective recovery of lithium ion in seawater using a λ-MnO_2 adsorbent
23.09.2004

Dr. T. Suzuki, University of Kitakyushu
Speckle image observations using high coherent X-ray beams focused by Fresnel Zone Plate
23.09.2004

Prof. K. Inoue, Saga University
Remediation of polluted environment by using biomass wastes
12.10.2004

Prof. F. Vögtle, Universität Bonn
Funktionelle Dendrimere – Synthesen, Eigenschaften und Anwendungen in den Material- und Lebenswissenschaften
28.10.2004

Prof. S. Waldvogel, Universität Bonn, Kekulé-Institut für Organische Chemie
Synthese, Eigenschaften und Anwendungen von künstlichen Koffeinrezeptoren
09.12.2004

INTERNAL SEMINARS

Dr. B. Noll
Monitoring Gentherapie
24.03.2004

A. Höhne
^{18}F-Markierung von COX-2-Inhibition
07.04.2004

Dr. B. Beuthien-Baumann
Parkinson-Diagnostik mit PET
28.04.2004

J. Schlesinger
^{86}Y-Markierung von Neurotensin (8-13)
19.05.2004

T. Heinrich
Entwicklung von stabilen und anpassbaren Re-Komplexen mit verbrückten DMSA-Chelatoren
09.06.2004

E. Schiller
Stabile Re-188-Komplexe mit Phoshin-Liganden
30.06.2004

S. Gester
Markierung von Polyphenolen und Flavonoiden mit PET-Radioisotopen
25.08.2004

D. Möckel
Validierung von Methoden zur Bewegungskorrektur bei PET
06.10.2004

J. Langner
Entwicklung einer parallelisierten Methode zur Bewegungskorrektur bei Hirnuntersuchungen in der Positronen-Emissions-Tomographie
27.10.2004

Dr. C. Haase
Modulation der Tau-Protein-Eigenschaften durch Pseudophosphorylierung
15.12.2004

V. PERSONNEL

Director (provisional)

Prof. Dr. van den Hoff, J.

Administrative Staff

Forker, S.
Neubert, G.

Scientific Staff

Dr. Berndt, M.*
Dr. Bergmann, R.
Dr. Füchtner, F.
Dr. Grote, M.*
Dr. Haase, C.*
Dr. Knieß, T.
Künstler, J.-U.*
Mäding, P.
Dr. Noll, B.
Dr. Noll, S.
Dr. Pawelke, B.*
Dr. Pietzsch, H.-J.
Dr. Pietzsch, J.
Preusche, S.
Dr. Rother, A.*
Dr. Seifert, S.
Dr. Spies, H.*
Dr. Stephan, H.
Dr. Strobel, K.*
Dr. Walther, M.*
Dr. Will, E.
Dr. Wüst, F.
Dr. Zessin, J.

Technical Staff

Barth, M.*
Dohn, N.
Gläser, H.
Görner, H.
Große, B.
Hentges, A.
Herrlich, R.
Herzog, W.
Jährig, P.*
Kasper, H.
Kolbe, U.
Krauß, E.
Krauß, T.*
Kreisl, B.
Landrock, K.
Lehnert, S.
Lenkeit, U.
Lipps, B.
Lücke, R.*
Rode, K.*
Roß, H.
Sterzing, R.
Suhr, A.**

PhD Students

Gester, S.
Hecht, M.
Heinrich, T.
Hultsch, C.
Just, U.
Langner, J.
Pötzsch, C.
Schiller, E.
Schlesinger, J.
Steiniger, B.

Former Personnel

(who left during the period covered by the report)

Scientific Staff:
Kretzschmar, M.
Dr. Pönisch, F*

* term contract
** on maternity leave